THE *IN-VITRO* SELECTION AND BIOCHEMICAL CHARACTERIZATION OF METALLODNAZYMES

BY

HANNAH ELIZABETH IHMS

THESIS

Submitted in partial fulfillment of the requirements
for the degree of Master of Science in Chemistry
in the Graduate College of the
University of Illinois at Urbana-Champaign, 2012

Urbana, Illinois

Advisor:

Professor Yi Lu

Abstract

DNAzymes are strands of catalytic DNA. First discovered in 1994, they have proved themselves capable of catalyzing many different types of reactions with significant rate enhancements. Because they often require divalent metal-ion cofactors, DNAzymes have readily been developed into metal-ion sensors, in some cases with part-per-trillion sensitivity.

These enzymes are currently isolated through *in vitro* selection. With little to base a DNAzyme selection's sequence upon, *in vitro* selections typically begin with randomized DNA pools. As more is learned about the properties of DNAzymes, more efficient means of isolation involving rational design will become more feasible.

Fundamental inquiries into the properties of heavy-metal-ion-dependent DNAzymes was the theme of this work. Heavy metal ions have significant health impacts, and thus are an active area of research in bioinorganic chemistry. Additionally, DNAzymes have proven their ability to distinguish between various metal ions with as high as million-fold selectivities. Such selectivities between metal ions with similar charge, ionic radii, and other properties are fundamentally intriguing.

Co^{2+} and Zn^{2+} are two closely related metal ions, and the factors governing one DNAzyme family's ability to distinguish between them were examined. During the course of a DNAzyme selection, it is customary to truncate the selected sequence to transform a *cis*-cleaving construct into a *trans*-cleaving construct. This general method was found to be ineffective in the case of this family, because peripheral sequences enhanced these DNAzymes' selectivity for Co^{2+} over Zn^{2+} and Pb^{2+}.

While DNAzymes have been successfully selected against Mg^{2+}, Zn^{2+}, Hg_2^{2+}, Mn^{2+}/Mg^{3+}, and other divalent cations, Cd^{2+}-, Fe^{2+}-, and Fe^{3+}-dependent DNAzymes have not yet been isolated. A DNAzyme pair selective for Fe^{2+} and Fe^{3+} is of particular interest, because of their interconversion in an biological environment and the fundamental understanding a comparison of the DNAzymes selective for each would provide about DNAzymes' abilities to distinguish between metal ions.

Finally, the Pb^{2+}-dependent DNAzyme 17E was mutated at the $G^{1.1}$ position with the guanine analogs inosine, diaminopurine, and 2-aminopurine to analyze its catalytic mechanism.

17E contains the 8-17 motif that has dominated selections carried out by multiple labs under a multiplicity of conditions.

By investigating the basic properties of DNAzymes, more light can be shed on the structure-function of these molecules, and expand the library of catalytic DNA ready to be used in new applications.

To Jesus, who calls me friend

Acknowledgments

A huge thank you to my advisor, Dr. Lu, for giving me the opportunity and resources to do this work. Thank you for your optimism and advice!

I could not have completed this work without my friends and family. Whether it was early-morning wake-up calls, mid-afternoon chats, or late-night counseling sessions, you have always been there for me. Mom and Dad, thank you, thank you, thank you for all that you have taught me about chemistry, life, and God. I cannot express how much your love and presence mean to me. Eli and Tida, thank you for being awesome siblings! Lab mates, it was worth coming to grad school just to meet you! Priya and Nandini, thank you for patiently teaching me how to do selections (and for not laughing at me when I tried to image cardboard)! Tian Lan (desk buddy, yeah! you are the definition of calm!), Dr. Ying He (your kindness has carried me through!), Li Huey (we've been through thick and thin!), Dr. Eric Null (chef extraordinaire!), Brian Wong (coffee meister!)… I could go on and on: thank you to all you Lu labbers for being the most incredible labmates on the surface of the earth!

Dr. Vickie Hess, Drs. John and Heidi Lakanen, Dr. Dennis Brinkman, Dr. Michael Goff, Dr. David Dueker, Dr. Willem van de Merwe, Dr. Daniel Jones, and Ron Mazellan, thank you for mentoring me at Indiana Wesleyan University and preparing me for this journey.

Rebekah Leitner, Nina Sekerak, Diana West, Stephanie Chung, Jerri-Ann Houser, Jane Christensen, Meg Hedlund, John-Paul Deddens, Gabe Hartwig, Jerry Vachaparambil, Amanda Cuevas, Corinne Kohler, Shirley Kolb, and Rudi & Judy Laufhutte, thank you for your friendship!

Julie Sides, Connie Knight, Theresa Struss, and Beth Myler, you light up this place with your kind hearts and willing hands. Dr. Ellen Wang Althaus and Dr. Alexander Scheeline, thank for your incredible advice and support, especially during a time of upheaval in my life!

Jesus, thank you for giving me something to live for. Thank you for carrying me through days of darkness and reminding me of the plan You have for each of us. Thank you for creating matter, and for being willing to enter space and time to deliver us from death itself. "You are worthy, our Lord and God, to receive glory and honor and power, for You created all things, and by Your Will they were created and have their being." It's in You we live, and move, and have our being!

Table of Contents

Chapter 1: Introduction 1

Chapter 2: Peripheral Sequences' Effects on the Selectivity and Activity of Co^{2+}-Dependent DNAzymes 13

Chapter 3: The *In-Vitro* Selections of Cd^{2+}-, Fe^{2+}-, and Fe^{3+}-Dependent DNAzymes 41

Chapter 4: Evaluating the Potential of an Acid/Base Catalysis Mechanism in the Pb^{2+}-Dependent 17E DNAzyme by Examining $G^{1.1}$-Mutants 76

Chapter 1: Introduction

1.1 Catalytic Nucleic Acids

1.1.1 Ribozymes

The central dogma of biology, that information is transmitted from DNA to RNA, and finally to protein, was challenged by the 1982 discovery of ribozymes—catalytically active RNA.[1] For the first time, RNA was seen not as a passive substrate for protein to act upon, but a key player with a dynamic role in cellular metabolism. Some commonly occurring ribozymes are shown in Figure 1.1.

1.1.2 DNAzymes

The isolation of an increasing number of ribozymes raised the question if ribozymes had a DNA counterpart. Ribonucleic and deoxyribonucleic acid differ by a single hydroxyl group, and it was an open question whether this drew the line between catalytically active and inactive sequences. In 1994, Breaker and Joyce reported their answer in the form of a deoxyribozyme,[2] and the known role of DNA has been expanding ever since.[3,4,5,6]

RNA-cleaving and Pb^{2+}-dependent, the first deoxyribozyme (also called catalytic DNA or a DNAzyme) foreshadowed many of the RNA-cleaving, metal-dependent DNAzymes that would follow. These nucleic acid enzymes are intriguing from a basic-science or an application-centered perspective. The three-dimensional structures which enable DNAzymes to participate in a wide range of activity are in the infancy of characterization, yet these enzymes have proven their ability to catalyze not only many different reactions, from RNA cleavage to porphyrin metallation, but to make use of many different metal cofactors, such as Mg^{3+}/Mn^{2+},[7] Co^{2+},[8] Cu^{2+},[9] Zn^{2+},[10] Hg_2^{2+},[11] Pb^{2+},[12] Ce^{3+}/Eu^{3+}/ Yb^{3+},[13] and UO_2^{2+} [14] (see Figure 1.2 and Table 1.1).

Novel DNAzymes are most often discovered through *in vitro* selection, a combinatorial technique that amplifies sequences with preferred activity in the presence of a target analyte (Figure 1.3). As shown in Table 1.1, the size of the random region used in this method can vary widely, with those shown here falling within the range of 40 to 228 nucleotides.

1.1.2.1 DNAzyme Applications

DNAzymes' simplicity yet functionality have opened the door for a wide variety of applications.[4,5,6] Heavy-metal-ion detection is crucial, whether in the rapid evaluation of environmental (water, soil, or industrial waste) or biological samples (blood, or urine), or the real-time imaging of transition metal ions in living cells. Heavy metal contamination affects people in many locations and occupations, and can be a major source of concern both for those who live in at-risk areas and those who do not wish to.[15] The development of cheap, rapid, robust methods of on-site transition metal ion detection that require only simple operating directions will narrow the gap between awareness and action: people concerned about possible contaminants in their home and surroundings will be able to collect and analyze their own samples. Also, rapid tests to evaluate blood or urine for transition metal ion contamination could decrease the turn-around time for sample processing and subsequent laboratory costs on the clinical level. Finally, transition metal ions have diverse biological roles, and improving the methods by which these ions can be visualized will enhance the level of understanding of their roles in normal and pathological processes.

The original DNAzyme selected by Breaker and Joyce has been developed into a fluorimetric Pb^{2+}-selective sensor 40,000 times more selective for Pb^{2+} than for Zn^{2+}, with a detection limit of 3.7 nM.[16] A single DNAzyme can be used in a broad range of techniques, because a DNAzyme-based sensor's sensing moiety is distinct from its signal-transducing moiety (see Figure 1.4). For example, another Pb^{2+}-dependent DNAzyme, the 8-17 DNAzyme, has been developed into colorimetric,[17] fluorimetric, and electrochemical sensors.[18]

Their thermal and chemical stability, ease of synthesis, cost-effectiveness, and environmentally benignity, have allowed DNAzymes to be used in many different ways; they have been used in lateral-flow ("dipstick") devices,[17] immobilized on electrodes,[18] and incorporated into molecular beacons.[19] The chemical nature of DNAzymes can also be tailored for specific applications. For example, to make a DNAzyme-based sensor more temperature independent, mismatches were introduced between the substrate and enzyme strands.[20]

Label-free sensing with DNAzymes is also possible, either by using the molecular beacon design cited above or by adding a vacant site to the substrate of a DNAzyme. In the vacant site

design, when the DNAzyme's target analyte is not present, the vacant site binds the extrinsic fluorophore 2-amino-5,6,7-trimethyl-1,8-naphthyridine (ATMND) and quenches its fluorescence. When the target analyte is added, the DNAzyme cleaves its substrate, the vacant site is released, and ATMND's fluorescence is recovered. The result is a turn-on sensor. The UO_2^{2+}-dependent DNAzyme 39E and the Pb^{2+}-dependent DNAzyme 17E were recently modified by this method and the resulting sensors had detection limits of 3 nM and 8 nM respectively.[21] A label-free approach can reduce the time and cost of DNA synthesis, and since the technique is generalizable, it is available for all DNAzymes.

1.1.2.2 Structural Characterization of DNAzymes

In contrast to the number of successful DNAzyme applications, attempts to rationally design DNAzymes have been less straightforward. Thus, while DNA can be ordered from any known sequence up to a certain length, there is currently no way to predict the sequence of a DNAzyme with desired properties. Current efforts to understand the structure-function relationships of DNAzymes focus on what is known about metal ions' catalytic capabilities—for example, that they can act as general acid-bases in phosphodiester cleavage, as Lewis acids, or as electrophilic catalysts[22] (see Figure 1.5)--and about the structure of DNAzymes.

A first approximation of the secondary structure of a DNAzyme can be obtained through mfold. Mfold uses thermodynamic considerations to predict the formation of hairpin loops and other common structures.[23] Such insights can be useful when truncating sequences and gaining an overall sense of the relative shape of a DNAzyme.

Circular dichroism (CD) has also been used to study the global folding of DNAzymes. When the activity and general folding of the hammerhead ribozyme and the 8-17 DNAzyme were compared, it was found that the hammerhead ribozyme has a ~10-fold higher dependence on monovalent cations for activity. Additionally, while all monovalent cations tested induced 8-17 to fold, those that enhanced its activity had higher binding affinities. In all cases except Pb^{2+}, the metal ion charge, binding affinity, and enzyme activity were positively correlated, implying that these effects were due to electrostatics. The fact that Pb^{2+} was an exception points to its using a different mechanism to induce activity in 8-17.[24]

Another technique used to interrogate global folding is fluorescence-detected resonance energy (FRET). A FRET-based study of the UO_2^{2+}-dependent DNAzyme 39E was recently carried out.[25] 39E's global folding was found to be highly dependent on the specific metal ions present as well as the overall ionic strength. In the presence of Mg^{2+}, Ca^{2+}, Sr^{2+}, and Zn^{2+}, 39E assumed a compact, nonreactive structure. In the presence of Pb^{2+} and UO_2^{2+}, however, 39E remained unfolded and catalytically active. A lock-and-key mode of catalysis had previously been observed in the Pb^{2+}-dependent 8-17 DNAzyme,[26] and this result shows that this mode also exists in other DNAzymes.

1.2 Research Focus

While DNAzymes are currently being used in a plethora of applications, the bottleneck in the field of DNAzymes is the selection of new sequences. This process can be streamlined by better understanding the structure-function relationships of known DNAzymes so that future selections can be rationally designed. The work described in this thesis involves the investigation of fundamental properties of DNAzymes as well as the attempted selections of new DNAzymes. Chapter 2 examines the effect of peripheral sequences on the selectivity of a family of Co^{2+} -dependent DNAzymes. Chapter 3 describes the attempted selections of Cd^{2+}-, Fe^{2+}-, and Fe^{3+}-dependent DNAzymes, and Chapter 4 presents the insights gained into the Pb^{2+}-dependent 17E DNAzyme's function by substituting nucleotides for $G^{1.1}$ in its conserved core.

1.3 Figures and Tables

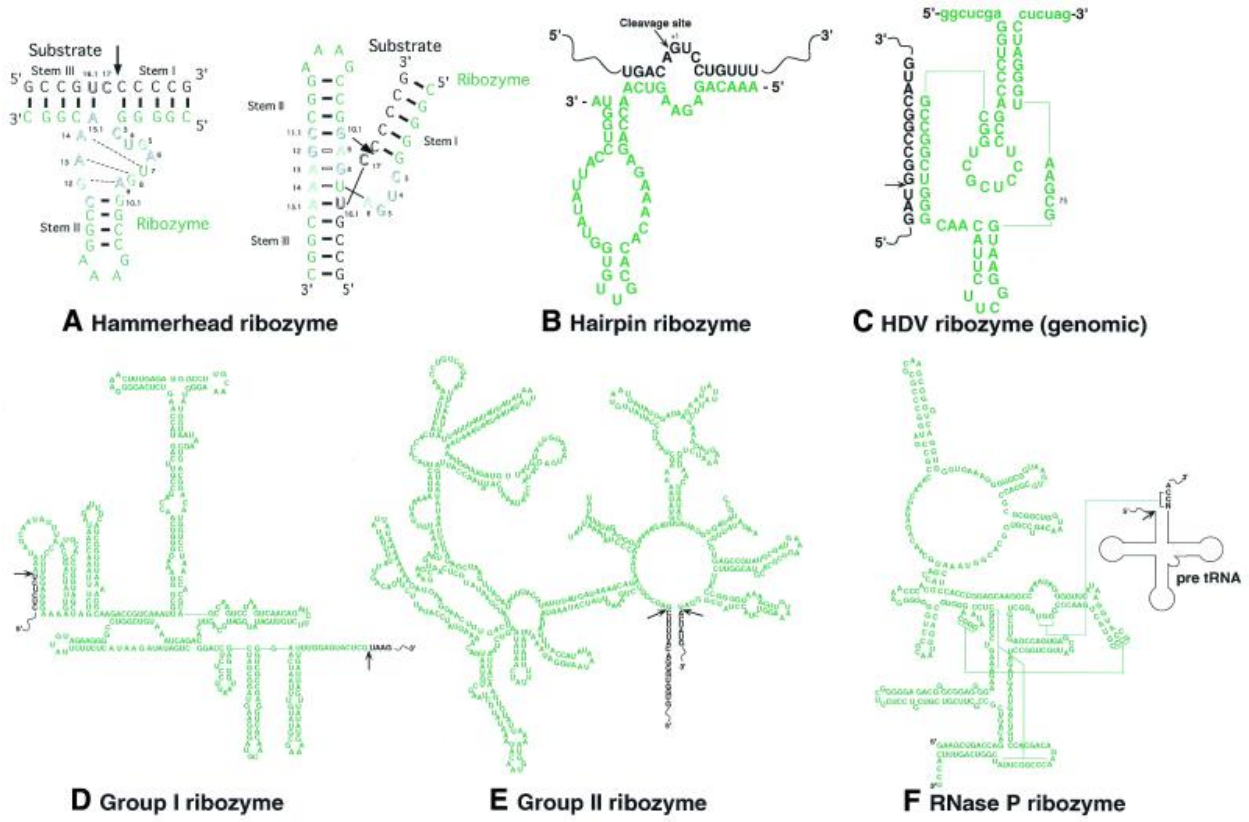

Figure 1.1. Examples of Ribozymes. A) The hammerhead ribozyme. B) The hairpin ribozyme. C) The HDV ribozyme. D) The group I ribozyme. E) The group II ribozyme. F) The RNase P ribozyme. From ref. 22.

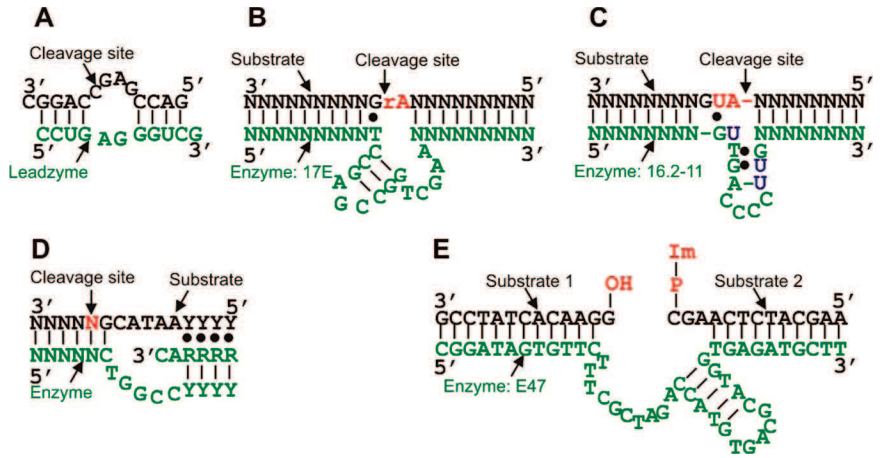

Figure 1.2. Examples of DNAzymes. N denotes any nucleotide. A) The leadzyme: a Pb^{2+}-dependent RNA-cleaving ribozyme. B) The Pb^{2+}-specific 8-17 DNAzyme. C) The Zn^{2+}-dependent DNAzyme. U denotes a C5-imidazole-functionalized deoxyuridine. D) The Cu^{2+}-dependent DNA-cleaving DNAzyme. Y denotes pyrimidine, and R denotes purine. E) The Cu^{2+}-specific DNA ligation DNAzyme. Im denotes an imidazole group. From ref. 5.

Reaction Catalyzed	Cofactor	k_{cat}/k_{uncat}	Random nt.	Bond	Reference
RNA cleavage	Pb^{2+}	~10^5	50	O-P	2
	Mg^{2+}	n.d.	50	O-P	27
	none	~10^8	40	O-P	28
RNA ligation (3'→5' and other)	Zn^{2+}	2 x 10^4	40	O-P	29
RNA ligation (3'→5')	Mg^{2+}	~10^4	40	O-P	30
	Zn^{2+}	~10^5	40	O-P	30
RNA ligation (branch formation)	Mn^{2+}	5 x 10^6	40	O-P	31
	Mg^{2+}	~10^5	40	O-P	32
RNA ligation (lariat formation)	Mn^{2+}	~10^5	40	O-P	33
DNA phosphorylation	Mn^{2+}	~10^9	70	O-P	34
DNA adenylation (capping)	Mg^{2+} + Cu^{2+}	2 x 10^{10}	70	O-P	35
DNA ligation	Cu^{2+} or Zn^{2+}	3 x 10^3	116	O-P	36
	Mn^{2+}	~10^5	150	O-P	37
Nucleopeptide linkage formation	Mg^{2+} or Mn^{2+}	5 x 10^5	40	O-P	38
Oxidative DNA cleavage	Cu^{2+}	~10^6	50	C-O	39
DNA depurination	Ca^{2+}	9 x 10^5	85	C-N	40
DNA depurination (IO_4^- dependent)	none	n.d.	70	C-N	41
Diels-Alder reaction	Ca^{2+}	4 x 10^5	36	C-C	42
Thymine dimer photoreversion	none	3 x 10^4	40	C-C	43
Phosphoramidate cleavage	Mg^{2+}	~10^3	72	N-P	44
Porphyrin metallation	Cu^{2+} or Zn^{2+}	1 x 10^3	228	Cu-N	45

Table 1.1. Some of the DNAzymes obtained by *in vitro* selection. "Random nt." denotes the size of the random region in the selection pool. n.d. denotes "not determined." Adapted from ref. 6.

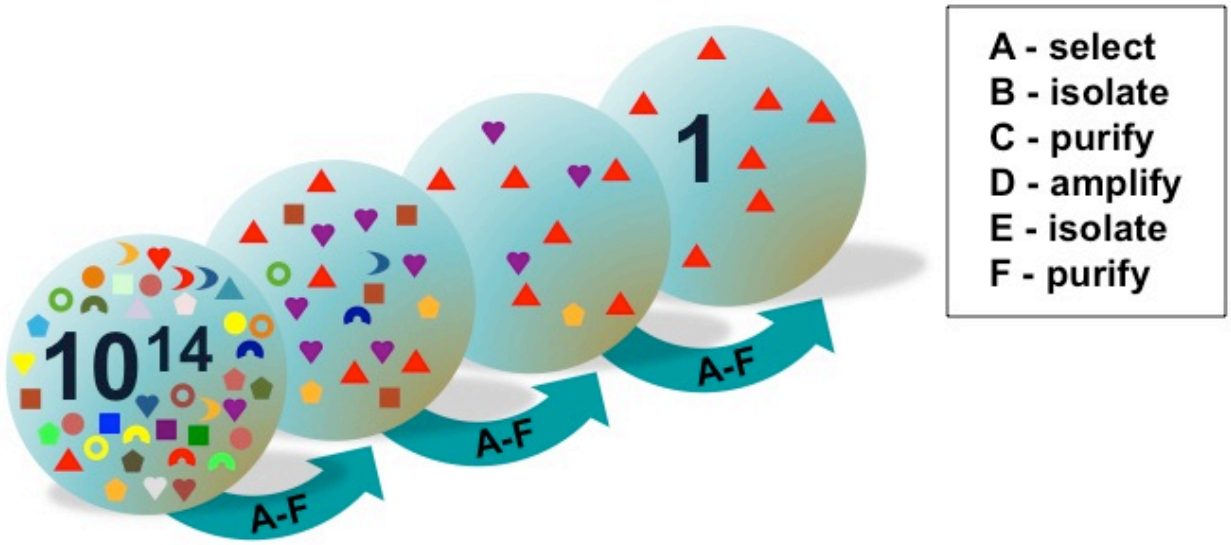

Figure 1.3. *In vitro* selection. A random DNA pool of approximately 10^{14} sequences (the variously colored shapes) is incubated with a selection buffer containing the target analyte, and winners from each round are isolated, purified, amplified, and carried on to the next step. Over time, the winners (the red triangles) are enriched in the pool.

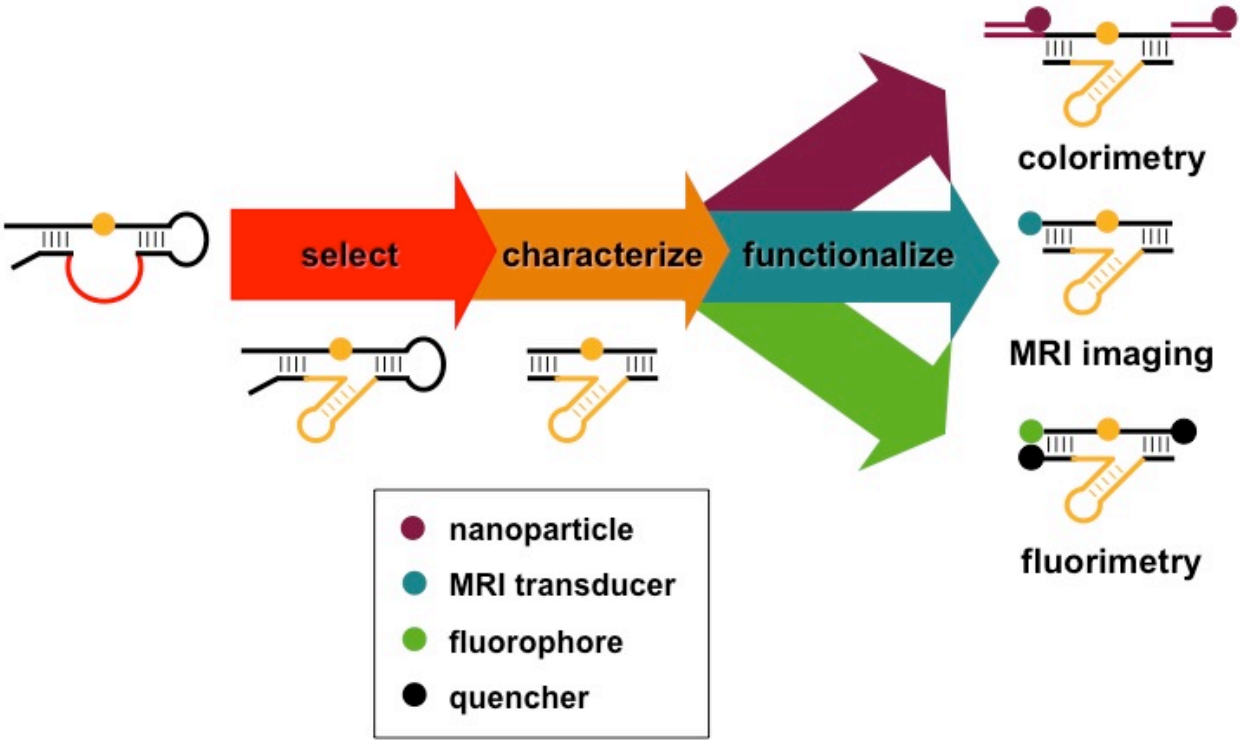

Figure 1.4. The development of DNAzyme-based sensors. The DNAzyme isolated by *in vitro* selection is truncated, transforming the *cis*-cleaving construct into a *trans*-cleaving construct. It can then be further modified for use in one of many different applications. (The modifications are not shown to scale).

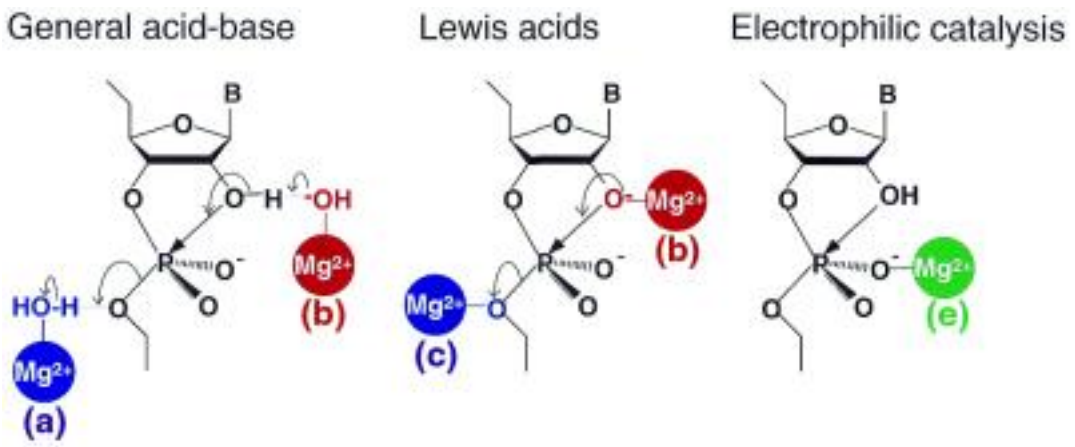

Figure 1.5. Possible catalytic mechanisms for metal ions in the cleavage of a phosphodiester bond. Metal ions can act as a) a general acid catalyst, b) a general base catalyst, c) a Lewis acid that stabilizes the leaving group, d) a Lewis acid that enhances the deprotonation of the attacking nucleophile and e) an electrophilic catalyst that increases the electrophilicity of the phosphorus atom. From ref. 22.

1.4 References

1. Kruger, K.; Grabowski, P.; Zaug, A.; Sands, J.; Gottschling, D.; Cech, T. "Self-Splicing RNA: Autoexcision and Autocyclization of the Ribosomal RNA Intervening Sequence of Tetrahymena." *Cell* **1982**, *31*, 147-157.

2. Breaker, R; Joyce, G. "A DNA Enzyme that Cleaves RNA." *Chem. Biol.* **1994**, *1*, 223–229.

3. Silverman, S. K. "Deoxyribozymes: Selection Design and Serendipity in the Development of DNA Catalysts." *Acc. Chem. Res.* **2009**, *42*, 1521-1531.

4. a) Sun, L. Q.; Cairns, M. J.; Saravolac, E. G.; Baker, A.; Gerlach, W. L. "Catalytic Nucleic Acids: From Lab to Applications." *Pharmacol. Rev.*, **2000**, *52*, 325-347. b) Emilsson, G. M.; Breaker, R. R. "Deoxyribozymes: New Activities and New Applications." *Cell. Mol. Life Sci.* **2002**, *59*, 596-607. c) Silverman, S. "Catalytic DNA (Deoxyribozymes) for Synthetic Applications: Current Abilities and Future Prospects." *Chem. Comm.* **2008**, *30*, 3467–3485. d) Zhang, X.-B.; Wang, Z.; Xing, H.; Xiang, Y.; Lu, Y. "Catalytic and Molecular Beacons for Amplified Detection of Metal Ions and Organic Molecules with High Sensitivity." *Anal. Chem.* **2010**, *82*, 5005-5011. e) Silverman, S. K. "DNA as a Versatile Chemical Component for Catalysis, Encoding, and Stereocontrol." *Angew. Chem.* **2010**, *122*, 7336–7359. *Angew. Chem. Int. Ed.* **2010**, *49*, 7180-7201. f) Nagraj, N.; Lu, Y. "Catalytic Nucleic Acid Biosensors for Environmental Monitoring" in "Nucleic Acid Biosensors for Environmental Pollution Monitoring," Ilaria Palchetti, Marco Mascini, eds.; Royal Society of Chemistry; pp. 82-98 (2011). g) Zhang, X.-B.; Kong, R.-M.; Lu, Y. "Metal Ion Sensors Based on DNAzymes and Related DNA Molecules." *Annu. Rev. Anal. Chem.* **2011**, *4*, 105-128. h) Lan, T.; Lu, Y. "Metal Ion-Dependent DNAzymes and Their Applications as Biosensors" in "Interplay between Metal Ions and Nucleic Acids," Metal Ions in Life Sciences, Vol. 10, Astrid Sigel, Helmut Sigel, Roland K. O. Sigel, eds.; Springer Netherlands; pp. 217-248 (2012).

[5] Liu, J.; Cao, Z.; Lu, Y. "Functional Nucleic Acid Sensors." *Chem. Rev.* **2009**, *109*, 1948-1998.

[6] Baum, D. A.; Silverman, S. K. "Deoxyribozymes: Useful DNA Catalysts *In Vitro* and *In Vivo*." *Cell. Mol. Life Sci.* **2008**, *54*, 2156-2174.

7. Feldman, A.; Sen, D. "A New and Efficient DNA Enzyme for the Sequence-specific Cleavage of RNA." *J. Mol. Biol.* **2001**, *313*, 283-294.

8. a) Bruesehoff, P. J.; Li, J.; Augustine III, A. J.; Lu, Y. "Improving Metal Ion Specificity During In Vitro Selection of Catalytic DNA." *Comb. Chem. High Throughput Screening* **2002**, *5*, 327–335. b) Liu, Z.; Mei, S. H. J.; Brennan, J. D.; Li, Y. "Assemblage of Signaling DNA Enzymes with Intriguing Metal-Ion Specificities and pH Dependences." *J. Am. Chem. Soc.* **2003**, *125*, 7539–7545.

9. Liu, J.; Lu, Y. "Colorimetric Cu^{2+} Detection with a Ligation DNAzyme and Nanoparticles." *Chem. Comm.* **2007**, 4972-4974.

10. Nelson, K.; Bruesehoff, P.; Lu, Y. "*In Vitro* Selection of High Temperature Zn^{2+}-Dependent DNAzymes." *J. Mol. Evol.* **2005,** *61*, 216-225.

11. Thomas, J.; Ting, R.; Perrin, D. "High Affinity DNAzyme-Based Ligands for Transition Metal Cations–A Prototype Sensor for Hg^{2+}." *Org. Biomol. Chem.* **2004**, *2*, 307-312. b) Hollenstein, M.; Hipolito, C.; Lam, C.; Dietrich, D.; Perrin, D. "A Highly Selective DNAzyme Sensor for Mercuric Ions." *Angew. Chem.* **2008**, *120*, 4418-4422. *Angew. Chem. Int. Ed.*, **2008**, *47*, 4346-4350. c) Liu, J.; Lu, L. "Rational Design of 'Turn-On' Allosteric DNAzyme Catalytic Beacons for Aqueous Mercury Ions with Ultrahigh Sensitivity and Selectivity." *Angew. Chem. Int. Ed.* **2007**, *46*, 7587 –7590.

12. Brown, A.; Li, J.; Pavot, C.; Lu, Y. “A Lead-Dependent DNAzyme with a Two-Step Mechanism.” *Biochemistry* **2003**, *42,* 7152-7161.

13. Dokukin, V.; Silverman, S. "Lanthanide Ions as Required Cofactors for DNA Catalysts." *Chem. Sci.*, **2012**, *3*, 1707-1714.

14. a) Brown, A. K.; Liu, J.; Lu, Y. "Biochemical Characterization of a Uranyl Ion-Specific DNAzyme." *ChemBioChem* **2009**, *10*, 486-492. b) Liu, J.; Brown, A.; Meng, X.; Cropek, D.; Istok, J.; Watson, D. Lu, Y. “A catalytic beacon sensor for uranium with parts-per-trillion sensitivity and millionfold selectivity.” *PNAS*, **2007**, *104*, 2056-2061.

15. Weber, O.; Scholz, R.; Bühlmann, R.; Grasmück, D. *Risk Analysis*, **2001**, *21,* 967-977.

16. Lan, T.; Furuya, K.; Lu, Y. "A Highly Selective Lead Sensor Based on a Classic Lead DNAzyme." *Chem. Commun*. **2010**, *46*, 3896-3898.

17. Mazumdar, D.; Liu, J.; Lu, G.; Zhou, J.; Lu, Y. "Easy-to-Use Dipstick Tests for Detection of Lead in Paints Using Non-Cross-Linked Gold Nanoparticle-DNAzyme Conjugates." *Chem. Comm.* **2010**, *46*, 1416-1418.

18. Xiao, Y.; Rowe, A.; Plaxco, K. "Electrochemical Detection of Parts-Per-Billion Lead via an Electrode-Bound DNAzyme Assembly." *J. Am. Chem. Soc.* **2007**, *129*, 262-263.

19. Song, P.; Xiang, Y.; Xing, H.; Zhou, Z.; Tong, A.; Lu, Y. "Label-Free Catalytic and Molecular Beacon Containing an Abasic Site for Sensitive Fluorescent Detection of Small Inorganic and Organic Molecules." *Anal. Chem.* **2012**, *84*, 2916-2922.

20. Nagraj, N.; Liu, J.; Sterling, S.; Wu, J.; Lu, Y. "DNAzyme Catalytic Beacon Sensors that Resist Temperature-Dependent Variations." *Chem. Commun.* **2009**, 4103-4105.

21. Xiang, Y.; Wang, Z.; Xing, H.; Wong, N. Y.; Lu, Y. "Label-Free Fluorescent Functional DNA Sensors Using Unmodified DNA: A Vacant Site Approach." *Anal. Chem.* **2010**, *82*, 4122-4129.

22. Takagi, Y.; Warashina, M.; Stec, W. J.; Yoshinari, K.; Taira, K. "Recent Advances in the Elucidation of the Mechanisms of Action of Ribozymes." *Nucleic Acids Res.* **2001**, *29*, 1815-1834.

23. Zuker, M. “Mfold Web Server for Nucleic Acid Folding and Hybridization Prediction.” *Nucleic Acids Res.* **2003**, *31*, 3406–3415.

24. Mazumdar, D.; Nagraj, N.; Kim, H.-K.; Meng, X.; Brown, A.; Sun, Q.; Li, W.; Lu, Y. "Activity, Folding and Z-DNA Formation of the 8-17 DNAzyme in the Presence of Monovalent Ions." *J. Am. Chem. Soc.* **2009**, *131*, 5506–5515.

25. He, Y.; Lu, Y. "Metal-Ion-Dependent Folding of a Uranyl-Specific DNAzyme: Insight into Function from Fluorescence Resonance Energy Transfer Studies." *Chem.-Eur. J.* **2011**, *17*, 13732-13742.

26. a) Liu, Y.; Sen, D. "A Contact Photo-Cross-linking Investigation of the Active Site of the 8-17 Deoxyribozyme." *J. Mol. Bio.* **2008**, *381*, 845-859. b) Liu, Y.; Sen, D. "Local Rather than Global Folding Enables the Lead-dependent Activity of the 8-17 Deoxyribozyme: Evidence from Contact Photo-crosslinking." *J. Mol. Biol.* **2010**, *395*, 234-241.

27. Santoro, S. W.; Joyce, G. F. “A General Purpose RNA-Cleaving DNA Enzyme.” *Proc. Natl. Acad. Sci. U. S. A.* **1997**, *94*, 4262-4266.

28. Geyer, C. R.; Sen, D. "Evidence for the Metalcofactor Independence of an RNA Phosphodiester-Cleaving DNA Enzyme." *Chem. Biol.* **1997**, *4*, 579-593.

29. Hoadley, K. A., Purtha, W. E., Wolf, A. C., Flynn-Charlebois, A.; Silverman, S. K. "Zn^{2+}-Dependent Deoxyribozymes that Form Natural and Unnatural RNA Linkages." *Biochemistry* **2005**, *44*, 9217-9231.

30. Purtha, W. E., Coppins, R. L., Smalley, M. K.; Silverman, S. K. "General Deoxyribozyme-Catalyzed Synthesis of Native 3'–5' RNA Linkages." *J. Am. Chem. Soc.* **2005**, *127*, 13124-13125.

31. a) Wang, Y.; Silverman, S. K. "Deoxyribozymes that Synthesize Branched and Lariat RNA." *J. Am. Chem. Soc.* **2003**, *125*, 6880-6881. b) Wang, Y.; Silverman, S. K. "Characterization of Deoxyribozymes that Synthesize Branched RNA." *Biochemistry* **2003**, *42*, 15252-15263.

32. a) Coppins, R. L.; Silverman, S. K. "A DNA Enzyme that Mimics the First Step of RNA Splicing." *Nat. Struct. Mol. Biol.* **2004**, *11*, 270-274. b) Coppins, R. L.; Silverman, S. K. "A Deoxyribozyme that Forms a Three-Helix-Junction Complex with Its RNA Substrates and Has General RNA Branch-Forming Activity." *J. Am. Chem. Soc.* **2005**, *127*, 2900-2907.

33. a) Pratico, E. D.; Wang, Y.; Silverman, S. K. "A Deoxyribozyme that Synthesizes 2',5'-Branched RNA with any Branch-Site Nucleotide." *Nucleic Acids Res.* **2005**, *33*, 3503-3512. b) Wang, Y.; Silverman, S. K. "Efficient One-Step Synthesis of Biologically Related Lariat RNAs by a Deoxyribozyme." *Angew. Chem.* **2005**, *117*, 6013-6016. *Angew. Chem. Int. Ed.* **2005**, *44*, 5863-5866.

34. Wang, W.; Billen, L. P.; Li, Y. “Sequence Diversity, Metal Specificity, and Catalytic Proficiency of Metal-Dependent Phosphorylating DNA Enzymes.” *Chem. Biol.* **2002**, *9*, 507-517.

35. Li, Y.; Liu, Y.; Breaker, R. R. “Capping DNA with DNA.” *Biochemistry* **2000**, *39*, 3106-3114.

36. Cuenoud, B.; Szostak, J. W. “A DNA Metalloenzyme with DNA Ligase Activity.” *Nature* **1995**, *375*, 611-614.

37. Sreedhara, A.; Li, Y.; Breaker, R. R. “Ligating DNA with DNA.” *J. Am. Chem. Soc.* **2004**, *126*, 3454-3460.

38. Pradeepkumar, P. I.; Höbartner, C.; Baum, D. A.; Silverman, S. K. “DNA-Catalyzed Formation of Nucleopeptide Linkages.” *Angew. Chem.* **2008**, *120*, 1777-1781. *Angew. Chem. Int. Ed.* **2008**, *47*, 1753-1757.

39. a) Carmi, N.; Shultz, L. A.; Breaker, R. R. “*In Vitro* Selection of Self-Cleaving DNAs.” *Chem. Biol.* **1996**, *3*, 1039-1046. b) Carmi, N.; Balkhi, S. R.; Breaker, R. R. “Cleaving DNA with DNA.” *Proc. Natl. Acad. Sci. U. S. A.* **1998**, *95*, 2233-2237. c) Carmi, N.; Breaker, R. R. “Characterization of a DNA-Cleaving Deoxyribozyme.” *Bioorg. Med. Chem.* **2001**, *9*, 2589-2600.

40. Sheppard, T. L.; Ordoukhanian, P.; Joyce, G. F. “A DNA Enzyme with *N*-Glycosylase Activity.” *Proc. Natl. Acad. Sci. U. S. A.* **2000**, *97*, 7802-7807.

41. Höbartner, C.; Pradeepkumar, P. I.; Silverman, S. K. “Site-Selective Depurination by a Periodate-Dependent Deoxyribozyme. *Chem. Commun.* **2007**, 2255-2257.

42. Chandra, M.; Silverman, S. K. “DNA and RNA can be Equally Efficient Catalysts for Carbon-Carbon Bond Formation.” *J. Am. Chem. Soc.* **2008**, *130*, 2936-2937.

43. Chinnapen, D. J.; Sen, D. “A Deoxyribozyme that Harnesses Light to Repair Thymine Dimers in DNA.” *Proc. Natl. Acad. Sci. U. S. A.* **2004**, *101*, 65-69.

44. Burmeister, J.; von Kiedrowski, G.; Ellington, A. D. “Cofactor-Assisted Self-Cleavage in DNA Libraries with a 3'-5' Phosphoramidate Bond.” *Angew. Chem.* **1997**, *109*, 1379-1381. *Angew. Chem. Int. Ed.* **1997**, *36*, 1321-1324.

45. a) Li, Y.; Sen, D. “A Catalytic DNA for Porphyrin Metallation.” *Nat. Struct. Biol.* **1996**, *3*, 743-747. b) Li, Y.; Sen, D. “Toward an Efficient DNAzyme.” *Biochemistry* **1997**, *36*, 5589-5599.

Chapter 2: Peripheral Sequences' Effects on the Selectivity and Activity of Co^{2+}-Dependent DNAzymes

2.1 Note and Acknowledgments

This work was done in direct collaboration with Dr. Kevin Nelson. Dr. Peter Bruesehoff performed the initial *in-vitro* selection of the DNAzyme, and subsequent characterizations were performed by Debapriya Mazumdar. This chapter is the basis for a published manuscript: Dr. Kevin E. Nelson, Hannah E. Ihms, Dr. Debapriya Mazumdar, Dr. Peter Bruesehoff, Prof. Yi Lu. "The Importance of Peripheral Sequences in Determining the Metal Selectivity of an *In Vitro*-Selected Co^{2+}-Dependent DNAzyme." *ChemBioChem* **2012**, *13*, 381-391.

2.2 Introduction

DNAzymes are catalytically active DNA molecules that use metal cofactors for their enzymatic functions. While a growing number of DNAzymes with diverse functions and metal selectivities have been reported, the relationships between metal-ion selectivity, conserved sequences and structures responsible for selectivity remain to be elucidated. To address this issue, we report biochemical assays of a family of previously reported *in-vitro*-selected DNAzymes. This family includes the Clone 11 DNAzyme, which was isolated by positive and negative selection, and the Clone 18 DNAzyme, which was isolated by positive selection alone. The Clone 11 DNAzyme has a higher selectivity for Co^{2+} over Pb^{2+} compared with Clone 18. The reasons for this difference are explored here through phylogenetic comparison, mutational analysis and stepwise truncation. A novel DNAzyme truncation method incorporated a nick in the middle of the DNAzyme to allow for truncation close to the nicked site while preserving peripheral sequences at both ends of the DNAzyme. The results demonstrate that peripheral sequences within the substrate binding arms, most notably the stem loop, Loop II, are sufficient to restore its selectivity for Co^{2+} over Pb^{2+} to levels observed in Clone 11. A comparison of these sequences' secondary structures and Co^{2+} selectivities suggested that metastable structures affect metal ion selectivity. The Co^{2+} selectivity of the Clone 11 DNAzyme showed that the metal ion binding and selectivities of small, *in-vitro*-selected DNAzymes may be more complex than previously appreciated, and that Clone 11 may be more similar to larger ribozymes than to other small DNAzymes in its structural complexity and behavior. These factors should be taken

into account when metal-ion selectivity is required in rationally designed DNAzymes and DNAzyme-based biosensors.

The discovery of the first catalytic DNA molecule (also called a DNAzyme or deoxyribozyme) settled a fundamental question: whether DNA, from a four-letter alphabet of building blocks lacking the 2'-hydroxyl present in RNA, could form sufficiently complex secondary and tertiary structures to achieve DNA catalysis. Since 1994, when the first DNAzyme was isolated through *in vitro* selection,[1] many DNAzymes with significant rate enhancements over uncatalyzed reactions, high substrate selectivities, and diverse catalytic functions have been isolated; they have also been shown to have potential as pharmaceutical drugs, sensors, and logic gate mathematical regulators.[2] In contrast to the significant advances in isolating and applying DNAzymes, the understanding of the structure–function relationships of these DNAzymes is progressing much more slowly. Understanding these relationships will enrich our knowledge of chemical biology and nucleic acid biochemistry, and will, in turn, produce more customizable DNAzymes for practical applications.

DNAzymes have been shown to selectively recruit metal ions to perform diverse functions similar to those performed by protein and RNA enzymes. For example, the 8-17 RNA-cleaving DNAzyme[3-5] is more than 100 times more selective for Pb^{2+} than for any other metal ion. In addition, a number of DNAzymes with high selectivities for Co^{2+},[6,7] Cu^{2+},[8] Hg^{2+},[9,10] Mg^{2+},[4] Mn^{2+},[7] Pb^{2+},[1] Zn^{2+},[5,11] and porphyrins[12] have been reported. Finally, a recently selected DNAzyme has selectivity for UO_2^{2+} that is a million-fold higher than for other metal ions.[13, 14] These high metal ion selectivities have established DNAzymes as a new class of efficient metal ion sensors,[9,13,15] with detection limits as low as 45 pM or 11 ppt.[13]

In contrast to metalloprotein enzymes, and to a certain degree even ribozymes,[16] relatively little is known about the factors that determine DNAzymes' metal-ion selectivities. This is because no three-dimensional structure of a DNAzyme in an active conformation has yet been reported. To address this issue, studies on the interactions between DNA and inorganic metal complexes,[17] and between nucleotides and metal ions[18] have provided insights into ligand preferences and ligand geometries in larger nucleic acid strands. Metal ions are essential for the folding and optimal activity of almost all reported DNAzymes, and divalent metal ions

have been implicated as direct participants in catalysis. Metal ions have also been reported to affect the tertiary structures and mechanisms of DNAzymes and ribozymes.[19–21] An improved understanding of the process by which metalloenzymes selectively bind metal ions will be invaluable to engineer DNAzymes with high activity and selectivity for use as biosensors.

A primary example of the challenge in understanding metal ion selectivity is finding metalloenzymes that can differentiate Co^{2+} from Zn^{2+}. Not only do these metal ions have identical charges, they also have nearly identical ionic radii and ligand donor set preferences.[22] Therefore, designing a molecule with high selectivity for Co^{2+} over Zn^{2+} is very difficult. In fact, although metalloproteins are known to bind metal ions with high selectivity, most Zn^{2+}-binding proteins can bind Co^{2+} with almost 100% activity. The problem of selectivity is further compounded for RNA-cleaving DNAzymes because of the background hydrolytic activity of Zn^{2+} and Co^{2+}.[23] To find molecules that differentiate between these two metal ions, we previously performed *in vitro* selection centered on phosphodiester cleavage. We used a negative-selection approach to obtain DNAzymes more selective for Co^{2+} over Zn^{2+} and Pb^{2+}.[6] Two alternative selection methods were carried out to isolate Co^{2+}-selective sequences. Selection 1 resulted in a DNAzyme population that was active in the presence of Co^{2+}, but was also active in the presence of Zn^{2+} and Pb^{2+}. To address this limitation, Selection 2 incorporated several rounds of negative selection to increase the Co^{2+} selectivity by removing DNAzymes active in the presence of Zn^{2+} and Pb^{2+}. This negative selection approach produced a population with increased selectivity for Co^{2+} over both Zn^{2+} and Pb^{2+}. Several of the sequences obtained in these selections are shown in Figure 2.1A. The Clone 11 DNAzyme, isolated during Selection 2, was the most selective for Co^{2+}(Co:Zn 1.6, Co:Pb 4.5) and had the highest activity (k_{obs} 0.18 min^{-1}) of all of the DNAzymes isolated by either selection method. Clone 11's sequence was similar to that of Clone 18, a DNAzyme isolated by Selection 1. By using mfold to predict the secondary structures,[24] Clone 11 was found to have two putative secondary structures: 11A and 11B (Figure 2.1B). While the secondary structures of 11A and Clone 18 were identical, Clone 18 had poor Co^{2+} selectivity and only moderate activity (k_{obs} 0.044 min^{-1}). Interestingly, a comparison of Clones 11 and 18 showed that only four different nucleotides, C72, T77, T78 and T80 (Figure 2.1B), decreased the Co^{2+} selectivity nearly eightfold (Table 2.1). It was hypothesized, then, that

Clone 11's enhanced selectivity and activity resulted from the 11B secondary structure.

To elucidate the relationship between Co^{2+} selectivity and DNAzyme sequence and structure in these systems, phylogenetic comparison, mutational analysis and stepwise truncation were performed. We found that peripheral sequences elements enhanced the activity and Co^{2+} selectivity of Clone 11, and that metastable structures might also play a role.

2.3 Materials and Methods

2.3.1 Materials

NaCl, $CoCl_2$, $ZnCl_2$ and $Pb(CH_3COO)_2$ were purchased from Alfa Aesar at puratronic grade (99.998% or greater purity, metals basis). HPLC-purified DNA oligonucleotides were purchased from Integrated DNA Technologies. Additional DNA-RNA chimeric oligomers were purchased from TriLink Biotechnologies and were purified by the company unless otherwise indicated. HEPES was purchased from Sigma–Aldrich. All buffers were treated with Chelex 100 (Sigma–Aldrich) to remove divalent metal ions. The radiolabeling of DNA-chimeric substrates was carried out using redivue [γ-^{32}P]-ATP (Amersham Biosciences) and T4 polynucleotide kinase (Invitrogen).

2.3.2 Artificial Phylogenetic Analysis and Design of Clone 11 Constructs

The sequences used in the alignment, including Clone 11 and 18, were derived from previously described *in vitro* selection experiments.[6] Sequence alignments of sequences from Selections 1 and 2 were constructed using the MultAlin folding program.[57] Highly conserved sequences have greater than 90% consensus, moderately conserved sequences have between 50% and 90% consensus, and nonconserved sequences have less than 50% consensus.

The design of constructs for the Co^{2+} selectivity studies was based on the sequence and structure of Clone 11, Clone 18 or the 11B-*trans*-cleaving construct (11B-*trans*), as predicted by the mfold DNA folding algorithm.[24] Oligonucleotides were purchased from Integrated DNA Technologies. Mutations were introduced at key locations as determined by factors such as the alignment of Selection 1 and 2 sequences, previously tested truncations, attempts to minimize self-complementarity among enzyme and substrate strands, or attempts to stabilize or destabilize secondary structures predicted for *trans*-cleaving Clone 11 constructs. The 11B-*trans*

construct was designed by truncating nucleotides 1–15, 38–43, and 78–107. Alternative truncation strategies were developed to investigate the Co^{2+} selectivity. Truncated constructs were designed that retained nucleotides 38–43 while truncating positions 1–15 and 78–107 to various degrees. An additional strategy was developed that placed a single nick at one of two locations within the 5'-substrate-binding arm of Clone 11. Mutations were made that retained the predicted secondary structure and activity of Clone 11 and stabilized the formation of the nicked helix. Additional truncated "nicked" constructs were designed that contained nucleotides 1–15 and 78–107 to various degrees (Clone 11 numbering). The sequences of all constructs tested are shown in Figure 2.3A.

2.3.3 Kinetic Assays

The kinetics of the cleavage of *cis*- and *trans*-constructs at a single riboadenosine was monitored by a radioactive assay. Preparation of ^{32}P-radiolabeled DNA substrates for assays was carried out as follows: the DNA substrate or *cis*-cleaving construct (20 pmol), [γ-^{32}P]-ATP (Amersham, 0.3 mM), and T4 polynucleotide kinase (1.25 U/μL) were heated at 37 °C for 45 min. in a reaction mixture that contained Tris·HCl (70 mM, pH 7.6), KCl (0.1 M), $MgCl_2$ (10 mM), and 2-mercaptoethanol (1 mM). The labeled product was then desalted using a Sep-Pak Plus C-18 cartridge, flash frozen, and lyophilized. DNA samples were prepared at twice the final concentration in HEPES buffer (50 mM, pH 7.0) with NaCl (500 mM). The NaCl concentration was chosen because the Co^{2+}-dependent activity begins to plateau at 300 mM NaCl (Bruesehoff and Lu, unpublished data). Reactions were performed under single-turnover conditions using a DNAzyme (1 μM) and its ^{32}P-radiolabeled substrate (30 nM), where the concentrations listed are the final concentrations. Samples were annealed by heating to 95 °C for 3 min., then cooling to ambient temperature over 15 min. Each reaction was initiated by adding an equal volume of $CoCl_2$, $ZnCl_2$, or $Pb(CH_3COO)_2$ to the DNAzyme solution. Aliquots (5 μL) were removed periodically and transferred to stop buffer (10 μL) containing urea (8 M) and EDTA (50 mM). Samples were then separated on a 20% polyacrylamide gel and exposed to a storage phosphorscreen (Molecular Dynamics). Gels were analyzed by scanning the storage phosphorscreen on a Storm 840 phosphorimager (Molecular Dynamics). The cleavage efficiency was calculated at time *t* using the following equation: $y = 100 * [I_c / (I_u + I_c)]$, where *y* is the

percent cleaved product, I_c is the intensity of the cleaved substrate and I_u is the intensity of the uncleaved substrate. Pseudo-first-order rate constants were determined by fitting an equation of the form $y = y_o + a\,(1 - e^{-kt})$ to the data using SigmaPlot 8.0, where y is the percent cleaved product as a function of time t, y_o is the background product at time $t = 0$, a is the fraction of the pool cleaved at time $t = 1$, and k is the observed rate constant.

2.4 Results

2.4.1 Artificial Phylogenetic Analysis

To trace selectivity differences between the Clone 11 and Clone 18 DNAzymes, artificial phylogenetic analysis was performed for the sequences obtained from Selections 1 and 2.[6] We sought to test the premise that sequences showing similar metal selectivities would also show similar structural characteristics. A similar approach had been used in the early RNA secondary structure predictions (phylogenetic analysis and the hypothesis that RNAs with similar functions but different species of origin have similar structures).[25]

The artificial phylogenetic analysis used six sequences from Selection 1 and 15 sequences from Selection 2 (Figure 2.1A). These sequences were chosen based on the similarities between Clone 11 and Clone 18. Within the region randomized for selection, a highly conserved region from positions 53 to 70 was apparent, while nucleotides 71–86 showed considerable variability. By superimposing the sequence alignment in Figure 2.1A onto the active secondary structure of the Co^{2+}-selective Clone 11 DNAzyme, we showed that the highly conserved region between 53 to 70 helps form the 5'-substrate-binding arm, stem loop I, and the 3'-substrate-binding arm (Figure 2.1B). The more variable region (positions 71–86) coincides with the corresponding terminal 3'-substrate-binding arm that contains Loop IV and the adjacent 3'-single-stranded region. Surprisingly, the four positions that distinguish Clone 11from 18 (positions 72, 77, 78, and 80) show the highest variability. The variability at these positions was unexpected, because sequence or structural motifs that increase selectivity were expected to be highly conserved. The sequence variability at positions 72 and 73 suggests that Loop IV helps increase Co^{2+} selectivity. The short helical region distal to Loop IV contains T77, which may also play a role in Co^{2+} selectivity. While T78 and T80 are part of a region predicted to be unstructured, they may participate in tertiary interactions affecting Co^{2+} selectivity.

2.4.2 Stepwise Truncation of Peripheral Sequence Elements

Next, the effect of peripheral sequences on Co^{2+} selectivity was investigated by truncating the Clone 11 DNAzyme. After *in vitro* selection, constructs have been routinely truncated to contain only mfold-predicted secondary structures of interest. The *cis*-cleaving Clone 11 DNAzyme was truncated to the 11B *trans*-cleaving construct (11B-*trans*) based on the 11B-type active secondary structure (Figure 2.2A). Interestingly, truncation of the 5'- and 3'-peripheral sequences resulted in another predicted secondary structure (11B', Figure 2.2A) that resembled neither that of Clone 11 nor that of Clone 18. 11B' retained the base pairing within both substrate binding arms but had disruptions at stem loop I and at the base pairs at the cleavage site. Co:Pb selectivity of the truncated 11B-*trans* construct was four times less than that of Clone 11 (Table 2.1), and its Co:Zn selectivity was three times lower (Table 2.1). The distal 5'- and 3'-sequence elements (nucleotides 1–15 and 78–107) that are adjacent to the 3' substrate-binding-arm can be thought of as “peripheral”, but might also be integral to selectivity: the decrease in Co^{2+} selectivity might have been due to the deletion of portions of these regions.

As the large-scale truncation described above decreased the Co^{2+} selectivity, a systematic truncation approach was adopted to find which regions were responsible for the decreased selectivity. Short peripheral sequence elements were systematically deleted from the enzyme and substrate strands of Clone 11 (Figure 2.2B). This produced a series of *trans*-cleaving enzyme and substrate strands of various lengths, and every possible combination of enzyme and substrate strand was constructed and assayed for Co^{2+} selectivity. All truncated constructs were most active in the presence of Zn^{2+} and were less selective for Co^{2+} than Clone 11 (Table 2.2). Of the Co^{2+}, Zn^{2+}, and Pb^{2+} selectivities, the Co^{2+}-dependent activity typically showed the greatest decrease: Co:Zn selectivities decreased as much as 32-fold and Co:Pb selectivities decreased nearly 40-fold. These changes in Co^{2+} selectivity were surprising for the sequences that retained C72, T77, T78, and T80 (the four nucleotides that distinguish Clone 11 and Clone 18). Deleting only Loop II from Clone 11 produced a full-length, *trans*-cleaving Clone 11 variant that also had reduced Co^{2+} selectivity. There are several possible explanations for this. First, the mfold-predicted structures could be incorrect. However, the introduction of

point mutations (data not shown) and the activity of the *trans*-cleaving constructs designed by mfold support the mfold-derived Clone 11 structures. Another possibility is that interstrand secondary structure forms between the enzyme and substrates of the Loop II deletion constructs. Alternatively, the *trans*-cleaving configuration might inhibit formation of a selective Co^{2+} binding pocket, as Clone 11 was selected as a *cis*-cleaving DNAzyme. The results of the stepwise truncation prompted alternative truncation strategies, to investigate the role that Loop II and other peripheral sequences play in determining the Co^{2+} selectivity of Clone 11.

2.4.3 Alternative Truncation Strategies

Investigating the influence of peripheral sequences on Co^{2+} selectivity required sequences with Loop II intact ; therefore, alternatives to conventional DNAzyme truncation strategies[4, 5, 26] were developed. *Cis*-cleaving constructs with peripheral sequence truncations had poor Co^{2+} selectivities and were difficult to synthesize because of their length (>100 nucleotides) and embedded ribonucleotide. Instead, novel *trans*-cleaving constructs (Figure 2.3A) were designed to provide a platform preserving Loop II while testing the peripheral sequence elements' contributions to Co^{2+} selectivity. This platform placed a nick in the 5'-substrate-binding arm and incorporated Loop II as a terminal stem loop on either the enzyme or substrate strand. As shown in Figure 2.3A, "nicked" constructs were designed on the basis of mfold analysis, to choose sequences that 1) preserved the 11B-type secondary structure of Clone 11, 2) retained the primary sequence of the conserved Loop 1 region (nucleotides 51–66), and 3) retained substrate binding arm base-pairing. Criterion 2 was based on the results of the artificial phylogenetic analysis. In addition, preliminary mutational analysis showed that helical regions of the substrate binding arms were mutation tolerant and that Loops I and III were mutation intolerant (data not shown). Mutations in the substrate binding arms preserved substrate recognition in the 5'-substrate-binding arm and reduced the self-complementarity of the enzyme and substrate strands. During the design process, the 5'-substrate-binding arm was also lengthened by one base pair, converting the sixbase Loop II into a tetraloop. The additional base pair and tetraloop allowed the helical region of the terminal stem loop to participate in substrate recognition in the 5'-substrate-binding arm. The sequences of constructs designed for the truncation study are shown in Figure 2.3A.

Constructs 11BNick1–4, which were generated by this method, differ only in their substrate-binding arms; they contain no peripheral sequences and are predicted to form the 11B-type secondary structure. In addition, 11BNick1, 11BNick2, and 11BNick 4 were predicted to form the 11B'-type structure. Two additional constructs, 11BNick5 and 11BNick6, were designed to incorporate basepairs in place of Loop IV. 11BNick6 also has peripheral sequences (nucleotides 77–81) appended. Each nicked construct containing Loop II was tested for Co^{2+} selectivity (Table 2.3). 11BNick1 (Co:Zn 0.56 ± 0.15, Co:Pb 0.55 ± 0.16), 11BNick5 (Co:Zn 0.67 ± 0.11, Co:Pb 1.1 ± 0.3), and 11BNick6 (Co:Zn 0.64 ± 0.03, Co:Pb 1.1 ± 0.3) showed no improvement in Co^{2+} selectivity. Constructs 11BNick3 and 11BNick4 showed an increased preference for Co^{2+} over Pb^{2+}(Co:Pb 11BNick3 1.7-fold, 11BNick4 1.5-fold). In contrast, 11BNick2 showed an increased Co^{2+} selectivity over Zn^{2+} (Co:Zn 1.4 ± 0.3) and Pb^{2+} (Co:Pb 2.4 ± 0.5). 11BNicks2's selectivity for Co^{2+} over Zn^{2+} and Pb^{2+} was found to increase further as the metal-ion concentration was decreased to 50 μM (Co:Zn 1.6 ± 0.2, Co:Pb 3.2 ± 0.7, Table 2.4).

Although the near threefold increase in 11BNick2's Co:Zn and Co:Pb selectivity is modest, the reproducible effect supports a role for Loop II in Co^{2+} selectivity. The conversion of Loop II to a tetraloop and the absence of additional peripheral sequence elements in these constructs may have limited the magnitude of the increased Co^{2+} selectivity. The increased selectivity of these constructs, however, demonstrated the utility of this alternative truncation platform in investigating the Co^{2+} selectivity of the Clone 11 system. Also, because most DNAzyme configurations incorporate a small catalytic core flanked by substrate binding arms, further refinement of the alternative truncation platform may lead to a general method for retaining the selectivity and activity of RNA-cleaving DNAzymes.

2.4.4 Loop II is Sufficient to Increase Co^{2+} Selectivity

To further investigate the role of peripheral sequence elements in Co^{2+} selectivity, additional constructs were designed based on the alternative truncation platform. The 11BNick2 construct was selected for further study because of its improved Co^{2+} selectivity over both Zn^{2+} and Pb^{2+}, as shown above. Constructs based on 11BNick2 contained both Loop II and peripheral sequences elements such as T78 and T80 (Figure 2.3A). A unique secondary structure element, not predicted in the full-length Clone 11 *cis*- or *trans*-sequences or sequence variants,

was predicted for construct 11BNick7 in peripheral sequence regions (nucleotides 4-15, 78-88; Figure 2.3A).

These peripheral sequence elements' contributions to Co^{2+} selectivity was investigated in the 11BNick7 construct (Table 2.4). 11BNick7 and 11BNick8 showed reproducible but insignificant improvements in Co^{2+} selectivity (Co:Pb 1.3–1.4-fold) over the 11B construct. No improvement was observed in the Co:Zn selectivity. At lower concentrations of metal ions, however, the Co:Pb selectivity was improved for 11BNick7 (Co:Pb 1.5 ± 0.4) and 11BNick8 (Co:Pb 2.2 ± 0.8), with levels similar to those observed in the 11BNick2 construct. This level corresponds to an increase in Co^{2+} selectivity of up to 2.9-fold over Pb^{2+}, compared with the 11B-*trans* system. No increase in Co^{2+} selectivity was observed for 11B-*trans* at the same concentration of metal ions, suggesting that the effect is specific to the constructs using the 11BNick2 construct from the alternative truncation platform.

To investigate whether the peripheral sequences forming Loop II were alone sufficient to increase Co^{2+} selectivity, two additional constructs, 11B14 and 11B15, were designed using the conventional truncation approach (Figure 2.3B). Aside from the absence of Loop II, construct 11B14 is identical to 11BNick7, and 11B15 is identical to 11BNick8. The Co:Zn selectivity for both 11B14 (Co:Zn 0.55 ± 0.06) and 11B15 (Co:Zn 0.56 ± 0.10) showed no increase over the 11B-*trans* construct (Table 2.4). Both constructs mirrored the improvement in the Co:Pb selectivity seen with 11BNick7 and 11BNick8 at metal ion concentrations of 50 µM. The 11BNick 7 (Co:Pb 2.8 ± 0.7) construct, however, showed a more significant increase over 11B14 (Co:Pb 1.8 ± 0.3) or 11B15 (Co:Pb 1.8 ± 0.4). While constructs containing the 3'- and 5'-peripheral sequences showed increases in Co:Pb selectivity, the 11BNick2 construct utilizing the alternative truncation platform and Loop II showed over a threefold increase in Co:Pb selectivity exceeding gains in all other constructs.

2.4.5 Exploring Possible Metastable Structures

The investigation described above was based primarily on the most stable secondary structure predicted by mfold, and truncation was based on the 11B secondary structure. However, systematic truncation to preserve the most stable secondary structure mostly resulted in a loss of metal ion selectivity. We concluded that some metastable structures

predicted by mfold might play a role. Three distinct secondary structures—11A, 11B and 11B'—were predicted for DNAzyme constructs based on Clone 11 (Figure 2.2A). The third structure, 11B', was identified during the design of constructs for the truncation study. 11B and 11B' differ by the secondary structure adopted within the highly conserved region (nucleotides 51–67). Since this region is highly conserved, adopts two different secondary structures, and interfaces with the cleavage site, the structure within this region could be functionally important.

To investigate the effects of these metastable structures in the Clone 11 system, correlations between Co^{2+} selectivity and predicted secondary structure were examined (Table 2.5). A cursory look at the predicted secondary structures of the constructs used in this study revealed three different scenarios. Predicted secondary structures for Clone 11-related sequences fell into several categories: 11A only, 11B along with 11A or 11B', or 11B only. Clone 18 is an example of the first scenario, forming only the 11A-type structures and showing poor Co^{2+} selectivity (Co:Zn 0.46, Co:Pb 0.56). Constructs truncated based on the 11A-type structure were inactive. Considering the second situation, sequences forming the 11B- and 11B'-type structures also had decreased Co:Zn selectivity (0.06–0.79) relative to Clone 11. In addition, 11B2/Sub2 forms the 11A and 11B structures and shows low Co^{2+} selectivity (Co:Zn 0.41, Co:Pb 0.69). No increase in Co:Zn selectivity was observed for the 11BNick1, 11BNick3, and 11BNick4 constructs (Co:Zn 0.56–0.77), which form the 11B- and 11B'-type structures. These three sequences were predicted to form the 11B and 11B' structures. While 11BNick3 did show a mild improvement in Co:Pb selectivity, the Co:Zn selectivity was still limited. The 11B14 and 11B15 constructs were of particular interest because each contained additional peripheral sequence elements and were predicted to form all three secondary structures. Improvements in the Co:Pb selectivity among 11BNick7, 11BNick8, 11B14, and 11B15 (1.6–2.5-fold) did not appear to correlate with their predicted secondary structures. 11BNick2 was predicted to form only the 11B-type structure. It also contained Loop II and utilized the alternative truncation platform. This construct showed the largest improvement in Co:Pb selectivity (2.9-fold), restoring the Co:Pb selectivity to near Clone 11 levels.

2.5 Discussion

2.5.1 Role of Peripheral Sequence Elements in Determining Metal-Ion Selectivity

In this study, we carried out biochemical assays of a previously selected Co^{2+}-selective DNAzyme[6] to identify sequence elements responsible for its subtle Co^{2+} selectivity. This selectivity is characterized by the selectivity index, the ratio of a DNAzyme's phosphodiester transfer activity in the presence of Co^{2+} to its activity in the presence of the next-most competing ions, Zn^{2+} or Pb^{2+}. Even though the changes in the selectivity indices were relatively small, the differences in the rates of the reactions in the presence of different metal ions exceeded the error measurements. Such a small metal selectivity index reflects the fact that Co^{2+} and Zn^{2+} are highly similar metal ions with the same ionic radii and similar preferences in ligand donor sets. Even metalloproteins that are known to have extremely high selectivity for other metal ions display a much smaller selectivity index between Co^{2+} and Zn^{2+}, as Co^{2+} in almost all zinc proteins can be substituted for Zn^{2+} and retain ~100% activity.

The most important finding from this study is that truncating peripheral sequences in Clone 11 tended to reduce Co^{2+} selectivity, even though the phosphodiester transfer activity remained. Truncating peripheral sequences is common practice in DNAzyme research. It often results in a smaller DNAzyme with similar activity to the originally selection product. We show here that when subtle differences in the metal-ion selectivity of highly similar metal ions such as Co^{2+} and Zn^{2+} are concerned, the role played by peripheral sequences cannot be ignored. In the Clone 11 system, Loop II partially restored the Co^{2+} selectivity over Pb^{2+} to levels observed in the *cis*-cleaving Clone 11 DNAzyme.

Peripheral sequence elements have been found to modulate function of other DNAzymes and ribozymes. For example, the P5abc peripheral element facilitates the proper folding of the P4–P6 domain in the *Tetrahymena thermophila* group I intron.[27] A construct of the *Schistosoma mansoni* hammerhead ribozyme incorporating peripheral sequences showed an increase in activity.[28, 29] Folding studies have shown that other ribozymes also utilize peripheral sequences for proper folding and catalytic activity. In the case of DNAzyme systems, the activity of the X-motif DNAzyme relies on peripheral sequence elements for activity.[30] A group of recently isolated, transition-metal-dependent DNAzymes also utilizes peripheral

sequences to modulate catalytic activity[31, 32] and to stabilize the 8–17 motif within a larger DNAzyme structure.[32]

2.5.2 Sequence Elements Important for Enhanced Co^{2+} Selectivity

We found that the peripheral sequence forming Loop II in the alternative truncation platform is important for increased Co^{2+} selectivity. Restoring the Co^{2+} selectivity of 11BNick2 to levels similar to those observed in Clone 11 also led to insights into the structure-function relationships in Clone 11. First, the similarities between the ionic radii and coordination geometry of Co^{2+} and Zn^{2+} make the twofold increase in the Co:Zn selectivity of 11BNick2 particularly significant. The peripheral sequence element Loop II may assist in forming tertiary structural features that facilitate the three-dimensional arrangement of ligand donor elements contributing to Clone 11's Co:Zn selectivity. Second, the restoration of the Co^{2+} selectivity over Pb^{2+} remains equally significant because of the high background rate of Pb^{2+}-mediated phosphodiester hydrolysis. Additional peripheral sequences beyond Loop II may be required to produce a structure that further increases the selectivity over Zn^{2+} and Pb^{2+} to levels observed in Clone 11. The tertiary structure formed may involve Loop II along with the conserved region (positions 51–70) or the 3'-substrate-binding arm to provide a three-dimensional arrangement of functional groups leading to the preferential binding of Co^{2+}.

In the Clone 11 DNAzyme system, the results from "nicked" constructs lend credence to the idea that peripheral sequences increase Co^{2+} selectivity. For example, converting Loop II to a tetraloop or introducing mutations into the substrate-binding arms may have contributed to differential Co^{2+} selectivity. These possibilities, however, are unlikely to be the sole reasons for the increased Co:Zn selectivity. Loop II alone was sufficient to produce modest but reproducible increases in selectivity over those observed in Clone 11. It is also important to note that increased Co^{2+} selectivity over both Zn^{2+} and Pb^{2+} was observed in a construct that contains only two of the four nucleotides that distinguish Clone 11 from Clone 18. This raises the possibility that nucleotides 72 and 77 contribute to a three-dimensional structure that preferentially binds Co^{2+} either through direct Co^{2+} binding or through a tertiary fold that uses these nucleotides to form a Co^{2+}-selective metal-binding pocket. The modest increase in Co^{2+} selectivity over Zn^{2+} also suggests that secondary or tertiary elements present in the full-length

Clone 11 DNAzyme are only approximated in the truncated "nicked" platform. These results support the possibility that peripheral sequence elements contribute to a tertiary structure with sufficient complexity to arrange DNAzyme ligand donor groups in a Co^{2+}-selective metal-binding pocket.

2.5.3 Role of Secondary Structure in Metal Selectivity

Comparing structural features present in Clone 11 with those of other DNAzyme/ribozyme systems provided further insights. The poor conservation of an element essential for selectivity in Clone 11 is mirrored in the Sc.ai5g group II self-splicing intron, which shows poor conservation of the sequence required for substrate recognition.[33] A Mg^{2+}-dependent secondary structure rearrangement at this substrate recognition site in the group II intron is proposed to facilitate substrate binding.[34] In other ribozyme systems, secondary structural motifs contribute to metal binding and tertiary structure formation. Loop–loop interactions mediate tertiary contacts necessary for the optimal activity of many ribozymes as well as the ribosome.[20,28,35,36] A single-stranded loop in the hammerhead ribozyme stabilizes the tertiary fold and facilitates catalytic core formation.[37] Loop regions have also been implicated in G-quartet formation and stability,[38] as observed in a recently isolated kinase DNAzyme that uses the loop region of a G-quartet to form a distal tertiary contact required for activity and G-quartet formation.[39] Helical junctions, also present in Clone 11, facilitate the assembly of the tertiary structure in many large and small ribozymes,[36,40,41] the RNA component of telomerase, and most notably in the recently isolated nuclease[4,5,42] and ligase[43] DNAzymes. The triple-helix junction in the 8–17 system comprises the catalytic core and serves as a hinge point for tertiary folding.[44] Crystal structures of the ribosome[20] and the L1 ligase ribozyme[45] both demonstrate the formation of tertiary contacts and the organization of divalent metal ion binding pockets mediated by helical junctions. Further studies on the Clone 11 system are likely to confirm that secondary structure motifs perform similar functions: forming a tertiary structure that contributes to the DNAzyme's ability to bind Co^{2+} with high selectivity.

2.5.4 Role of Metastable Structures in Determining Metal Selectivity

Our results also suggest that metastable structures predicted by mfold may affect metal selectivity. Metastable structures are involved in the folding and function of many other DNA and RNA systems. Differential folding and metal ion-dependent secondary and tertiary structure rearrangements in many ribozymes are likely to proceed through metastable structures.[23,46-48] For example, metastable structures contribute to the folding of the hepatitis delta virus[48] and the P4-P6 domain of the group I intron,[47] as well as mediating splicing activity of the thymidylate synthase group I intron.[47] The group II intron has also demonstrated differential folds based on the identity of the metal-ion cofactor.[49] Riboswitches have also been shown to undergo metal-ion-dependent structural transitions that affect cofactor binding and activation.[50] In the case of DNAzymes, *in-vitro*-selected transition-metal-ion-dependent systems show multiple structures for similar sequences.[31] In addition, allosteric DNAzymes undergo analyte-dependent structural changes.[51] Other effects of metastable structures are seen in the transcription and activity of viral and mRNA sequences.[40,47,52] Finally, a number of conditions, including monovalent[53] and divalent metal ion concentration,[21,54] temperature,[51] pH,[53] and peripheral sequence elements[27,55] affect the folding behavior and prevalence of metastable structures.

The influence of metastable structures on the metal selectivity of Clone 11 is supported by its Co^{2+} selectivity and multiple predicted secondary structures, as well as the precedent of metastable structures observed in other DNA/RNA systems. Results from truncation studies show that the largest decreases in Co:Zn and Co:Pb selectivity (Table 2.5) correlate with constructs showing multiple predicted secondary structures. Interestingly, two of these predicted secondary structures, 11B and 11B', lie within a sequence region that is highly conserved and intolerant to point mutations. The correlation of Co^{2+} selectivity with multiple predicted secondary structures suggests the possibility of interconversion between the 11B and 11B' structures. A structural rearrangement may have the functional role of repositioning the single riboadenosine, which is predicted to be base-paired in the 11B-type structure, to allow for the incoming nucleophile's in-line attack on the scissile phosphate. Competing metastable structures may also help explain the persistence of Pb^{2+}- and Zn^{2+}-dependent activity after

multiple rounds of negative selection, as observed with the persistence of inactive sequences following negative selection.[56] Finally, peripheral sequences and Co^{2+} metal ions may help stabilize the 11B-type structure, an effect mediated by both peripheral sequences and metals in other DNAzymes/ribozymes[27,32,55] and only approximated in truncated constructs in the Clone 11 system. A complex but synergistic relationship may exist between metal-ion cofactors and peripheral sequence elements that contribute to Co^{2+} selectivity in Clone 11.

2.6 Conclusions

Clone 11 requires both its primary sequence and the peripheral sequence element Loop II to be selective for Co^{2+} over Zn^{2+} and Pb^{2+}. Loop II's structural features and nucleotides 72 and 77 likely contribute tertiary contacts that either stabilize or form a Co^{2+}-selective binding pocket. This study provides a foundation to further investigate the relationship between DNAzyme structure and analyte selectivity. The success of the "nicked" strategy in reintroducing peripheral sequence elements and in restoring Co^{2+} selectivity suggests the potential of this approach as a general method for truncating and studying DNAzymes/ribozymes when the traditional truncation method fails to work. As the effects of peripheral sequences and secondary structure on cofactor selectivity are better understood, increasing or altering cofactor selectivity may be possible through rational design and *in vitro* selection based on established motifs. With its increased selectivity at low metal-ion concentrations, Clone 11 is a good candidate for the analyte-responsive element of a biosensor. Finally, insights about the potential contributions of secondary structures to a DNAzyme's overall function may be important in future DNAzyme/ribozyme-based biotechnology applications that require high activity and high analyte selectivity.

2.7 Figures and Tables

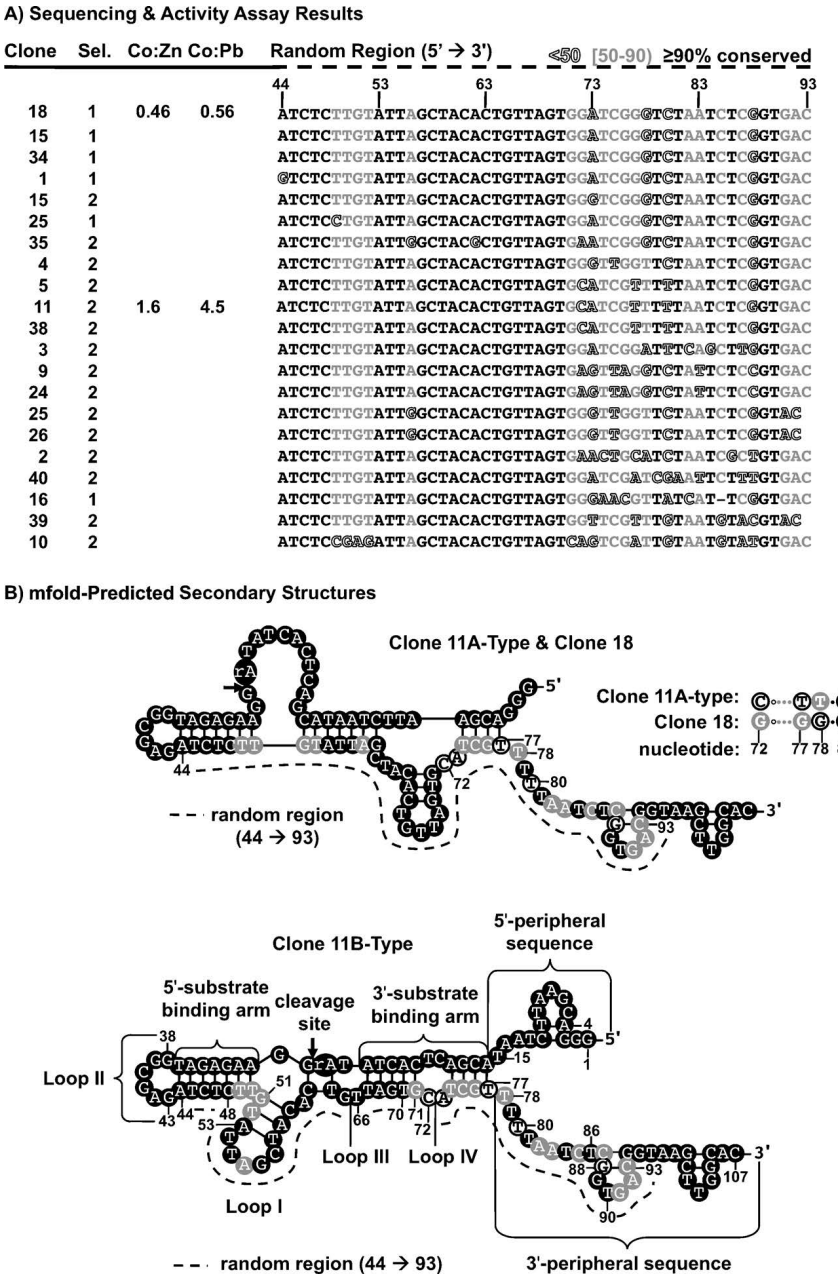

Figure 2.1. The artificial phylogenetic analysis and secondary structures of the Clone 11 and Clone 18 DNAzymes. A) The aligned sequences from Selections 1 and 2 that were used for artificial phylogenetic analysis. Sequences are arranged according to similarity. Shading indicates the degree of nucleotide conservation: positions that were highly (>90%) conserved are shown in black, positions that were moderately (50–90%) conserved are shown in grey, and nonconserved (<50%) positions are outlined. Positions 71–83 were highly variable. Nucleotide positions are based on the full-length Clone 11 sequence. B) The sequence variability of each sequence overlaid with their mfold-predicted secondary structures. Cleavage sites are indicated by arrows. Two secondary structures were predicted for Clone 11: the 11A-type and the 11B-type secondary structure. Clone 18 differs from Clone 11 by only four nucleotides (72, 77, 78 and 80), and the single secondary structure predicted for Clone 18 is identical to that of the 11A-type secondary structure.

Construct	k_{obs} (min^{-1})			Co:Zn	Co:Pb
	Co^{2+}	Zn^{2+}	Pb^{2+}		
Clone 11	0.18	0.11	0.040	1.6	4.5
Clone 18	0.044	0.096	0.078	0.46	0.56
11B	0.088	0.15	0.079	0.59	1.1

Table 2.1. The kinetic data and Co^{2+} selectivity of clones 11 and 18 and the 11B-*trans*-cleaving DNAzymes. Kinetic data was obtained at pH 7.0 with metal ions (500 µM) and NaCl (500 mM).

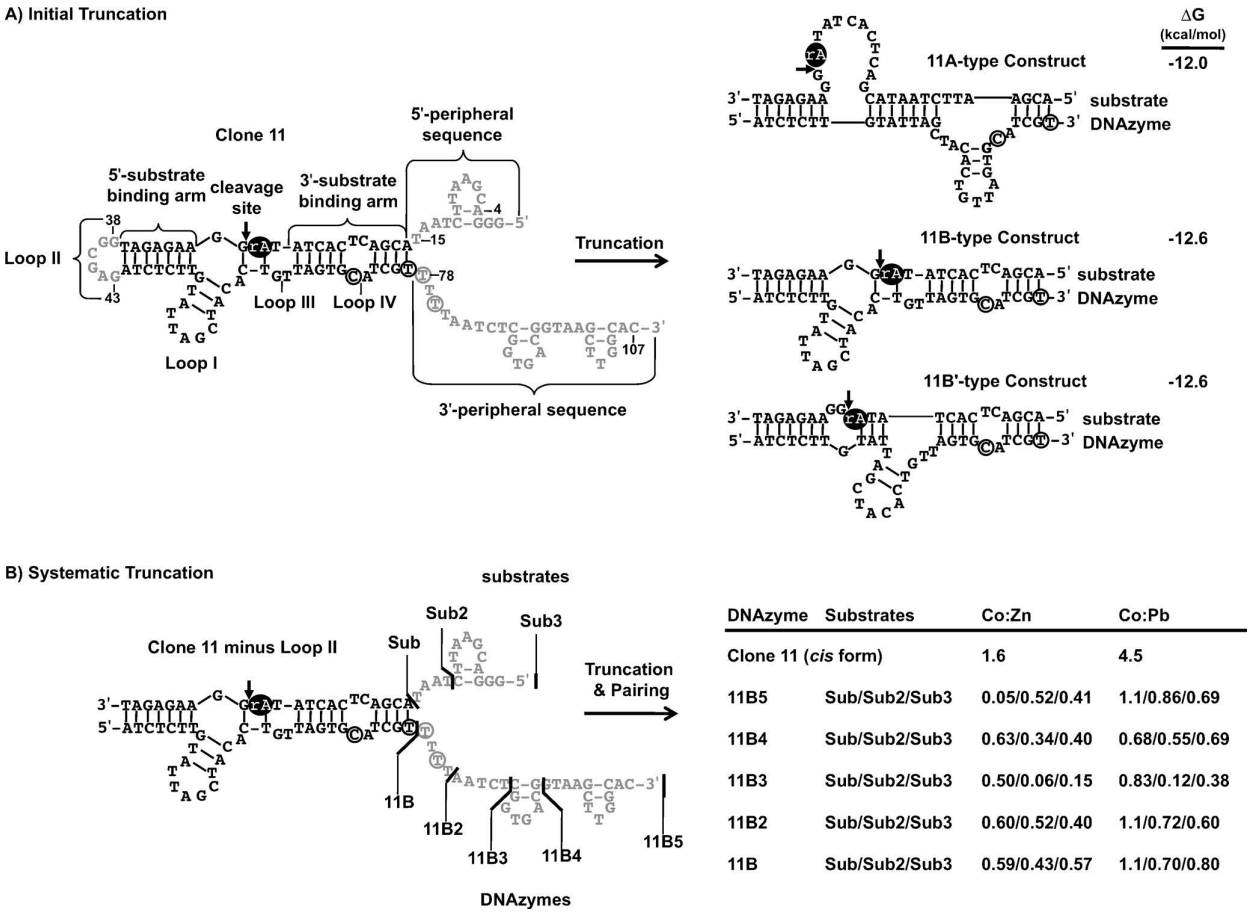

DNAzyme	Substrates	Co:Zn	Co:Pb
Clone 11 (*cis* form)		1.6	4.5
11B5	Sub/Sub2/Sub3	0.05/0.52/0.41	1.1/0.86/0.69
11B4	Sub/Sub2/Sub3	0.63/0.34/0.40	0.68/0.55/0.69
11B3	Sub/Sub2/Sub3	0.50/0.06/0.15	0.83/0.12/0.38
11B2	Sub/Sub2/Sub3	0.60/0.52/0.40	1.1/0.72/0.60
11B	Sub/Sub2/Sub3	0.59/0.43/0.57	1.1/0.70/0.80

Figure 2.2. Truncation of the Clone 11 *cis*-cleaving DNAzyme. The portions of Clone 11 that were removed are shown in grey and the ribonucleotide is shown as a black oval. A) The clone 11 *cis*-cleaving DNAzyme was initially truncated to the 11B-*trans* cleaving DNAzyme (11B-*trans*) by deleting Loop II and all peripheral sequences. Mfold predicted three different secondary structures for 11B-*trans*: 11A-type, 11B-type, and 11B' (shown here with corresponding DG values). The 11B and 11B' structures differ only at positions 51–67, and 11B' has a single-stranded region immediately following the cleavage site. Only 5–6 base pairs differ between 11B and 11B'. B) The clone 11 *cis*-cleaving DNAzyme was then modified by deleting Loop II and systematically truncating peripheral sequences by small increments. This produced three substrate variants (Sub3, Sub2 and Sub) and five DNAzyme variants (11B5, 11B4, 11B3, 11B2 and 11B). These sequences were paired in every possible permutation and their metal-dependent activities were measured. Co:Zn and Co:Pb selectivity indices for each permutation are reported for the results using Co^{2+}, Zn^{2+}, and Pb^{2+} (500 µM). The full results are listed in Table 2.2.

Construct	k_{obs} (min^{-1})			Co:Zn	Co:Pb
	Co^{2+}	Zn^{2+}	Pb^{2+}		
11B5/Sub3	0.045	0.11	0.065	0.41	0.69
11B5/Sub2	0.057	0.11	0.066	0.52	0.86
11B5/Sub	0.025	0.53	0.022	0.05	1.1
11B4/Sub3	0.043	0.10	0.062	0.40	0.69
11B4/Sub2	0.048	0.14	0.087	0.34	0.55
11B4/Sub	0.075	0.12	0.11	0.63	0.68
11B3/Sub3	0.015	0.099	0.039	0.15	0.38
11B3/Sub2	0.014	0.24	0.12	0.06	0.12
11B3/Sub	0.070	0.14	0.084	0.50	0.83
11B2/Sub3	0.018	0.045	0.030	0.40	0.60
11B2/Sub2	0.094	0.18	0.13	0.52	0.72
11B2/Sub	0.12	0.20	0.11	0.60	1.1
11B/Sub3	0.008	0.014	0.010	0.57	0.80
11B/Sub2	0.069	0.16	0.099	0.43	0.70
11B/Sub	0.088	0.15	0.079	0.59	1.1

Table 2.2. The Co^{2+} selectivity over Zn^{2+} and Pb^{2+} is shown for each stepwise truncation of Clone 11. Pseudo-first-order rate constants for substrate cleavage by truncated Clone 11 constructs were determined. The enzyme strand is denoted by "11B" followed by the substrate strand. All permutations of enzyme and substrate strands were assayed. Note that 11B/Sub is the 11B-*trans* construct. All data were obtained from assays with Co^{2+}, Zn^{2+}, or Pb^{2+} (500 μM).

Construct	k_{obs} (min^{-1})			Co:Zn	Co:Pb
	Co^{2+}	Zn^{2+}	Pb^{2+}		
11B	0.088 ± 0.006	0.15 ± 0.01	0.079 ± 0.016	0.59 ± 0.06	1.1 ± 0.2
11BNick1	0.042 ± 0.004	0.075 ± 0.019	0.076 ± 0.021	0.56 ± 0.15	0.55 ± 0.16
11BNick2	0.010 ± 0.002	0.0073 ± 0.0008	0.0041 ± 0.0004	1.4 ± 0.3	2.4 ± 0.5
11BNick3	0.027 ± 0.004	0.038 ± 0.010	0.016 ± 0.002	0.71 ± 0.22	1.7 ± 0.3
11BNick4	0.015 ± 0.002	0.019 ± 0.003	0.010 ± 0.002	0.79 ± 0.14	1.5 ± 0.3
11BNick5	0.18 ± 0.01	0.27 ± 0.04	0.16 ± 0.04	0.67 ± 0.11	1.1 ± 0.3
11BNick6	0.18 ± 0.01	0.28 ± 0.01	0.16 ± 0.05	0.64 ± 0.03	1.1 ± 0.3

Table 2.3. The Co^{2+} selectivity over Zn^{2+} or Pb^{2+} for constructs 11BNick1–6. The effect of the alternative truncation platform involving a nick in the 5'-substrate-binding arm is examined. Metal-ion selectivities and pseudo-first-order rate constants for each construct are shown. All data were obtained from assays with Co^{2+}, Zn^{2+}, or Pb^{2+} (500 μM).

Construct	Conc. (μM)	k_{obs} (min^{-1})			Co:Zn	Co:Pb
		Co^{2+}	Zn^{2+}	Pb^{2+}		
11B	500	0.088 ± 0.006	0.15 ± 0.01	0.079 ± 0.016	0.59 ± 0.06	1.1 ± 0.2
	50	0.022 ± 0.002	0.025 ± 0.002	0.021 ± 0.001	0.88 ± 0.09	1.1 ± 0.1
11BNick2	500	0.010 ± 0.002	0.0073 ± 0.0008	0.0041 ± 0.0004	1.4 ± 0.3	2.4 ± 0.5
	50	0.0016 ± 0.0001	0.0010 ± 0.0001	0.0005 ± 0.0001	1.6 ± 0.2	3.2 ± 0.7
11BNick7	500	0.13 ± 0.01	0.17 ± 0.04	0.086 ± 0.022	0.76 ± 0.20	1.5 ± 0.4
	50	0.034 ± 0.001	0.037 ± 0.003	0.012 ± 0.003	0.92 ± 0.09	2.8 ± 0.7
11BNick8	500	0.094 ± 0.008	0.14 ± 0.01	0.065 ± 0.008	0.67 ± 0.08	1.4 ± 0.2
	50	0.022 ± 0.001	0.029 ± 0.002	0.010 ± 0.004	0.76 ± 0.07	2.2 ± 0.8
11B14	500	0.077 ± 0.001	0.14 ± 0.02	0.11 ± 0.03	0.55 ± 0.06	0.70 ± 0.18
	50	0.022 ± 0.003	0.026 ± 0.003	0.012 ± 0.001	0.85 ± 0.15	1.8 ± 0.3
11B15	500	0.056 ± 0.007	0.10 ± 0.01	0.074 ± 0.014	0.56 ± 0.10	0.76 ± 0.17
	50	0.013 ± 0.002	0.015 ± 0.001	0.0071 ± 0.0004	0.87 ± 0.15	1.8 ± 0.4

Table 2.4. The Co^{2+} selectivity of nicked constructs containing peripheral sequence elements. The increase in Co^{2+} selectivity attributable to the presence of Loop II and peripheral sequence elements is examined. Pseudo-first-order rate constants and metal selectivities are shown for the given metal ion concentration.

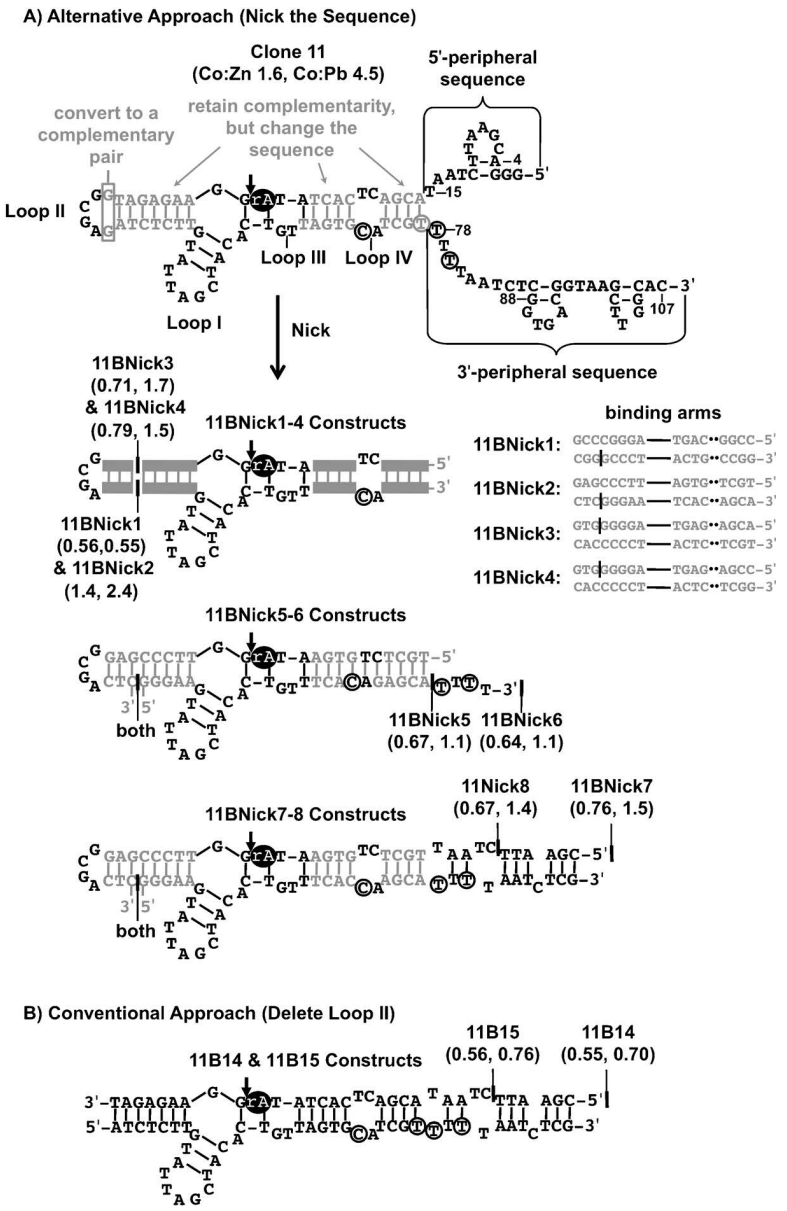

Figure 2.3. Truncation of the Clone 11 *cis*-cleaving DNAzyme by conventional and alternative truncation approaches. The portions of Clone 11 that were changed during truncation are shown in grey. The ribonucleotide is shown as a black oval. A) An alternative truncation approach to the conventional method (shown in Figure 2.2B) preserved the secondary structure of 11B, retained many conserved nucleotides from Clone 11, and preserved the substrate-binding-arm base pairs. The nucleotides within Clone 11's binding arms were modified, but its base pairing interactions were preserved. Then the 5' substrate-binding arm was nicked at one of two positions. Thus the two resulting truncated constructs retained Loop II. In order to preserve the base pairing in the 5'-substrate-binding arm, two nucleotides in Loop II were base-paired, converting Loop II to a tetraloop. The peripheral sequences were then systematically truncated. In 11BNick5 and 11BNick6, two additional point mutations were introduced in Loop IV to increase the substrate binding arm complementarity. The mfold-predicted secondary structures of each of the constructs obtained by the alternative approach (11BNick1–8) are shown. 11BNick1–4 have secondary structures that differ only in the substrate binding arm sequences, as shown. Their Co:Zn and Co:Pb selectivity indices are shown in parentheses. B) The truncation of Clone 11 by the conventional approach described in Figure 2.2B produced two additional constructs: 11B14 and 11B15. Modifications included 1) deleting Loop II and 2) systematically truncating the peripheral sequences.

Construct	Predicted Structure	Co:Zn	Co:Pb
Clone 11	11A/11B	1.6[a]	4.5[a]
Clone 18	11A	0.46[a]	0.56[a]
11B/Sub	11B/11B'	0.59 ± 0.06[a]	1.1 ± 0.2[a]
		0.88 ± 0.091	1.1 ± 0.1
11B5/Sub3	11A/11B	0.41[a]	0.69[a]
11B5/Sub	11B/11B'	0.05[a]	1.1[a]
11B3/Sub2	11B/11B'	0.06[a]	0.12[a]
11BNick1	11B/11B'	0.56 ± 0.15	0.55 ± 0.16
11BNick2	11B	1.4 ± 0.3[a]	2.4 ± 0.5[a]
		1.6 ± 0.2	3.2 ± 0.7
11BNick3	11B/11B'	0.71 ± 0.22	1.7 ± 0.3
11BNick4	11B/11B'	0.79 ± 0.14	1.5 ± 0.3
11BNick5	11B	0.67 ± 0.11	1.1 ± 0.3
11BNick6	11B	0.64 ± 0.03	1.1 ± 0.3
11BNick7	11B	0.76 ± 0.20[a]	1.5 ± 0.4[a]
		0.92 ± 0.09	2.8 ± 0.7
11BNick8	11B	0.67 ± 0.08[a]	1.4 ± 0.2[a]
		0.76 ± 0.07	2.2 ± 0.8
11B14	11A/11B/11B'	0.55 ± 0.06[a]	0.70 ± 0.18[a]
		0.85 ± 0.15	1.8 ± 0.27
11B15	11A/11B/11B'	0.56 ± 0.10[a]	0.76 ± 0.17[a]
		0.87 ± 0.15	1.8 ± 0.4

Table 2.5. Effect of metastable structures on selectivity. The predicted metastable structures for selected constructs are compared with the observed metal selectivity. Constructs predicted to form only the 11B structure show higher Co^{2+} selectivity. All metal selectivity values were determined at 50 μM metal concentration unless otherwise stated. [a]Values obtained at 500 μM.

2.8 References

1. Breaker, R. R.; Joyce, G. F. "A DNA Enzyme that Cleaves RNA." *Chem. Biol.* **1994**, *1*, 223– 229.

2. a) Sen, D.; Geyer, C. R. "DNA Enzymes." *Curr. Opin. Chem. Biol.* **1998**, *2*, 680–687; b) Breaker, R. R. "Making Catalytic DNA." *Science* **2000**, *290*, 2095–2096; c) Lu, Y. "New Transition-Metal-Dependent DNAzymes as Efficient Endonucleases and as Selective Metal Biosensors." *Chem. Eur. J.* **2002**, *8*, 4588–4596; d) Peracchi, A. "DNA Catalysis: Potential, Limitations, Open Questions." *ChemBioChem* **2005**, *6*, 1316–1322; e) Dass, C. R.; Choong, P. F. M.; Khachigian, L. M. "DNAzyme Technology and Cancer Therapy: Cleave and Let Die." *Mol. Cancer Ther.* **2008**, *7*, 243–251; f) Silverman, S. K. "Catalytic DNA (Deoxyribozymes) for Synthetic Applications—Current Abilities and Future Prospects." *Chem. Commun.* **2008**, 3467–3485; g) Liu, J. ; Cao, Z.; Lu, Y. "Functional Nucleic Acid Sensors." *Chem. Rev.* **2009**, *109*, 1948–1998; h) Schlosser, K.; Li, Y. "Biologically Inspired Synthetic Enzymes Made from DNA." *Chem. Biol.* **2009**, *16*, 311–322; i) Zhang, X.-B.; Kong, R.-M.; Lu, Y. "Metal Ion Sensors Based on DNAzymes and Related DNA Molecules." *Annu. Rev. Anal. Chem.* **2011**, *4*, 105–128.

3. a) Faulhammer, D.; Famulok, M. "The Ca^{2+} Ion as a Cofactor for a Novel RNA-Cleaving Deoxyribozyme." *Angew. Chem.* **1996**, *108*, 2984–2988; *Angew. Chem. Int. Ed.* **1996**, *35*, 2837 –2841; b) Peracchi, A. "Preferential Activation of the 8–17 Deoxyribozyme by Ca^{2+} Ions: Evidence for the Identity of 8-17 with the Catalytic Domain of the Mg5 Deoxyribozyme." *J. Biol. Chem.* **2000**, *275*, 11693–11697; c) Brown, A. K.; Li, J.; Pavot, C. M.-B.; Lu, Y. "A Lead-Dependent DNAzyme with a Two-Step Mechanism." *Biochemistry* **2003**, *42*, 7152–7161; d) Cruz, R. P. G.; Withers, J. B.; Li, Y. "Dinucleotide Junction Cleavage Versatility of 8-17 Deoxyribozyme." *Chem. Biol.* **2004**, *11*, 57–67; e) Schlosser, K.; Gu, J.; Sule, L.; Li, Y. "Sequence-Function Relationships Provide New Insight into the Cleavage Site Selectivity of the 8–17 RNA-Cleaving Deoxyribozyme." *Nucleic Acids Res.* **2008**, *36*, 1472–1481.

4. Santoro, S. W.; Joyce, G. F. "A General Purpose RNA-Cleaving DNA Enzyme." *Proc. Natl. Acad. Sci. U. S. A.* **1997**, *94*, 4262–4266.

5. Li, J.; Zheng, W.; Kwon, A. H.; Lu, Y. "*In Vitro* Selection and Characterization of a Highly Efficient Zn(II)-Dependent RNA-Cleaving Deoxyribozyme." *Nucleic Acids Res.* **2000**, *28*, 481–488.

6. Bruesehoff, P. J.; Li, J.; Augustine III, A. J.; Lu, Y. "Improving Metal Ion Specificity During *In Vitro* Selection of Catalytic DNA." *Comb. Chem. High Throughput Screening* **2002**, *5*, 327–335.

7. Liu, Z.; Mei, S. H. J.; Brennan, J. D.; Li, Y. "Assemblage of Signaling DNA Enzymes with Intriguing Metal-Ion Specificities and pH Dependences." *J. Am. Chem. Soc.* **2003**, *125*, 7539–7545.

8. Carmi, N.; Balkhi, H. R.; Breaker, R. R. "Cleaving DNA with DNA." *Proc. Natl. Acad. Sci. U. S. A.* **1998**, *95*, 2233–2237.

9. Liu, J.; Lu, Y. "Rational Design of 'Turn-On' Allosteric DNAzyme Catalytic Beacons for Aqueous Mercury Ions with Ultrahigh Sensitivity and Selectivity." *Angew. Chem.* **2007**, *119*, 7731–7734; *Angew. Chem. Int. Ed.* **2007**, *46*, 7587–7590.

10. Hollenstein, M.; Hipolito, C.; Lam, C.; Dietrich, D.; Perrin, D. M. "A Highly Selective DNAzyme Sensor for Mercuric Ions." *Angew. Chem.* **2008**, *120*, 4418–4422; *Angew. Chem. Int. Ed.* **2008**, *47*, 4346–4350.

11. a) Santoro, S. W.; Joyce, G. F.; Sakthivel, K.; Gramatikova, S.; Barbas III, C. F. "RNA Cleavage by a DNA Enzyme with Extended Chemical Functionality." *J. Am. Chem. Soc.* **2000**, *122*, 2433–2439; b) Hoadley, K. A.; Purtha, W. E.; Wolf, A. C.; Flynn-Charlebois, A.; Silverman, S. K. "Zn^{2+}-Dependent Deoxyribozymes That Form Natural and Unnatural RNA Linkages." *Biochemistry* **2005**, *44*, 9217–9231.

12. Li, Y.; Sen, D. “Toward an Efficient DNAzyme.” *Biochemistry* **1997**, *36*, 5589–5599.

13. Liu, J.; Brown, A. K.; Meng, X.; Cropek, D. M.; Istok, J. D.; Watson, D. B.; Lu, Y. “A Catalytic Beacon Sensor for Uranium with Parts-per-Trillion Sensitivity and Millionfold Selectivity.” *Proc. Natl. Acad. Sci. U. S. A.* **2007**, *104*, 2056–2061.

14. Brown, A. K.; Liu, J.; He, Y.; Lu, Y. “Biochemical Characterization of a Uranyl Ion-Specific DNAzyme.” *ChemBioChem* **2009**, *10*, 486–492.

15. a) Li, J.; Lu, Y. “A Highly Sensitive and Selective Catalytic DNA Biosensor for Lead Ions.” *J. Am. Chem. Soc.* **2000**, *122*, 10466–10467; b) Liu, J.; Lu, Y. *J. Am. Chem. Soc.* **2003**, *125*, 6642–6643; c) Lu, Y.; Liu, J.; Li, J.; Bruesehoff, P. J.; Pavot, C. M.-B.; Brown, A. K. “New Highly Sensitive and Selective Catalytic DNA Biosensors for Metal Ions.” *Biosens. Bioelectron.* **2003**, *18*, 529–540; d) Achenbach, J. C.; Chiuman, W.; Cruz, R. P. G.; Li, Y. “DNAzymes: From Creation *In Vitro* to Application *In Vivo*.” *Curr. Pharm. Biotechnol.* **2004**, *5*, 321–336; e) Chiuman, W.; Li, Y. “Efficient Signaling Platforms Built from a Small Catalytic DNA and Doubly Labeled Fluorogenic Substrates.” *Nucleic Acids Res.* **2007**, *35*, 401–405; f) Liu, J.; Lu, Y. “A DNAzyme Catalytic Beacon Sensor for Paramagnetic Cu^{2+} Ions in Aqueous Solution with High Sensitivity and Selectivity.” *J. Am. Chem. Soc.* **2007**, *129*, 9838–9839; g) Shen, Y.; Mackey, G.; Rupcich, N.; Gloster, D.; Chiuman, W.; Li, Y.; Brennan, J. D. “Entrapment of Fluorescence Signaling DNA Enzymes in Sol−Gel-Derived Materials for Metal Ion Sensing.” *Anal. Chem.* **2007**, *79*, 3494–3503; h) Zhao, W.; Chiuman, W.; Lam, J. C.; Brook, M. A.; Li, Y. “Simple and Rapid Colorimetric Enzyme Sensing Assays Using Non-Crosslinking Gold Nanoparticle Aggregation.” *Chem. Commun.* **2007**, 3729–3731; i) Lee, J. H.; Wang, Z.; Liu, J.; Lu, Y. “Highly Sensitive and Selective Colorimetric Sensors for Uranyl (UO_2^{2+}): Development and Comparison of Labeled and Label-Free DNAzyme-Gold Nanoparticle Systems.” *J. Am. Chem. Soc.* **2008**, *130*, 14217–14226; j) Zhao, W.; Lam, J. C.; Chiuman, W.; Brook, M. A.; Li, Y. “Enzymatic Cleavage of Nucleic Acids on Gold Nanoparticles: A Generic Platform for Facile Colorimetric Biosensors.” *Small* **2008**, *4*, 810–816.

16. a) DeRose, V. J. “Metal Ion Binding to Catalytic RNA Molecules.” *Curr. Opin. Struct. Biol.* **2003**, *13*, 317– 324; b) Sigel, R. K. O.; Pyle, A. M. “Alternative Roles for Metal Ions in Enzyme Catalysis and the Implications for Ribozyme Chemistry.” *Chem. Rev.* **2007**, *107*, 97–113.

17. a) Boerner, L. J. K.; Zaleski, J. M. “Metal Complex–DNA Interactions: from Transcription Inhibition to Photoactivated Cleavage.” *Curr. Opin. Chem. Biol.* **2005**, *9*, 135–144; b) Jiang, Q.; Xiao, N.; Shi, P.; Zhu, Y.; Guo, Z. “Design of Artificial Metallonucleases with Oxidative Mechanism.” *Coord. Chem. Rev.* **2007**, *251*, 1951–1972; c) Zeglis, B. M.; Boland, J. A.; Barton, J. K. “Recognition of Abasic Sites and Single Base Bulges in DNA by a Metalloinsertor.” *Biochemistry* **2009**, *48*, 839–849; d) Zeglis, B. M.; Pierre, V. C.; Kaiser, J. T.; Barton, J. K. “A Bulky Rhodium Complex Bound to an Adenosine-Adenosine DNA Mismatch: General Architecture of the Metalloinsertion Binding Mode.” *Biochemistry* **2009**, *48*, 4247–4253; e) Dong, X.; Wang, X.; Lin, M.; Sun, H.; Yang, X.; Guo, Z. “Promotive Effect of the Platinum Moiety on the DNA Cleavage Activity of Copper-Based Artificial Nucleases.” *Inorg. Chem.* **2010**, *49*, 2541–2549.

18. a) Lippert, B. “Ligand-pK_a Shifts through Metals: Potential Relevance to Ribozyme Chemistry.” *Chem. Biodiversity* **2008**, *5*, 1455–1474; b) Mucha, A.; Knobloch, B.; Jezowska-Bojczuk, M.; Kozlowski, H.; Sigel, R. K. “Effect of the Ribose Versus 2'-Deoxyribose Residue on the Metal Ion-Binding Properties of Purine Nucleotides.” *Dalton Trans.* **2008**, 5368–5377; c) Nakano, S.; Hirayama, H.; Sugimoto, N. “Investigations of the Cation Binding to Nucleotides by Monitoring the Hairpin-Duplex Equilibrium of a Self-Complementary Sequence.” *Nucleic Acids Symp. Ser.* **2009**, *53*, 229–230; d) Sigel, R. K. O.; Sigel, H. “A Stability Concept for Metal Ion Coordination to Single-Stranded Nucleic Acids and Affinities of Individual Sites.” *Acc. Chem. Res.* **2010**, *43*, 974–984; e) Khutia, A.; Sanz Miguel, P. J.; Lippert, B. “’Directed’ Assembly of Metallacalix[*n*]arenes with Pyrimidine Nucleobase Ligands of Low Symmetry: Metallacalix[*n*]arene Derivatives of *cis*-$[a_2M(\text{cytosine-}N3)_2]^{2+}$ ($M=Pt^{II}$, Pd^{II}; *n*=4 and 6).” *Chem. Eur. J.* **2011**, *17*, 4195–4204.

19. a) Li, Y.; Breaker, R. R. “Deoxyribozymes: New Players in the Ancient Game of Biocatalysis.” *Curr. Opin. Struct. Biol.* **1999**, *9*, 315–323; b) Liu, Y.; Sen, D. “Local Rather than Global Folding Enables the Lead-dependent Activity of the 8-17 Deoxyribozyme: Evidence from Contact Photo-crosslinking.” *J. Mol. Biol.* **2010**, *395*, 234–241.

20. Klein, D. J.; Moore, P. B.; Steitz, T. A. “The Contribution of Metal Ions to the Structural Stability of the Large Ribosomal Subunit.” *RNA* **2004**, *10*, 1366–1379.

21. Pyle, A. “Metal Ions in the Structure and Function of RNA.” *J. Biol. Inorg. Chem.* **2002**, *7*, 679–690.

22. Cotton, F. A.; Wilkinson, G.; Murillo, C. A.; Bochmann, M. *Advanced Inorganic Chemistry*, 6th ed., Wiley, New York, 1999.

23. Erat, M. C.; Sigel, R. K. O. “Divalent metal ions tune the self-splicing reaction of the yeast mitochondrial group II intron *Sc*.ai5γ.” *J. Biol. Inorg. Chem.* **2008**, *13*, 1025–1036.

24. Zuker, M. “Mfold Web Server for Nucleic Acid Folding and Hybridization Prediction.” *Nucleic Acids Res.* **2003**, *31*, 3406–3415.

25. Fox, G. E.; Woese, C. R. “5S RNA Secondary Structure.” *Nature* **1975**, *256*, 505–507.

26. a) Bruesehoff, P. J. “*In Vitro* Selection and Characterization of Transition Metal-Dependent DNAzymes and RNAzymes.” Dissertation/Thesis, University of Illinois at Urbana-Champaign (USA), 2003; b) Mei, S. H. J.; Liu, Z.; Brennan, J. D.; Li, Y. “An Efficient RNA-Cleaving DNA Enzyme that Synchronizes Catalysis with Fluorescence Signaling.” *J. Am. Chem. Soc.* **2003**, *125*, 412–420.

27. Engelhardt, M. A.; Doherty, E. A.; Knitt, D. S.; Doudna, J. A.; Herschlag, D. “The P5abc Peripheral Element Facilitates Preorganization of the *Tetrahymena* Group I Ribozyme for Catalysis.” *Biochemistry* **2000**, *39*, 2639–2651.

28. Osborne, E. M.; Schaak, J. E.; Derose, V. J. “Characterization of a Native Hammerhead Ribozyme Derived from Schistosomes.” *RNA* **2005**, *11*, 187–196.

29. Roychowdhury-Saha, M.; Burke, D. H. “Extraordinary Rates of Transition Metal Ion-Mediated Ribozyme Catalysis.” *RNA* **2006**, *12*, 1846–1852.

30. Lazarev, D.; Puskarz, I.; Breaker, R. R. “Substrate Specificity and Reaction Kinetics of an X-motif Ribozyme.” *RNA* **2003**, *9*, 688–697.

31. Chiuman, W.; Li, Y. “Revitalization of Six Abandoned Catalytic DNA Species Reveals a Common Three-way Junction Framework and Diverse Catalytic Cores.” *J. Mol. Biol.* **2006**, *357*, 748–754.

32. Schlosser, K.; Lam, J. C. F.; Li, Y. “Characterization of Long RNA-Cleaving Deoxyribozymes with Short Catalytic Cores: The Effect of Excess Sequence Elements on the Outcome of *In Vitro* Selection.” *Nucleic Acids Res.* **2006**, *34*, 2445–2454.

33. Kruschel, D.; Sigel, R. K. “Divalent Metal Ions Promote the Formation of the 5'-Splice Site Recognition Complex in a Self-Splicing Group II Intron.” *J. Inorg. Biochem.* **2008**, *102*, 2147–2154.

34. Erat, M. C.; Kovacs, H.; Sigel, R. K. O. “Metal Ion-N7 Coordination in a Ribozyme Branch Domain by NMR.” *J. Inorg. Biochem.* **2010**, *104*, 611–613.

35. a) Pley, H. W.; Flaherty, K. M.; McKay, D. B. “Model for an RNA Tertiary Interaction from the Structure of an

Intermolecular Complex between a GAAA Tetraloop and an RNA Helix." *Nature* **1994**, *372*, 111–113; b) Wilson, T. J.; Lilley, D. M. J. "Metal Ion Binding and the Folding of the Hairpin Ribozyme." *RNA* **2002**, *8*, 587–600; c) Saksmerprome, V.; Roychowdhury-Saha, M.; Jayasena, S.; Khvorova, A.; Burke, D. H. "Artificial Tertiary Motifs Stabilize *Trans*-Cleaving Hammerhead Ribozymes under Conditions of Submillimolar Divalent Ions and High Temperatures." *RNA* **2004**, *10*, 1916–1924.

36. Lilley, D. M. J. "The Varkud Satellite Ribozyme." *RNA* **2004**, *10*, 151–158.

37. Baird, N. J.; Westhof, E.; Qin, H.; Pan, T.; Sosnick, T. R. "Structure of a Folding Intermediate Reveals the Interplay Between Core and Peripheral Elements in RNA Folding." *J. Mol. Biol.* **2005**, *352*, 712–722.

38. Fujimoto, T.; Miyoshi, D.; Tateishi-Karimata, H.; Sugimoto, N. "Thermal Stability and Hydration State of DNA G-Quadruplex Regulated by Loop Regions." *Nucleic Acids Symp. Ser.* **2009**, *53*, 237–238.

39. McManus, S. A.; Li, Y. "A Deoxyribozyme with a Novel Guanine Quartet-Helix Pseudoknot Structure." *J. Mol. Biol.* **2008**, *375*, 960–968.

40. Krasilnikov, A. S.; Xiao, Y.; Pan, T.; Mondragón, A. "Basis for Structural Diversity in Homologous RNAs." *Science* **2004**, *306*, 104–107.

41. Zappulla, D. C.; Cech, T. R. "Yeast Telomerase RNA: A Flexible Scaffold for Protein Subunits." *Proc. Natl. Acad. Sci. U. S. A.* **2004**, *101*, 10024–10029.

42. a) Chiuman, W.; Li, Y. "Evolution of High-Branching Deoxyribozymes from a Catalytic DNA with a Three-Way Junction." *Chem. Biol.* **2006**, *13*, 1061–1069; b) Shen, Y.; Chiuman, W.; Brennan, J. D.; Li, Y. "Catalysis and Rational Engineering of trans-Acting pH6DZ1, an RNA-Cleaving and Fluorescence-Signaling Deoxyribozyme with a Four-Way Junction Structure." *ChemBioChem* **2006**, *7*, 1343–1348.

43. Coppins, R. L.; Silverman, S. K. "A Deoxyribozyme that Forms a Three-Helix-Junction Complex with its RNA Substrates and has General RNA Branch-Forming Activity." *J. Am. Chem. Soc.* **2005**, *127*, 2900–2907.

44. Liu, J.; Lu, Y. "FRET Study of a Trifluorophore-Labeled DNAzyme." *J. Am. Chem. Soc.* **2002**, *124*, 15208–15216.

45. Robertson, M. P.; Scott, W. G. "The Structural Basis of Ribozyme-Catalyzed RNA Assembly." *Science* **2007**, *315*, 1549–1553.

46. Andersen, A. A.; Collins, R. A. "Intramolecular Secondary Structure Rearrangement by the Kissing Interaction of the *Neurospora* VS Ribozyme." *Proc. Natl. Acad. Sci. U. S. A.* **2001**, *98*, 7730–7775.

47. Nagel, J. H. A.; Pleij, C. W. A. "Self-Induced Structural Switches in RNA." *Biochimie* **2002**, *84*, 913–923.

48. Brown, T. S.; Chadalavada, D. M.; Bevilacqua, P. C. "Design of a Highly Reactive HDV Ribozyme Sequence Uncovers Facilitation of RNA Folding by Alternative Pairings and Physiological Ionic Strength." *J. Mol. Biol.* **2004**, *341*, 695–712.

49. Steiner, M.; Rueda, D.; Sigel, R. K. O. "Ca^{2+} Induces the Formation of Two Distinct Subpopulations of Group II Intron Molecules." *Angew. Chem.* **2009**, *121*, 9920–9924; *Angew. Chem. Int. Ed.* **2009**, *48*, 9739–9742.

50. Yamauchi, T.; Miyoshi, D.; Kubodera, T.; Nishimura, A.; Nakai, S.; Sugimoto, N. "Roles of Mg^{2+} in TPP-Dependent Riboswitch." *FEBS Lett.* **2005**, *579*, 2583–2588.

51. Zivarts, M.; Liu, Y.; Breaker, R. R. "Engineered Allosteric Ribozymes that Respond to Specific Divalent Metal Ions." *Nucleic Acids Res.* **2005**, *33*, 622–631.

52. Suo, Z.; Johnson, K. A. “RNA Secondary Structure Switching during DNA Synthesis Catalyzed by HIV-1 Reverse Transcriptase.” *Biochemistry* **1997**, *36*, 14778–11485; Paiva, A. M.; Sheardy, R. D.; “The Influence of Sequence Context and Length on the Kinetics of DNA Duplex Formation from Complementary Hairpins Possessing (CNG) Repeats.” *J. Am. Chem. Soc.* **2005**, *127*, 5581–5585.

53. Inoue, M.; Miyoshi, D.; Sugimoto, N. “Structural Switch of Telomere DNA by pH and Monovalent Cation.” *Nucleic Acids Symp. Ser.* **2005**, *49*, 243–244.

54. a) Pyle, A. M. “Ribozymes: A Distinct Class of Metalloenzymes.” *Science* **1993**, *261*, 709–714; b) Miyoshi, D.; Nakao, A.; Toda, T.; Sugimoto, N. “Effect of Divalent Cations on Antiparallel G-Quartet Structure of d($G_4T_4G_4$).” *FEBS Lett.* **2001**, *496*, 128–133; c) Li, W.; Miyoshi, D.; Nakano, S.; Sugimoto, N. “Structural Competition Involving G-Quadruplex DNA and Its Complement.” *Biochemistry* **2003**, *42*, 11736–11744.

55. Michel, F.; Westhof, E. “Modelling of the Three-Dimensional Architecture of Group I Catalytic Introns Based on Comparative Sequence Analysis.” *J. Mol. Biol.* **1990**, *216*, 585–610.

56. a) Soukup, G. A.; Breaker, R. R. “Allosteric Nucleic Acid Catalysts.” *Curr. Opin. Struct. Biol.* **2000**, *10*, 318–325; b) Roth, A.; Breaker, R. R. “Selection *In Vitro* of Allosteric Ribozymes.” Methods in Molecular Biology, Vol. 252: Ribozymes and siRNA Protocols (Ed.: M. Sioud), Humana, Totowa, 2004, pp. 145–164.

57. Corpet, F. “Multiple Sequence Alignment with Hierarchical Clustering.” *Nucleic Acids Res.* **1988**, *16*, 10881–10890.

Chapter 3: The *In-Vitro* Selections of Cd^{2+}-, Fe^{2+}-, and Fe^{3+}-Dependent DNAzymes

3.1 Note and Acknowledgements

This work was made possible through training by Dr. Debapriya Mazumdar and Dr. Nandini Nagraj. The Cd^{2+}-dependent DNAzyme selection is a continuation of work begun by Dr. Debapriya Mazumdar. Many thanks to Tian Lan, Dr. Ying He, Li Huey Tan, and Seyed-Fakhreddin Torabi for invaluable advice on this project. This project is being continued by Seyed-Fakhreddin Torabi.

3.2 Introduction

Heavy-metal-ion DNAzymes are intriguing on fundamental and application-oriented levels. While DNAzymes for many metal ions have already been selected, the periodic table offers an open frontier for further selections. No selection has yet successfully isolated DNAzymes selective for two oxidation states of the same element, and such a development would allow for the direct comparison of the analyte-binding pocket, and provide a deeper understanding of structural basis for DNAzyme selectivity.

3.2.1 Environmental Guidelines

This chapter presents selection attempts for DNAzymes dependent on Cd^{2+}-, Fe^{2+}-, and Fe^{3+}. All can be toxic at certain concentrations: the U.S. Environmental Protection Agency (EPA) has set a maximum contaminant level (MCL) of 0.005 mg/L cadmium in drinking water and a secondary standard of 0.3 mg/L iron in drinking water.[1] People regularly ingesting cadmium at or above the maximum contaminant level risk permanent kidney damage. The most likely sources of cadmium include industrial waste and leaching from natural sources.

3.2.2 Iron and Disease

Iron has a complex role as a biologically controlled substance with both beneficial and destructive qualities. The standard reduction potential for $Fe^{3+} + e^- \rightarrow Fe^{2+}$ is 0.771 V. This potential can be modulated by varying the protein bound to the iron ion. Iron superoxide dismutase with a reduction potential of +0.27 V, and ferredoxin with a reduction potential of -0.40 V show the broad range of protein-iron complexes' potentials, explaining their appearance in many vital cellular processes from the electron transport chain to oxygen

transport.[2] However, while these proteins require Fe^{2+} or Fe^{3+} for their activity, iron ions retain their activity, protein-bound or not. One reaction that iron participates in is the Fenton reaction, which produces reactive oxygen species: $Fe^{2+} + H_2O_2 \rightarrow Fe^{3+} + {}^{\bullet}OH + OH^-$ Thus, the very trait that makes Fe^{2+} and Fe^{3+} necessary in one environment makes them deadly in another environment. To prevent the production of reactive oxygen species through the Fenton reaction, the absorption, transport, and storage of iron in its various forms is carefully regulated.

No systematic excretion mechanisms exist for any iron species. Thus, iron ion absorption defects can rapidly lead to a diseased state, even if a person does not have a high rate of total iron ingestion or inhalation. Iron ions can have a causative or compounding role in disease. They can initiate the disease process, act as a promoting cofactor, or be abnormally deposited at a tissue site affected by another disease. Other diseases can interrupt the normal absorption of iron ions, causing abnormal and widespread iron loading. Iron ions participate in diseases affecting every organ system, from the nervous (Alzheimer's disease) to the cardiovascular (atherosclerosis), to the digestive system (viral hepatitis).[3] Once ingested, a significant amount of iron ions are reduced to the Fe^{2+} state and then rapidly absorbed across the apical membrane of epithelial intestinal enterocytes. Depending on the current total iron needs of the body, these incoming iron ions may be stored in this cell, or transported elsewhere. The excretion of iron ions by these cells is modulated by the protein exporter ferroportin and the peptide hormone hepcidin.[4] The cell transports and stores Fe^{2+} and Fe^{3+} as protein complexes. Transferrin can bind up to two Fe^{3+} ions, has a dissociation constant of 10^{-23}, and shuttles iron between cellular locations.[5] Ferritin binds and stores up to 4,500 Fe^{3+} ions intracellularly.

Even with these tightly regulated systems in place, some amount of non-protein-bound iron ions are present in the bloodstream and the cytoplasm. The concentration of these non-transferrin-bound iron (NTBI) ions has been measured at 0.3 ± 0.6 μM in the bloodstream,[6] and in the labile, intracellular pool the concentration of "free" iron may be as high as 11 μM in normal adults.[7] The exact chemical composition of this "free" iron ion population is not well characterized, but it is thought to contain ions bound to albumin as well as citrate and phosphate.[8] The average adult has approximately four grams of total iron in his body, but

patients with the iron-regulation disease hereditary hemochromatosis can collect as much as fifty grams of total iron during their lifetime. While three-quarters of iron ions are normally in an active role, with one-quarter in readily retrievable storage,[9] in an Fe^{2+}/Fe^{3+}-loaded individual, the physiological response to the influx of iron is to remove as much iron as possible from the bloodstream by depositing it in various tissues as ferritin complexes. Over time, these ferritin complexes can degrade, forming irretrievable hemosiderin deposits, which can be sources of free iron ions that can participate in the Fenton reaction.

3.2.3 Current Methods of Detecting Fe^0, Fe^{2+}, and Fe^{3+}

Iron deposits can be visualized by magnetic resonance imaging (MRI), due to the paramagnetic properties of Fe^{2+}/Fe^{3+}.[10] However, these images can only be obtained at advanced stages of the disease. Other changes can be detected earlier. In hemochromatic patients, the serum concentrations of transferrin and total ionic iron can increase as much as tenfold and fourfold, respectively.[11] This degree of change in the NTBI ion concentration is detectable by Fe^{2+}/Fe^{3+} sensors. Fe^{2+} or Fe^{3+} chromophores include bathophenanthroline,[12] ferene,[13] ferrocyanide,[14] ferrozine,[15] 3-{4-[2-(4-dibutylaminophenyl)vinyl]phenyl}-1-(4-[2,2':6',2'']terpyridin-4'-yl-benzyl)-3H-imidazol-1-ium bromide,[16] and tripyridyl-s-triazine.[17] Fe^{2+} and Fe^{3+} fluorophores include 3-hydroxypyridin-4-one,[18] AlexaFluor 488,[19] fluorescein-labeled apotransferrin,[20] calcein,[21] and phen green-SK.[22] Current clinical total blood iron tests do not distinguish between protein-bound and “free” ionic iron concentrations, nor do they retain any speciation information. Any protein-bound iron is removed from its protein carrier, and reduced or oxidized as a single pool for detection. While transferrin is not typically saturated even in iron-loaded individuals, there are cases when free iron is found in the bloodstream of patients whose transferrin is not saturated. Thus, Fe^{2+} and Fe^{3+} sensors can be used to determine the concentration and speciation of the “free” ionic iron population in the bloodstream, thus complementing the information currently available from a standard serum iron test. In addition, these sensors have real-time intracellular applications.

3.2.4 Limitations in Current Fe^{2+} and Fe^{3+} Detection Methods

Current Fe^{2+} and Fe^{3+} sensors are already being used in many different applications, but with significant limitations. Colorimetric sensors can be used for solution analysis and excised tissue staining, but not *in vivo* applications. Some iron sensors do not distinguish between Fe^{2+} and Fe^{3+}. Since transition metals quench fluorescence, many fluorimetric sensors for Fe^{2+}, or Fe^{3+} are "turn-off" sensors.[23] A challenge with "turn-off" sensors is that fluorescence quenching can be a nonspecific process. Also, there is currently no general method for the isolation of transition metal ion chromophores or fluorophores, which can delay an accurate understanding of the true toxicity of various oxidation states of the same element. One further limitation with current small molecule colorimetric sensors is that they may not be readily adapted to nanoparticle-based sensing. An attractive reason to use a nanoparticle-based approach is that the molar absorptivity of nanoparticles is four orders of magnitude higher than that of many colorimetric sensors. For example, the molar absorptivity of ferrozine is 28,000 $M^{-1}cm^{-1}$,[24] while the absorptivity of 13 nm gold nanoparticles is 2.7×10^8 $M^{-1}cm^{-1}$.[25] This substantially higher absorptivity can be used to produce a sensor with a lower detection limit. These limitations of small molecule sensors are due to the fact that their method of selection is not generalizable, and their analyte-detecting and signal-transducing moieties are usually one and the same. DNAzymes offer a solution on both points.

3.2.5 Benefits of DNAzyme-Based Sensing

DNAzymes are not prone to the denaturation that protein enzymes are susceptible to in the presence of heavy metals, extreme pH conditions, or thermal cycling. Also, DNAzymes offer a solution to the limitations faced by small molecule chromophores and fluorophores. For example, a DNAzyme selection strategy can be carried out for type of metal ion . Typically, no assumptions are made about the secondary or tertiary structures that a transition metal ion would require. DNAzyme-based sensors can be selected against either Fe^{2+} or Fe^{3+} by changing the incubation conditions for the random pool. Also, in a DNAzyme-based sensor, the detecting and transducing moieties are separate. Once a DNAzyme with preferred activity has been isolated, many different signal transducers can be used to report the cleavage of the DNAzyme in the presence of the analyte. The same molecular recognition event occurs in all cases; only

the transducer changes. In this way, the same DNAzyme can be the basis for a colorimetric or a fluorimetric sensor. Also, the fluorophore and quencher attached to a fluorimetric DNAzyme-based sensor can be tailored to a specific application, allowing for a broad range of wavelengths of excitation and detection. A DNAzyme-based fluorimetric sensor would be a "turn-on" sensor, since the fluorophore is released when the DNAzyme interacts with the otherwise quenching metal ion. For colorimetric sensing, a nanoparticle-functionalized uranyl DNAzyme-based sensor with a limit of detection of as low as 1 nM discernable by the naked eye has been developed.[26] This concept can be extended to other DNAzymes, as well. If this selection method produces DNAzymes that are capable of distinguishing between Fe^{2+} and Fe^{3+}, it could be extended to the various species of other transition elements. The bioavailability and toxicities of different forms of the same element can vary widely, yet much of the medical literature speaks only of the total concentration of a given element and its effects. DNAzymes specific for various species of the same element could address this.

3.2.6 *In Vitro* Selection

The process of selecting functional nucleic acids is termed "*in vitro* selection." One of the types of DNAzymes that is commonly selected for is the RNA-cleaving DNAzyme. Typically in the presence of a metal cofactor, the catalytic core of a RNA-cleaving DNAzyme enhances the rate of transesterification of a single RNA base in the substrate, as shown in Figure 3.1. A DNA pool design commonly used to select new RNA-cleaving DNAzymes is shown in Figure 3.2A, and the FeIIrCG pool is shown in Figure 3.2B. This pool hybridizes with itself, placing a random region opposite the single RNA base of the substrate. This random region is free to assume the secondary and tertiary structures necessary for its catalytic action. Selection rounds are carried out by incubating the random pool with analyte and isolating and purifying only those sequences that cleave in this environment (Figure 3.3). Primer-binding regions at the end termini of the random pool allow the sequence to be regenerated by polymerase chain reaction (PCR) after cleavage (Figure 3.4).

3.3 Materials and Methods

3.3.1 Materials

All DNA templates, primers, and markers were obtained from Integrated DNA Technologies (Coralville, IA) or TriLink Biotechnologies (San Diego, CA) in HPLC-purified form. Ultrapure ferrous ammonium sulfate and ferric chloride were obtained from Alpha Aesar (Ward Hill, MA). Chelex 100 sodium-form beads were obtained from Sigma-Aldrich (St. Louis, MO). All buffer and electrophoresis materials were obtained from Sigma-Aldrich, BIORAD (Hercules, CA), or the USB Corporation (Cleveland, OH). X-ray film for autoradiography was purchased from Eastman Kodak Co. (Rochester, NY). 250 μCi [α-^{32}P]-dATP and [γ-^{32}P]-ATP were obtained from Perkin-Elmer (Boston, MA). Platinum *Taq* DNA-polymerase, PCR-grade dNTPs, and T4 kinase were obtained from Invitrogen (Carlsbad, CA).

Millipore water was used to prepare all solutions. Any polypropylene tubes for the long-term storage of solutions, and all glassware were rinsed with concentrated nitric acid before use. Residual divalent cations in non-EDTA-containing solutions were removed by stirring 1 g of Chelex 100 beads in 100 mL of solution for five hours. Midget gas bubblers (7532-20) were obtained from Ace Glass, Inc. (Vineland, NJ). All selections were carried out at room temperature with either Cd^{2+} solution from a frozen-down stock or freshly prepared Fe^{2+} or Fe^{3+} solutions. Selections involving Fe^{2+} were carried out under N_2 or Ar in a glove bag using solutions and water samples that had been degassed under N_2 or Ar using a bubbler.

3.3.2 Methods

3.3.2.1 Pool Design

A previously developed, general *in vitro* method to isolate an analyte-dependent RNA-cleaving DNAzyme was the basis of these selection strategies. Since little is known about the preferred sequence and conformation of the DNA that would be active in the presence of Cd^{2+}, Fe^{2+}, or Fe^{3+}, a sizeable random region was incorporated into the DNA sequence to increase the probability of secondary structure forming. With a random region of fifty bases, there are 4^{50} or 1.27×10^{30} different sequences possible, though only a portion of this sequence space was

interrogated by this selection method. This is not necessarily problematic, however: DNAzyme motifs are often much less than 50 nt., and thus could appear multiple times in each pool.

Because selections are time-consuming, efficiency is a necessity. Figure 3.5 shows some of the various approaches possible. Figure 3.5A shows a single pool being used with a metal soup. This method has the benefit of selecting DNAzymes for multiple analytes simultaneously, but Fe^{2+} and Fe^{3+} selections present a unique problem. Because iron can interchange between the two oxidation states, it can be difficult to design a selection buffer that stabilizes both. Thus this method was decided against. Using a single pool for distinct selections can cause cross-contamination, if these selections are carried out at the same time. Thus, a single pool could be used for sequential selections (Figure 3.5B). This method is time-consuming, however, so alternate pools were designed and used in parallel (Figure 3.5C).

When designing a pool, the cleavage site and the overall folding were vital factors. The cleavage site is the dinucleotide junction between the RNA nucleotide to be cleaved, and the 3'-adjacent deoxynucleotide. The Yingfu Li lab has compared the characteristics of pools with all sixteen of the possible dinucleotide cleavage junctions,[27,28] and these results are summarized in Figure 3.6. Two of the characteristics compared were the rate of cleavage of pools with various dinucleotide junctions and these pools' propensity for developing the 8-17 DNAzyme motif. The 8-17 DNAzyme motif is a relatively small motif that has been isolated in *in vitro* selections in many different laboratories. It can be undesirable because it is often susceptible to Pb^{2+}-dependent cleavage.

As shown in Figure 3.6A, the various families of dinucleotide junctions produced regular patterns of activity, with the NG family showing the highest observed cleavage rates. Many of the pools also showed a high percentage of 8-17 motifs (Figure 3.6B). To compare these properties, the 8-17 percentage versus the observed rate of cleavage was plotted against one another (Figure 3.6C). This plot revealed a bimodal distribution, with more rapidly cleaving pools having a higher percentage of 8-17 motifs, and less rapidly cleaving pools having a lower percentage of 8-17 motifs. To select a dinucleotide junction which had a lower likelihood of producing the 8-17 motif (and thus potential Pb^{2+} sensitivity) while preserving a rate of activity,

the 5'-rCG-3' dinucleotide junction was selected (the filled square in Figure 3.6C). This dinucleotide junction was used for all Fe^{2+} and Fe^{3+} pools.

The further design of the pool involved its secondary structure, which was assessed by mfold, a DNA analysis tool that uses thermodynamic analysis to predict internucleotide interactions.[29] In this way, sequences giving rise to many undesirable formations could be discarded. The two desired binding arms were designed first, then a random sequence was generated for the remaining areas of the random pool. The random pool was then analyzed by mfold. Multiple predicted secondary structures were commonly obtained, but if the most stable structure formed did not have the desired binding arms, the sequence was modified and reanalyzed by mfold. The resulting secondary structures predicted by mfold are shown in Figure 3.7. The primers were also analyzed to ensure that they did not readily form hairpin loops.

The DNA used to form the final pools is shown in Table 3.1. Geng rCT, the pool used in the Cd^{2+} selection, was designed by Geng Lu, a previous group member. The FeIIrCG Pool and Gel Pool 1 and Gel Pool 2 were designed by the method explained herein. These pools have template and primers with identical lengths but unique sequences. With several pools available, multiple selections could be carried out in parallel. The two modifications used in these selections, Spacer 18 and biotin, are shown in Figure 3.8. The randomized markers used to gel purify the desired bands are shown in Table 3.2.

3.3.2.2 Experimental Conditions

The pool was constructed and purified by a method similar to that described by previous group members,[30] though some selection approaches varied the PCR annealing temperate, number of PCR cycles, and means of extraction. The pool was generated from three primers (forward primers P2 and P3 and reverse primer P4) and a template strand. To construct a pool, 210 pmoles of template, 990 pmoles of primer P3, and 1540 pmoles of primer P4 were used in two steps of polymerase chain reaction (PCR). The 210 pmoles of template are capable of producing up to 1.26×10^{14} sequences. The resulting 117-mer random pool was isolated on a 10% denaturing polyacrylamide gel electrophoresis (PAGE) gel, and run against γ–labeled DNA markers of equal length as the random pool and the cleaved pool. The resulting gel was imaged by autoradiography using X-ray film (during early selection approaches) or by exposure to a

phosphorscreen (during later selection approaches). When a phosphorscreen was used, it was scanned with an Amersham Biosciences Molecular Dynamics Storm 430 phosphorimager (Molecular Dynamics). A paper triangular marker was made radioactive, enclosed in plastic, and used to align the gel and the image so that the desired band could be excised.

The pool was extracted from the gel into soak solution (10 mM Tris, 1 mM $Na_2EDTA•2H_2O$, 300 mM NaCl, pH 7.5). It was then ethanol precipitated and lyophilized.

The pool was reconstituted in 2X selection buffer, denatured and annealed by heating to 95 ˚C, then slowly cooled to room temperature over the course of thirty minutes. To initiate a round of selection, an equal volume of 2X transition metal ion solution was mixed into the reconstituted DNA solution for a final reaction volume of 100 μL, and the selection was allowed to progress for 5 hours at room temperature. For Fe^{2+} and Fe^{3+} selections, in early approaches the pool was reconstituted and mixed with 2X metal solutions; in later approaches, the pool was reconstituted in 1X selection buffer, to which metal solutions 1X in selection buffer and 2X in metal concentration were added.

To stop a selection round, an equal volume of stop solution (8 M urea, 50 mM $Na_2EDTA•2H_2O$, and 1X TBE) was added to the selection solution. The cleaved pool was then purified by the same method as the originally generated pool. This cleaved pool, which is made up of the "winners" from that round of selection, was then regenerated through PCR. 40 pmoles of P2, 50 pmoles of P3, and 65 pmoles of P4 were added to the cleaved pool in a two-step PCR process made up of elongation (where the RNA-base-containing arm is reintroduced to the cleaved pool), and amplification (where the regenerated pool is produced in abundance) was carried out. The PCR products were purified by the same method as the original pool. The next rounds of selection will then take place, by the same method as described above.

Kinetic assays were carried out by γ-labeling P3, and using the resulting P3* to radiolabel the pool at a given round by performing PCR-2* and gel purifying it. After extraction, instead of ethanol precipitating the PCR-2* product (the radiolabeled pool from that round), it was purified by Sep-pak and lyophilized. To perform an assay, the PCR-2* product was reconstituted in selection buffer containing all but the target analyte. The radiolabeled pool was denaturated and annealed over a thirty-minute time period, first by heating to 95 °C, then cooling to room

temperature over the course of 30 min. It was then mixed with freshly prepared Fe^{3+} solution to initiate the reaction. Five-microliter aliquots of the reaction solution were mixed with stop solution to quench the reaction at appropriate time points (typically spaced between 0 and 5 h.). The reactions were then purified on a 20% denaturing PAGE gel and exposed to a storage phosphorscreen. Cleavage products were visualized and intensities were background subtracted by a phosphorimager. The cleavage efficiency was calculated at time *t* using the following equation: $y = 100 * [I_c / (I_u + I_c)]$, where *y* is the percent cleaved product, I_c is the intensity of the cleaved substrate and I_u is the intensity of the uncleaved substrate

3.4 Results

The selections undertaken are summarized in Table 3.3. Multiple variations were implemented, including changing the selection buffer, pH, PCR annealing temperature, number of PCR cycles, negative selections, and using a gel- or column-based pool.

The PCR results from some selections were extremely stable, in some cases for up to twenty-seven rounds. In other cases, the PCR results were unpredictable. One example of the latter case was seen in the Fe^{3+} selection shown in Figure 3.9.

Because PCR had such a profound effect on the progress of a selection, several variations in this area were made. One systematic study was performed to optimize the PCR annealing temperature and number of PCR cycles. The results are shown In Figures 3.10-3.13 and summarized in Table 3.4. A lower annealing temperature was found to increase the abundance of products, but lower the PCR stringency. Higher annealing temperatures were found to increase the stringency of PCR, and decrease the abundance of products.

To examine the metal-ion dependence of the FeIIrCG pool after various rounds of Fe^{3+} selection, kinetic assays with 10 mM of a suite of metal ions were performed. The results are shown in Figure 3.14-3.17. The pool was found to be inactive in the presence of metal ions other than Pb^{2+}, and to increase in activity in the presence of Pb^{2+} over the course of the selection.

3.5 Discussion

3.5.1 Choice of Selection Buffer

The selection buffer may be the single most important aspect of a selection, especially in the case where the metal ion is inherently unstable due to solubility or oxidation vulnerabilities. Its role is to stabilize the analyte of interest and to some degree simulate the sample matrix where it will be used. Selecting DNAzymes for Fe^{2+} and Fe^{3+} has a twin set of challenges: solubility and stability. Selection conditions should be as similar to the application conditions as possible, thus selections were begun at pH 7. Fe^{2+} is readily soluble at this pH, but it also readily oxidizes. Fe^{3+} is more stable to air oxidation at pH 7, but is also nearly insoluble. Carrying out a selection at a lower pH would help stabilize Fe^{2+}, but also is problematic because this is not the pH a Fe^{2+}-dependent DNAzyme would be used at biologically. Because pH had such a significant effect on Fe^{2+} stability, selections were attempted at pH 6 and pH 7. Fe^{3+} was solubilized by incorporating citrate into the selection buffer at twice the concentration of Fe^{3+}. Citrate itself introduces another level of complexity into the selection because iron chelated by citrate complexes may or may not be highly available for interactions with potential DNAzymes.

Another variation in the selection buffer was the inclusion of Mg^{2+}. Mg^{2+} is known to stabilize the secondary structure of DNA, but this divalent cation was originally absent from selection buffers so that it would not compete with Fe^{2+}. In the final Fe^{3+} selection approach, however, it was present.

3.5.2 PCR Variations

One point of considerable variation was the number of PCR cycles used to generate or regenerate the pool. The pool was designed to require PCR at both these steps. PCR is needed to generate the pool because the template is a slightly truncated complement to the desired pool: synthesizing an intact pool would reduce its stability and increase the uncertainty of its sequence because it includes an RNA nucleotide and its length is greater than 100 nt.

Because extraction is not 100% efficient, it is necessary to have more than one copy of each sequence. At the same time, there should not be too many PCR cycles. An excessive number of PCR cycles would bias the pool toward those sequences favored by PCR, instead of

those who are active in the presence of the target. In early selection approaches, ten rounds of PCR-1 and thirty rounds of PCR-2 were performed. In later approaches the number of cycles were optimized at each step. In the final selection approach, ten cycles of PCR-1 and PCR-2 were performed.

RT-PCR trials were carried out to determine whether undesirable PCR products could be eliminated. Two important variables in PCR are the annealing temperature and the number of PCR rounds. Based on a literature precedent, the annealing temperature was varied through a "step-down" protocol. The results decreased the side-products, but were also found to decrease the desired products to an unacceptable degree.

Molecular biology is trending toward miniaturization. Thus, while an older PCR thermocycler used in this lab could easily process 100 µL reaction volumes, a newer model had guaranteed results only through 50 µL reaction volumes. Thus, PCR volumes were reduced in later selection approaches.

In earlier approaches the lyophilized, regenerated pool was reconstituted in 60 µL and 30 µL were taken to the next step. In later approaches, the pool was reconstituted in 100 µL and 20 µL were used for PCR-1. The change was made in order to preserve more of the stock solution that was frozen down as a stock solution. The amount of template was kept within an order of magnitude, and the amplification of the pool was not negatively affected.

In early approaches, when PCR variations were attempted on the prep-scale, the entire pool was treated in the same way, and carried on to the next selection step as long as the pool regenerated. Over time, this was found to be an inefficient method. Instead, several 20-µL reactions were attempted at the same time, gel-purified on a larger gel, and compared. This allowed for more rapid PCR optimization, and a minimization of variations, since all the samples were compared on the same gel. This made comparing the simultaneous effects of altering the annealing temperature and number of PCR cycles much more efficient.

Much of the time spent in the course of these selections was spent optimizing PCR. This is partly due to the large number of PCR rounds attempted in many of the approaches before trying a different strategy. In the future, it may be more realistic to determine a reasonable number of PCR rounds to attempt for a given selection, instead of doing countless cycles of

PCR. When a selection has progressed for twenty-seven rounds without yielding the desired result, it is likely that conditions other than PCR need to be altered.

3.5.3 Negative Selections

Negative selections can be introduced into selections to remove DNAzymes active in the presence of interferents. In a negative selection, the pool is incubated with a potential interferent and after gel purification the cleaved pool is discarded and the uncleaved pool is retained. This may be especially helpful when perennial interferents have been identified. For example, as described in Chapter 2, enzymes active in the presence of Co^{2+} often are crossreactive with Zn^{2+}. When selecting a Co^{2+}-dependent DNAzyme, previous lab members wanted a DNAzyme with little cross-reactivity for Zn^{2+}; thus, in one selection negative selections against Zn^{2+} were performed. It should be noted that no parallel selections comparing the results from positive and negative selections have been carried out to directly compare the utility of incorporating negative selection rounds.

For the selections described here, negative selections were only used in the first selection approach. This was done because a negative control showed that the pool was cleaving in the presence of the selection buffer with no Fe^{3+}. A negative selection was performed against the selection buffer. In later approaches negative selections were not employed because the overall activity of the pool was low and it was deemed more prudent to preserve sequences that could still potentially show Fe^{3+} dependence and assay crossreactivity later.

3.5.4 Selection Pressures

Theoretically, several selection pressures can be applied to increase the stringency of the final pool. The most common selection pressures are time and concentration. At the beginning of a selection, when sequence diversity is the highest, the selection conditions may be relatively gentle: the selection round may be allowed to progress for 5 hours, and the concentration of target analyte may also be high.

Through the course of selection, these parameters can be reduced. This allows inactive or marginally active sequences to be removed while more desirable DNAzymes with high

affinity and activity are retained. These parameters were not used widely in these selections, because selection rounds typically showed minimally active populations. One approach did reduce the reaction time, from an initial 5-h. selection to a 30-min. selection. Unfortunately, as with other selections, there was very little cleavage activity overall.

3.5.5 Gel- and Column-Based Selections

Because selections are often time-consuming, efficiency is paramount. One method with a more rapid turnaround is column-based selection. This approach 5'-biotinylates the random pool, which allows it to be immobilized on a streptavidin column. As this columns is washed with various solutions, selection rounds can be carried out. Once standard practice in this lab, column-based DNAzyme selections fell into disuse because of the reduced amount of feedback: while gel-based methods allow the state of the pool to be rapidly assessed at each round, column-based methods provide no such feedback.

The increased speed of each selection step, however, was a motivating factor in designing a column-based pool. Gel Pool 1 was modified for use with a column by 5'-biotinylating P3 to produce P3b, and removing the $(AAC)_{12}$ and Spacer 18 regions from P4 to produce P1, and ordering the 5'-biotinylated P1 sequence called P1b (Table 3.1).

The column-based method was ultimately unsuccessful in these selections, because of the production of large molecular weight complexes. These complexes were most readily apparent on electrophoresis gels after PCR-2. Since the identity of these complexes was not ascertained, and they appeared in two different approaches which used different concentrations of Fe^{3+}, future column-based methods were not pursued in these selections.

3.5.6 Purification Method

Because of the large number of side-products formed during PCR, one selection approach gel-purified the pool after PCR-1 and after PCR-2. Ultimately, this method was abandoned because of the increased amount of time involved.

3.5.7 Imaging Techniques

Early selection approaches imaged prep-scale electrophoresis gels with X-ray film, using phosphorscreens only for kinetic assay gels which would be quantified. While easier to directly

align than images obtained from phosphorimager screens, X-ray film was less sensitive and more costly than other alternatives. Later approaches used phosphorscreens for both qualitative and quantitative gels. An added benefit to this switch was the lesser amount of time needed to image a gel. One implication of the new method was that phosphorimaging scales the entire image based on the most intense area; this makes it more challenging to process samples with varying degrees of radioactivity. Overall, the new method increased the reproducibility of results: the X-ray film developer was poorly maintained and gels were often incompletely fixed. Phosphorimaging also made the quantification of results routine instead of extraordinary, which heightened the ability to assess trends.

3.5.8 Extraction Method

Various methods of extracting the pool from the electrophoresis gel have been attempted. The first changes were simply to extraction time: the first approach was two extractions, each extraction consisting of rocking the excised band in 1 mL of extraction buffer for at four hours at room temperature. In later steps the extraction time was reduced to two 2-h. extractions. The latest change was much more efficient: after a single 1-h. rocking extraction at room temperature, the gel and extraction solution were placed at -80 °C and sonicated for 10 minutes. The extraction solution was then removed from the gel.

Definitive studies comparing the extraction efficiencies of each of these methods were not performed, but, for example, the last selection approach used this last extraction method exclusively and was able to see consistent amplification results.

3.5.9 Activity Assay Conditions

For the activity assays with the Fe^{3+}/citrate pool, it was important to remember that citrate also complexes other metal ions beside Fe^{3+}. In order to see if the pool was sensitive to these other metal ions, it was decided to carry out activity assays in the presence of other metal ions without citrate in the solution. It would have been best to use a solution buffered as the citrate solution was, but just not containing citrate, but this option was unfortunately not considered while doing the activity assays.

3.5.10 Common Sources of Error

A common source of error in selections is a mistake in designing or ordering DNA. Two examples that occurred in the course of these selections involved ordering an incomplete template, and ordering the reverse complement of a primer. To safeguard against such time-consuming errors, our lab instituted a "double-check" rule so that every strand of DNA ordered is looked over by two people before being ordered. Another standard practice is to perform mass spectrometry on all new DNA orders to ensure that their size corresponds to that ordered.

3.6 Conclusions and Future Directions

The selections described here were ultimately unsuccessful in isolating Cd^{2+}-, Fe^{2+}-, or Fe^{3+}-dependent DNAzymes. The Cd^{2+} pool amplification was unstable over time, showing many bands beyond those expected, and a gradual reduction in the length of the pool. The pools designed for Fe^{2+} and Fe^{3+} selections were more stable, but still produced no DNAzymes with the desired activities.

Seven major Fe^{2+} and Fe^{3+} selection attempts were carried out, in which the selection buffer, pH, PCR annealing temperature, number of PCR cycles, negative selections, pool type, and other conditions were varied. Over time, an increase in Pb^{2+}-dependent cleavage was observed. Pb^{2+} is not likely to be present at significant concentrations in the biological environments where Fe^{2+}/Fe^{3+}-dependent DNAzymes would be used. Thus the Pb^{2+} dependence of these selected pools is less concerning than the absence of Fe^{3+} dependence. Millipore water was used for all selections, but as a precaution, a representative sample was tested for lead by ICP-MS. The results showed no appreciable concentrations of lead. The increased Pb^{2+} dependence may then be simply due to an enrichment of the 8-17 motif in the pool, since the 8-17 motif is notoriously sensitive to Pb^{2+}. Though the cleavage site chosen for these selections had a reduced probability of forming this motif, it did not eliminate the possibility of its becoming abundant. Also, the activity of the 8-17 motif can cause it to predominate in a pool.

Given the lack of success in these attempts, a paradigm shift may be in order. The selection buffers for Fe^{2+} and Fe^{3+}may need to be significantly altered; one possible reason for the lack of positive results is that the Fe^{3+}/citrate complex is not accessible to the DNA. The pool

design may also need to be significantly altered so that reaction types beyond simply RNA-cleavage are assayed. Real-time PCR (RT-PCR) can also be implemented to analyze the efficiency of amplification. This will allow for rapid optimization without the costly requirement of running two analytical and one preparative-scale gels during each PCR step. These modifications should improve the outcome and efficiency of selections.

Once Cd^{2+}-, Fe^{2+}-, and Fe^{3+}-dependent pools are observed and their activity has stabilized, a representative aliquot from each pool will be sequenced. Families of related sequences will be determined, and the activity of representative examples from each family will be compared in the presence of the target analyte and likely interferents. If the activities of the sequences are low, these sequences will be the basis of a reselection. If the activity of a sequence or multiple sequences is adequate, the DNAzyme will be converted into a sensor. The sequence will be truncated to remove the primer-binding regions and extraneous bases in the random region, isolating the enzyme's catalytic core. After each successive truncation, the sequence's activity will be assessed to assure no loss of function. The melting temperature of the substrate and enzyme strands will be evaluated by absorption spectroscopy.

The transducing moiety will be specific for each application. Nanoparticle-based colorimetric sensors will be developed for a liquid-phase or dipstick analysis of drinking water, soil extracts, and blood samples. Intracellular fluorescent sensors will be developed for visualization in living cells. Fluorescent sensors for non-protein-bound Fe^{2+} and Fe^{3+} would allow for the detection of dynamic changes in the ratio of these two ions in a single cell, and the determination of the electrode potential at given locations in the cell. If used in conjunction with a fluorescent hydrogen peroxide sensor such as mitochondria peroxy yellow 1,[31] Fe^{2+}/Fe^{3+} sensors could also visualize the Fenton reaction occurring in the cell.

3.7 Figures and Tables

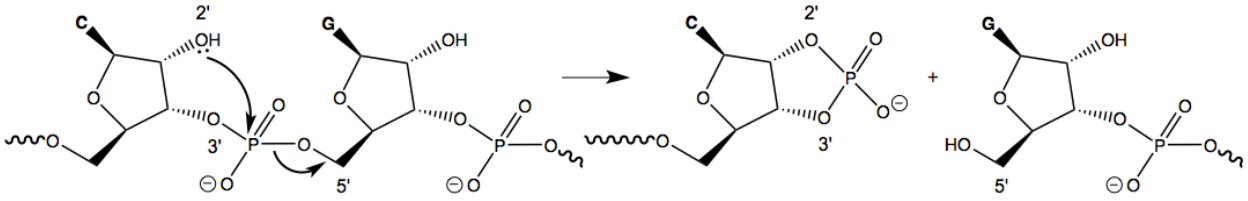

Figure 3.1. Transesterification, the reaction RNA-cleaving DNAzymes catalyze. A 5'-rCG-3' cleavage junction is shown.

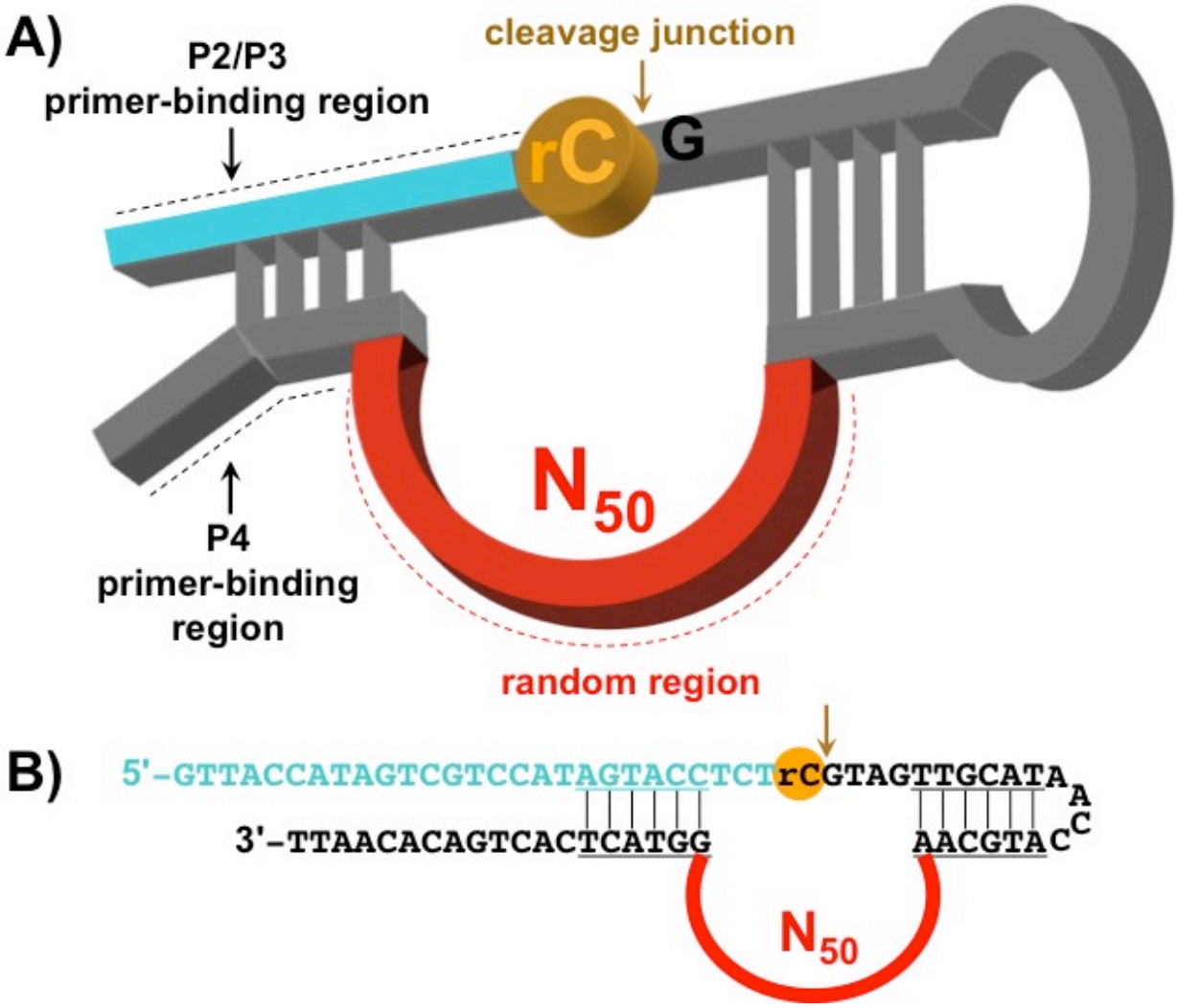

Figure 3.2. *In vitro* selection pool design. A) A generic RNA-cleaving DNAzyme with an N_{50} random region. B) The FeIIrCG random pool.

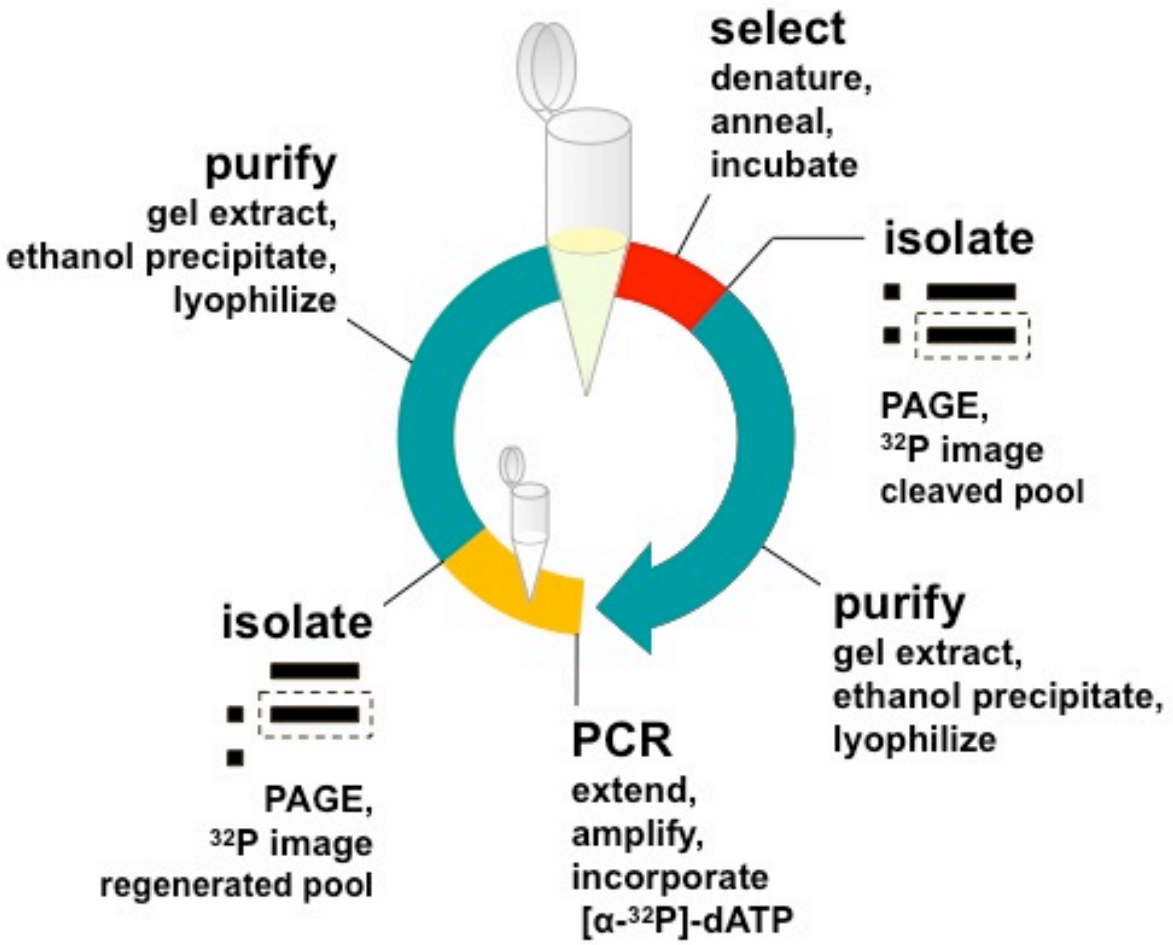

Figure 3.3. Overview of *in vitro* selection. *In vitro* selection is a cyclical process of polymerase chain reaction (PCR) followed by selection rounds, with purification in between. The images shown in the isolation step is an idealized image from polyacrylamide gel electrophoresis (PAGE). The small squares to the left of each band are the 90- and 118mer markers for the regenerated band and cleaved pool, respectively. The dashed rectangle shows the excision of the desired band for that step.

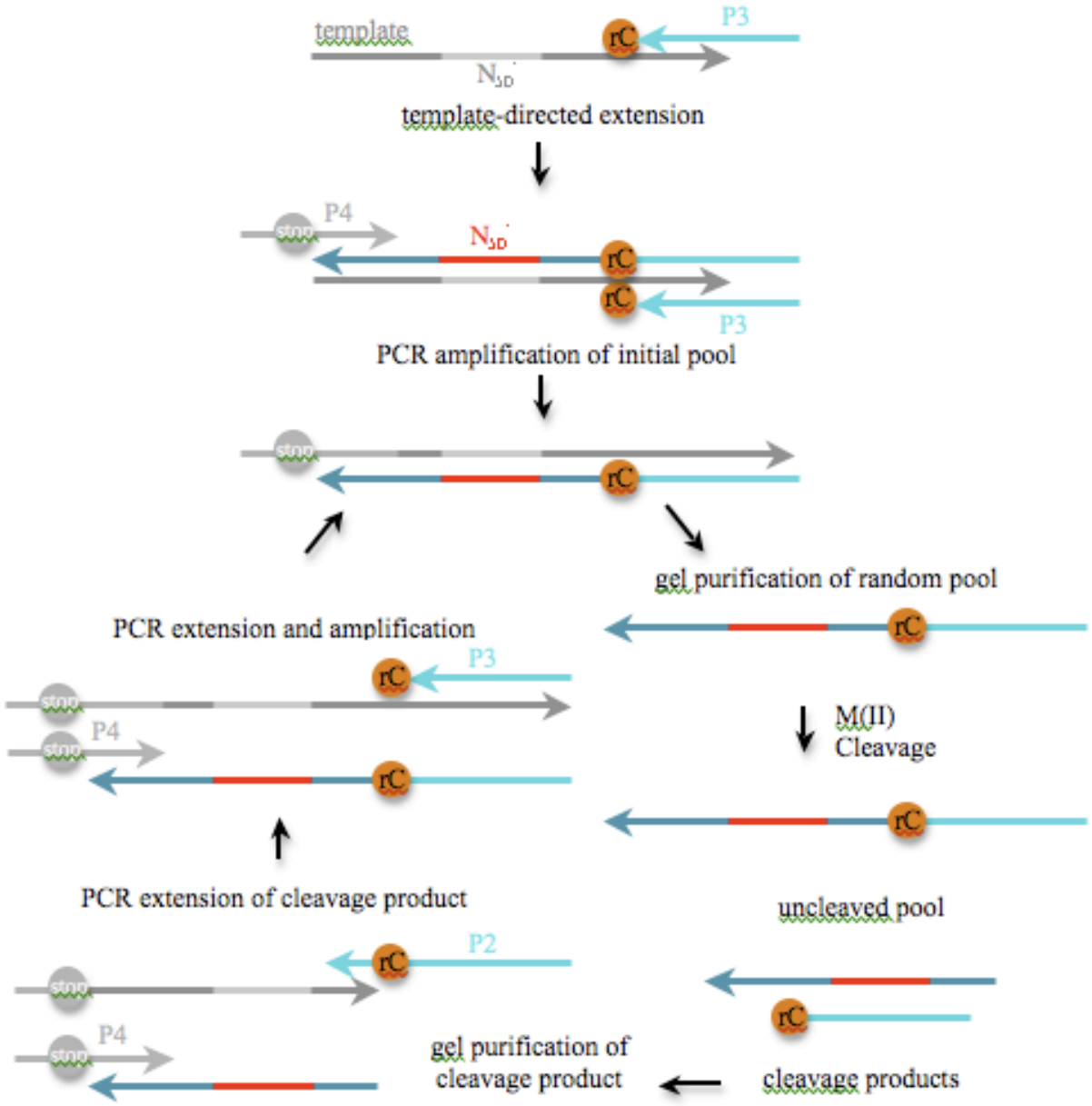

Figure 3.4. The generation and regeneration of the random pool by polymerase chain reaction (PCR). Three primers and a template are required. Primers P3 and P2 contain the same initial portions as the pool. They are simply different lengths: P3 ends at the ribonucleotide and binds to the complement of the uncleaved pool. P2 contains nucleotides after the ribonucleotide as is used with the complement of the cleaved pool. The template is the reverse complement of the pool, and is also ten nucleotides shorter than the pool. During the generation of the pool, P3 binds to the template, and as it is extended introduces the RNA base into the pool and provides the ten remaining nucleotides. P4 is complementary to the random pool and amplifies it. Because P4 contains a Spacer 18, or "Stop *Taq*" sequence, the complementary pool can be distinguished from the pool by gel electrophoresis. The pool is purified and used in a selection round. The cleaved pool is isolated and purified and taken on to a pool regeneration step. During pool regeneration, P4 produces the reverse complement of the cleaved pool. P2 then binds to this reverse complement and produces the regenerated pool which is amplified by P3 and P4. As with the generation step, because of the Spacer 18 in P4, the complementary pool can be distinguished from the pool by gel electrophoresis.

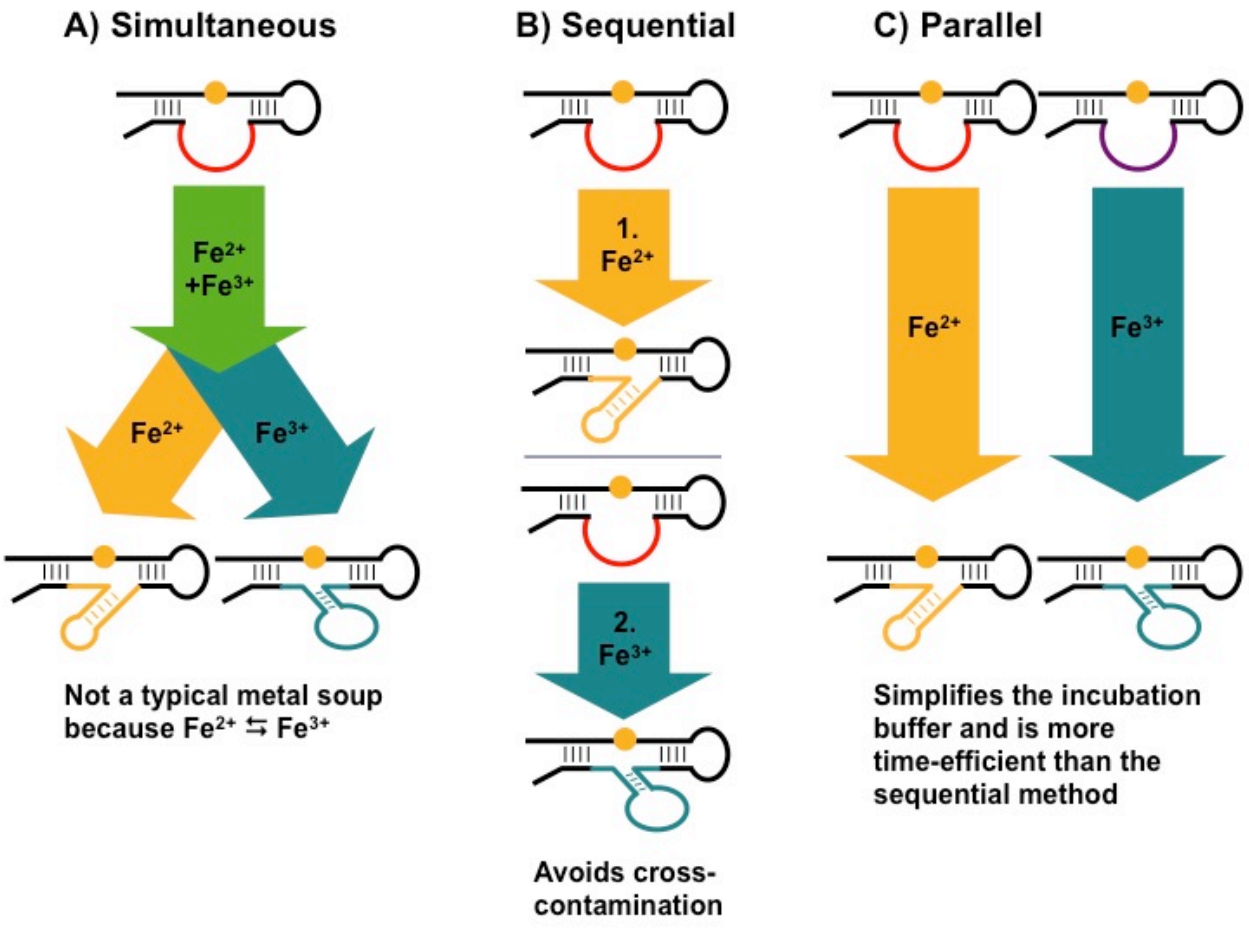

Figure 3.5. Selection types. A) Two or more DNAzymes are selected simultaneously using the same pool and a metal soup. B) The same pool is used to select two DNAzymes, but the selections are done sequentially. C) Two distinct pools are used concurrently to select two unique DNAzymes.

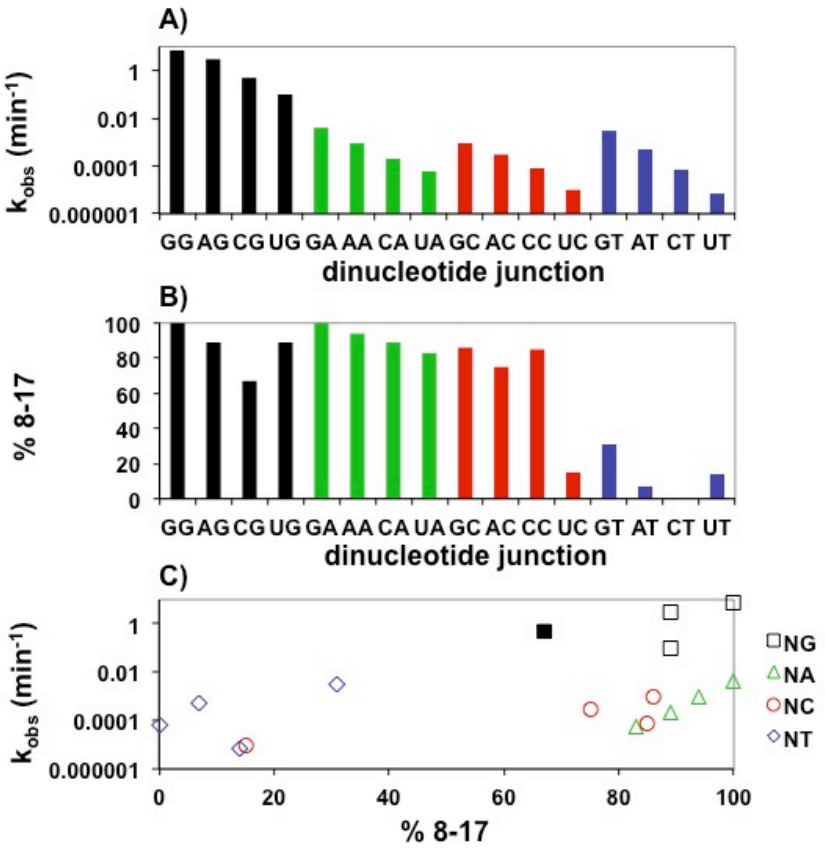

Figure 3.6. The properties of pools with various dinucleotide junctions. The junctions are listed from 5' → 3', with the ribonucleotide written before the dinucleotide. A) The variation in the observed rate of cleavage with dinucleotide junctions. B) The variation in the percent 8-17 DNAzyme motif with the dinucleotide junction. C) A combination of A) and B) showing the variation of % 8-17 motif with the overall activity of each pool. The classes of dinucleotide junctions are show with a closed square being the CG junction chosen for the Fe^{2+} and Fe^{3+} pools, open squares for the rest of the NG family, an open triangle for the NA family, an open circle for the NC family, and an open diamond for the NT family. This data is adapted from refs. 27 and 28.

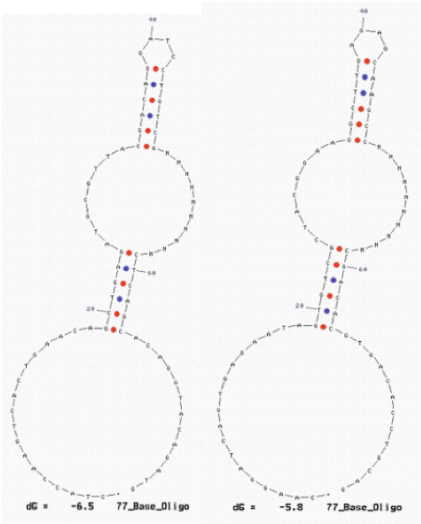

Figure 3.7. Secondary structures of Gel Pools #1 and #2, as predicted by mfold.

Pool	Name	Length (nt).	Sequence (5'→3')
Geng rCT Pool	Template	107	CTCGGATCCATACCCTGAAN_{50}'GACAACGAGGGTTGTCTGTCTATCTTCAGGTGATCTAG
	Primer 2 (P2)	43	GAATCACCTACTAGATCACCTGAAGATrCGACAGACAACCCTCG
	Primer 3 (P3)	28	GAATCACCTACTAGATCACCTGAAGATrC
	Primer 4 (P4)	51 + spacer	$(AAC)_{12}$**-Spacer18-**CTCGGATCCATACCC
	Random Pool	117	GAATCACCTACTAGATCACCTGAAGATrCGACAGACAACCCTCGTTGTCN_{50}TTCAGGGTATGGATCCGAG
FeIIrCG Pool	Template	107	AATTGTGTCAGTGAGTACCN_{50}'TTGCATGGTTATGCAACTACGAGAGGTACTATGGACGA
	P2	43	GTTACCATAGTCGTCCATAGTACCTCTrCGTAGTTGCATAACCA
	P3	28	GTTACCATAGTCGTCCATAGTACCTCTrC
	P4	51 + spacer	$(AAC)_{12}$**-Spacer18-**AATTGTGTCAGTGAG
	Random Pool	117	GTTACCATAGTCGTCCATAGTACCTCTrCGTAGTTGCATAACCATGCAAN_{50}GGTACTCACTGACACAATT
Gel Pool 1	Template	107	CATCTGTACCTGTCGTGAGN_{50}'CGACAGGATCCTGTCGTAACGCATCTCAGCTGTTCAGT
	P2	43	CTACCAAGTCACTGAACAGCTGAGATGrCGTTACGACAGGATCC
	P3	28	CTACCAAGTCACTGAACAGCTGAGATGrC
	P4	51 + spacer	$(AAC)_{12}$**-Spacer18-**CATCTGTACCTGTCG
	Random Pool	117	CTACCAAGTCACTGAACAGCTGAGATGrCGTTACGACAGGATCCTGTCGN_{50}CTCACGACAGGTACAGATG
Gel Pool 2	Template	107	CTGCAGGTGTCACGTGTCGN_{50}'GGCTTGTCTCCAAGCCCTTCGTAGCGACACTATTCTCA
	P2	43	CAAGGATCAGTGAGAATAGTGTCGCTArCGGAAGGCTTGAGAGC
	P3	28	CAAGGATCAGTGAGAATAGTGTCGCTArC
	P4	51 + spacer	$(AAC)_{12}$**-Spacer18-**CTGCAGGTGTCACGT
	Random Pool	117	CAAGGATCAGTGAGAATAGTGTCGCTArCGAAGGGCTTGGAGACAAGCCN_{50}CGACACGTGACACCTGCAG
Gel Pool 1 (add'l primers needed for column selection)	P1	15	CATCTGTACCTGTCG
	P1b	Biotin + 15	**Biotin-**CATCTGTACCTGTCG
	P3b	Biotin + 28	**Biotin-**CTACCAAGTCACTGAACAGCTGAGATGrC

Table 3.1. *In vitro* selection DNA. The template and primers were ordered, and used to construct the random pool. The spacer incorporated into P4 was "Spacer 18" is a PEGylated spacer; see Figure 3.%%%A for more information. Underlined sequences are regions where the pool hybridizes with itself in its final conformation. *N* is any nucleotide, with an equal probability of being G, C, T, or A.

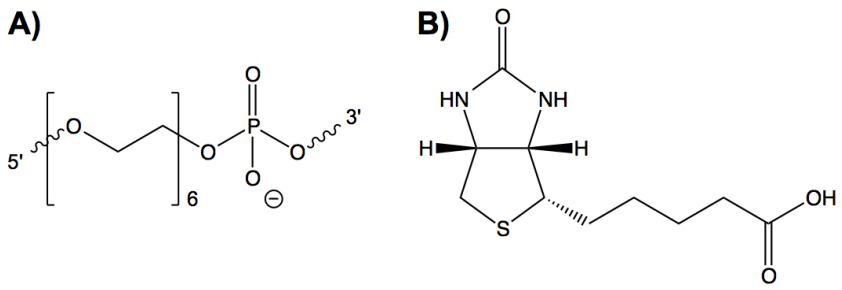

Figure 3.8. DNA Modifications. A) Spacer 18 from Integrated DNA Technologies used to internally modify P4. It is an 18-atom hexaethyleneglycol spacer, and the longest modification IDT offers for a single base. B) Biotin, used to 5'-modify primers P1 and P3 for column selections.

Name	Length (nt.)	Sequence (5'→3')
90mer Marker	90	ATA GCT AGC TTA GGT ACT CTA GCT GTC AGT CGA TCT ATA CTG CTA CTA CTA GCT CTA GCT CAT CGC TAG CTA CGT ACG TAC GTG CTA CGT
118mer Marker	118	ATG CGA TTG CCG GCT GCT ACT CAT GCT CAT GCC AAT TCT AGG TAC TCT AGC TGT CAG TCG ATC TAT ACT ATT AGG TGT AGC TCT AGC TCA TTA GAA GTT AGG TAT CTA CTT GGT TCG T

Table 3.2. Markers used for *in vitro* selection. Due to an arithmetic mistake when counting the number of nucleotides in the random pool, the 118mer Maker is one nucleotide longer than the random pool.

Approach	Ion	Pool	pH	Other Conditions	Results
C1	Cd^{2+}	Geng rCT Pool	7	10 cycles of PCR-1, 30 cycles of PCR-2	the PCR products were too unpredictable for further work
F1*	Fe^{3+}		7	"	taken to R-27; no increase in Fe^{3+}-dependent activity noted
F2	Fe^{2+}		7	"	solution oxidized too rapidly for stable selection conditions
F3	Fe^{2+}		6	"	complexes impeded selection progress
F4	Fe^{2+}		7	"	complexes impeded selection progress
F5	Fe^{3+}		7	"	no increase in Fe^{3+}-dependent activity noted
F6	Fe^{3+}		7.4	optimized number of PCR cycles at each step; used 50 µL PCR volumes; gel-purified after PCR-1 and after PCR-2	no increase in Fe^{3+}-dependent activity noted, and approach was too time-consuming
F7	Fe^{3+}		7.4	10 cycles of PCR-1, 10 cycles of PCR-2; used 50 µL PCR volumes	taken to R-12; no increase in Fe^{3+}-dependent activity noted

Table 3.3. Fe^{2+} and Fe^{3+} *in vitro* selection approaches attempted **. *** While F1 is listed as if it was a single selection, it was actually made up of many fits and starts. All PCR volumes were 100 µL unless otherwise noted.

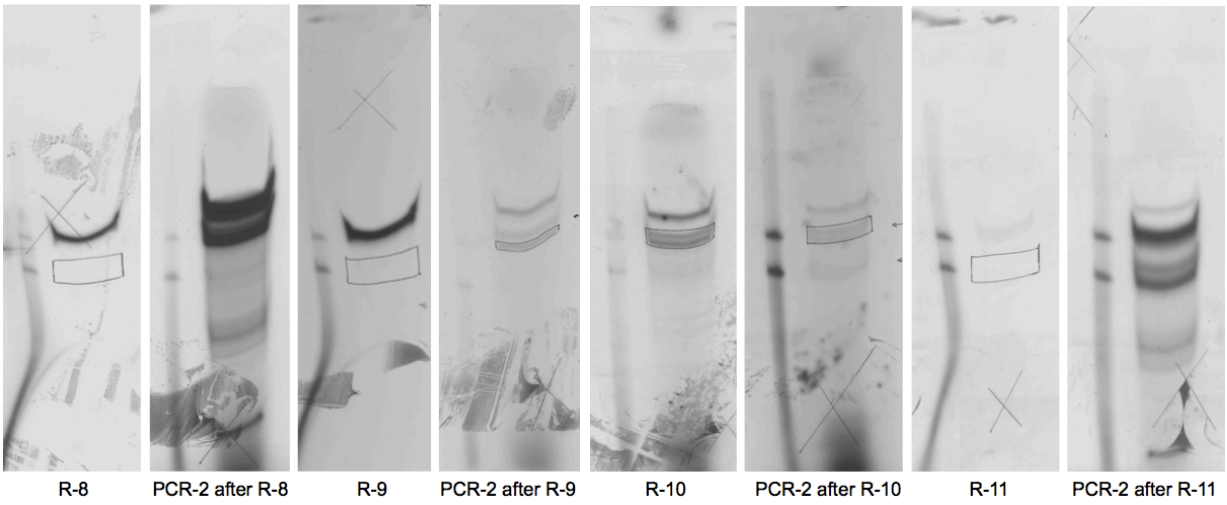

Figure 3.9. Gel images showing selection rounds 8-11. Selection rounds 1-8 showed stable PCR-2 results, but beginning with the PCR-2 after R-9, the PCR results were more varied.

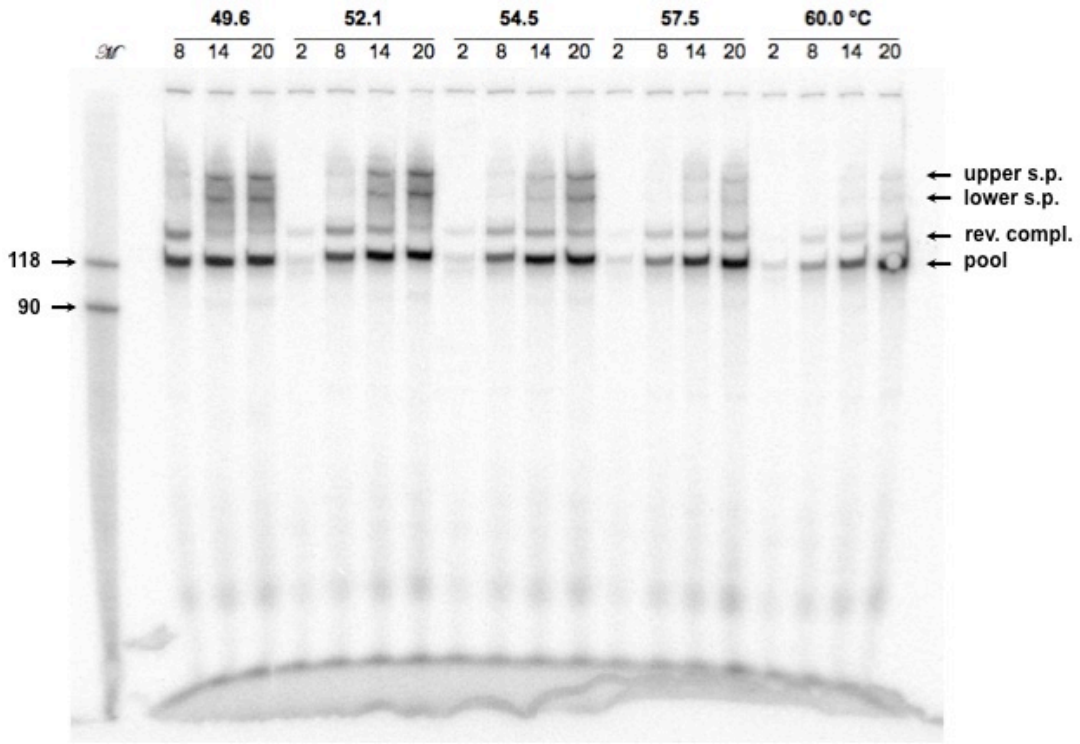

Figure 3.10. PCR variations for the FeIIrCG Pool. Annealing temperatures (T_a) from 49.6 to 60.0 °C and PCR-2 cycles from 2 to 20 were attempted. s.p. denotes side product and rev. compl. denotes reverse complement.

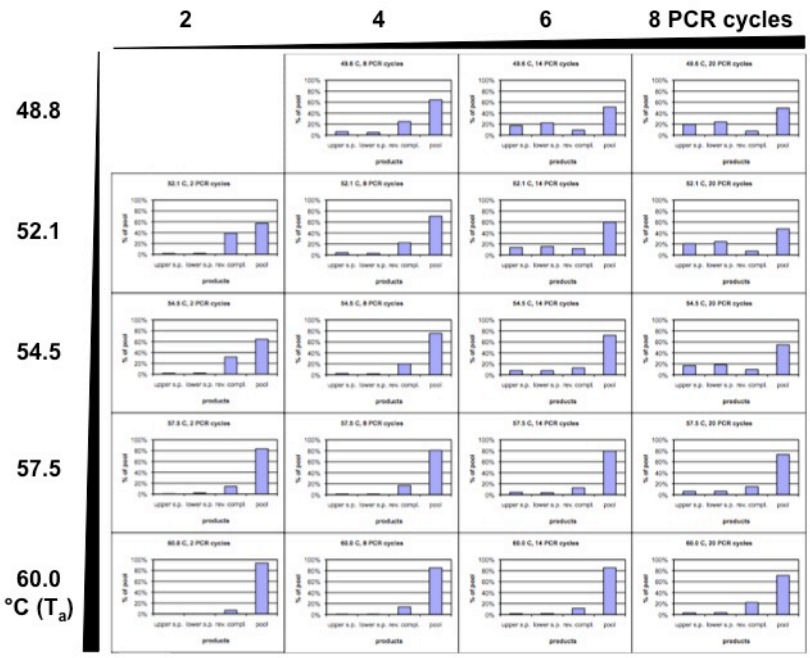

Figure 3.11. PCR variation results showing the percentage of total PCR products (normalized).

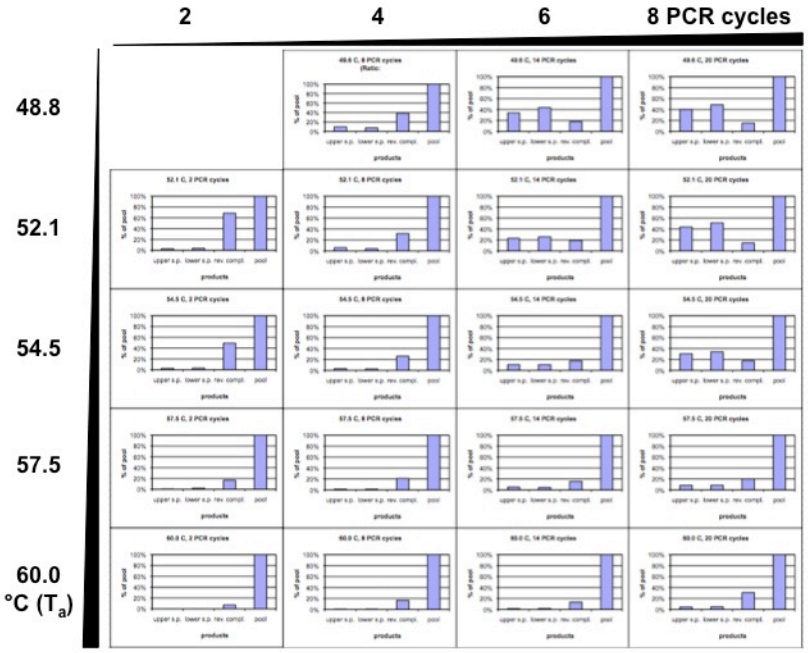

Figure 3.12. PCR variation results showing the percentage of pool (normalized).

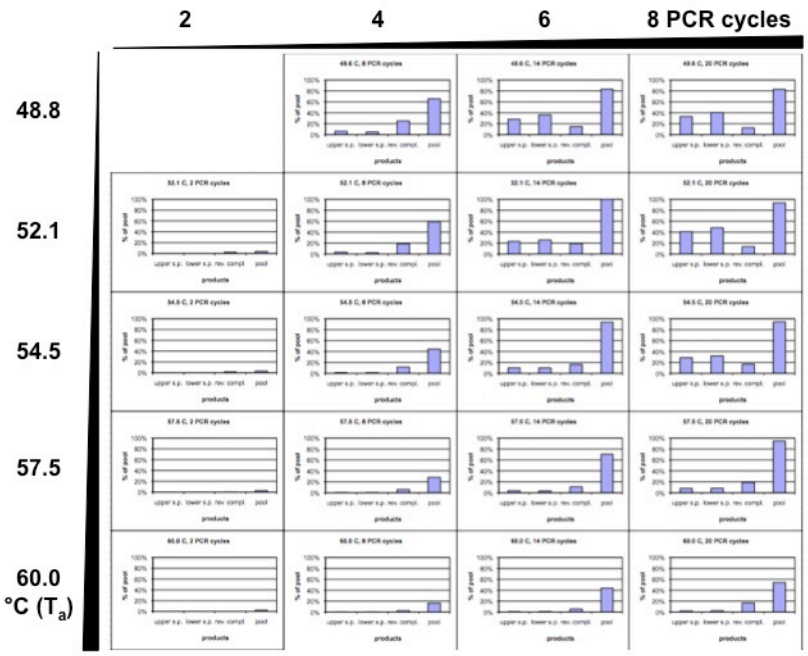

Figure 3.13. PCR variation results showing the percentage of most intense pool.

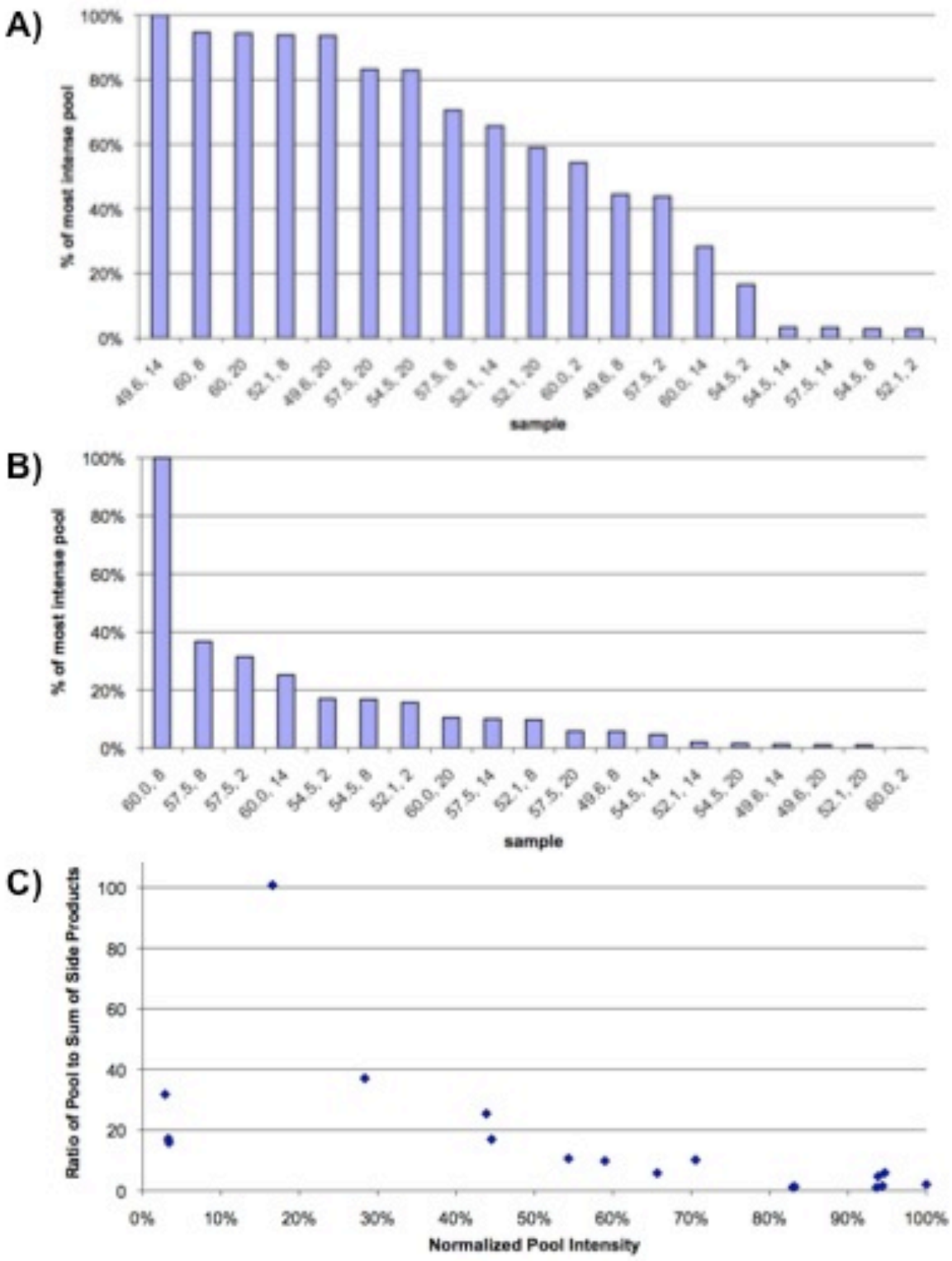

Figure 3.14. PCR variation results. A) Ranking of normalized pool intensities. B) Ranking of the ratios of pool intensities to the intensities of the side product (lowest value not shown). C) Normalized pool intensity versus the ratio of the pool to the sum of side products (lowest value not shown).

T_a (°C)	# Cycles	Normalized Pool Intensity	Ratio of Pool to Sum of S.P.
49.6	8	65.7%	5.8
	14	83.2%	1.3
	20	82.9%	1.1
52.1	2	3.4%	16
	8	59.0%	9.8
	14	100.0%	2.0
	20	93.6%	1.1
54.5	2	3.3%	17
	8	44.5%	17
	14	93.8%	4.7
	20	94.4%	1.6
57.5	2	2.9%	32
	8	28.3%	37
	14	70.6%	10
	20	94.7%	5.9
60.0	2	2.8%	-180
	8	16.6%	100
	14	43.9%	25.4
	20	54.3%	10.6

Table 3.4. PCR variation results. S.P. denotes side products.

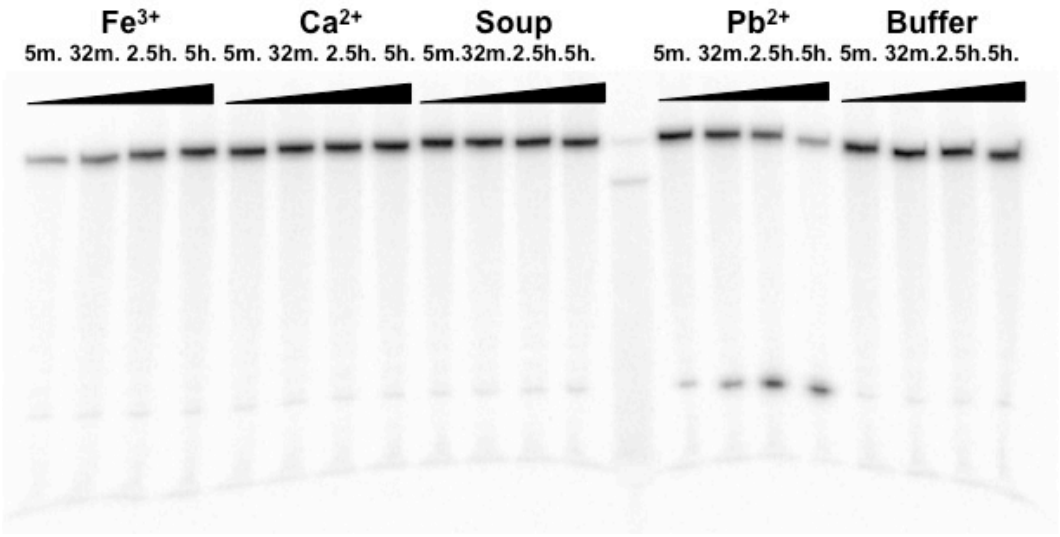

Figure 3.15. Fe^{3+} selection kinetic assay after R-25. The FeIIrCG pool was used. All cleavage assays were performed in the presence of 10 mM of the respective metal ions.

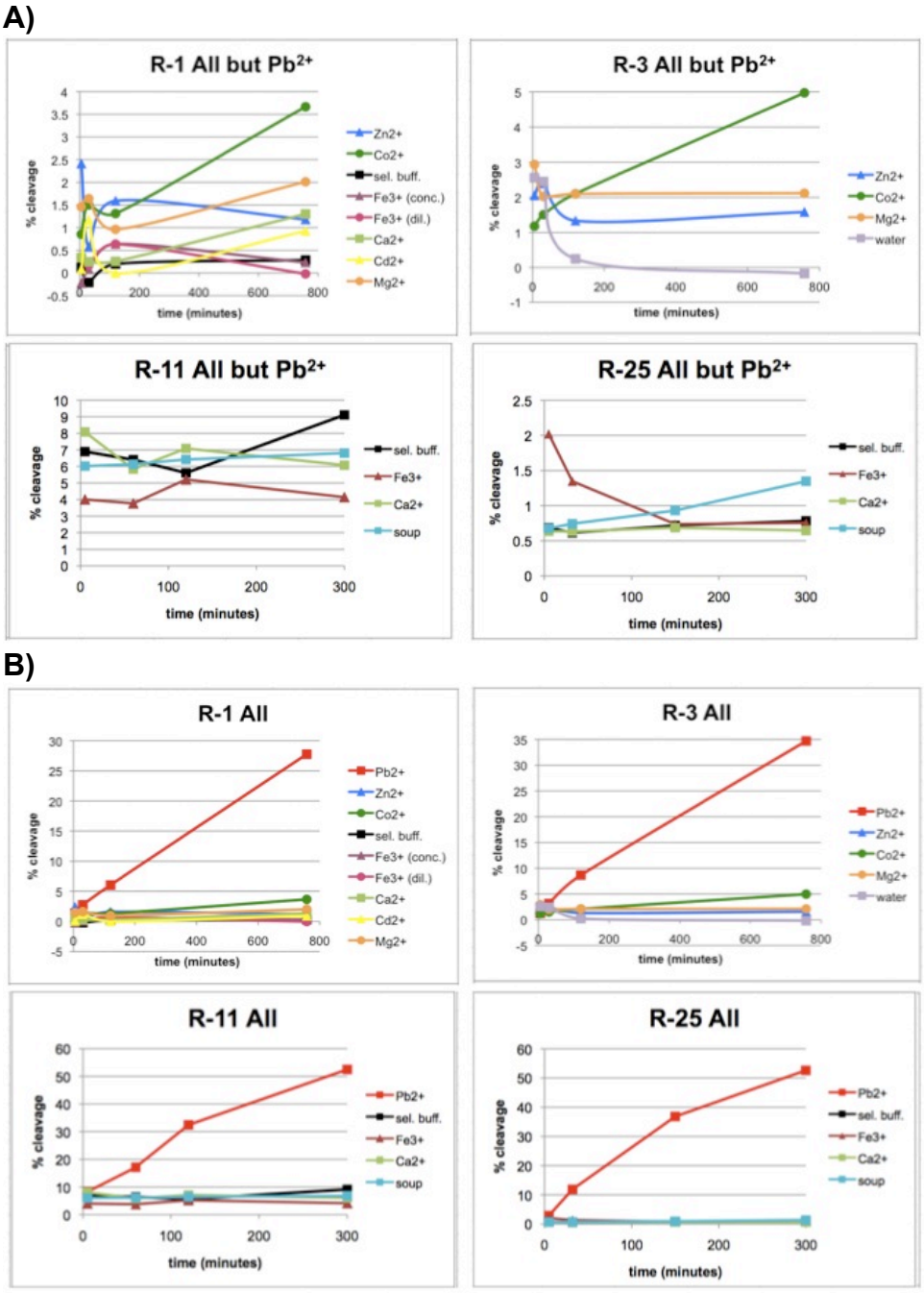

Figure 3.16. The metal dependence of the FeIIrCG pool after 1, 3, 11, and 25 rounds of Fe^{3+} selection. A) The percent cleavage of the pool in the presence of all metal ions but Pb^{2+}. B) The percent cleavage of the pool in the presence of all metal ions but Pb^{2+}.

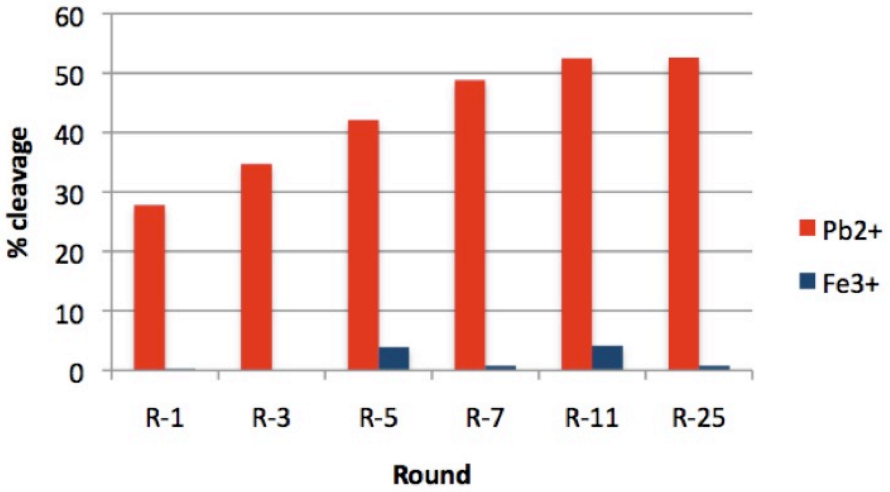

Figure 3.17. The percent cleavage of the FeIIrCG pool after 1, 3, 5, 7, 11, and 25 selection rounds.

3.8 References

1. U.S. EPA "Drinking Water Contaminants." 6 March 2012. Web. 15 April 2012. <http://water.epa.gov/drink/contaminants/index.cfm#Inorganic>

2. Crichton, Robert. "Inorganic Biochemistry of Iron Metabolism: From Molecular Mechanisms to Clinical Consequences." John Wiley & Sons, Ltd.; p. 3 (2001).

3. a) Harrison, S.; Bacon, B.; "Hereditary Hemochromatosis: Update for 2003." *J. Hepatol.* **2003**, *38*, S14-S23. b) Weinberg, E. "Iron Loading in Humans: A Risk Factor for Enhanced Morbidity and Mortality." *J. Nutr. Environ. Med.* **2007**, *16*, 43-51.

4. Drakesmith, H.; Prentice, A. "Viral Infection and Iron Metabolism." *Nat. Rev. Micro.* **2008**, *6*, 541-552.

5. De Domenico, I.; McVey Ward, D.; Kaplan, J. "Regulation of Iron Acquisition and Storage: Consequences for Iron-linked Disorders." *Nature Rev. Mol. Cell Biol.* **2008**, *9*, 72-81.

6. Breuer, W.; Cabantchik, Z. "A Fluorescence-Based One-Step Assay for Serum Non-Transferrin-Bound Iron." *Anal. Biochem.* **2001**, *299*, 194-202.

7. Tenopoulou, M.; Doulias, P.; Barbouti, A.; Brunk, U.; Galaris, D. "Role of Compartmentalized Redox-Active Iron in Hydrogen Peroxide-Induced DNA Damage and Apoptosis. *Biochem J.* **2005**, 703-710.

8. Breuer, W.; Cabantchik, Z. "A Fluorescence-Based One-Step Assay for Serum Non-Transferrin-Bound Iron." *Anal. Biochem.* **2001**, *299*, 194-202.

9. Blick, Kenneth, E.; Liles, Suzanne Martin. "Principles of Clinical Chemistry." John Wiley & Sons, Inc., pp. 347-348 (1985).

10. Stankiewicz, J.; Panter, S.; Neema, M.; Arora, A.; Batt, C.; Bakshi, R. "Iron in Chronic Brain Disorders: Imaging and Neurotherapeutic Implications." *Neurotherapeutics.* **2007**, *4*, 371-386.

11. Loreal, O.; Gosriwatana, I.; Guyader, D.; Porter, J.; Brissot, P.; Hider, R. "Determination of Non-Transferrin-Bound Iron in Genetic Hemochromatosis using a New HPLC-Based Method." *J. Hepatol.* **2000**, *32*, 727-733.

12. a) Perry, R.; San Clemente, C. "Determination of Iron with Bathophenanthroline Following an Improved Procedure for Reduction of Iron(III) Ions." *Analyst* **1977**, *102*, 114-119. b) Gosriwatana, I.; Loreal, O.; Lu, S.; Brissot, P.; Porter, J.; Hider, R. "Quantification of Non-Transferrin-Bound Iron in the Presence of Unsaturated Transferrin." *Anal. Biochem*. **1999**, *273,* 212-220.

13. Loreal, O.; Gosriwatana, I.; Guyader, D.; Porter, J.; Brissot, P.; Hider, R. "Determination of Non-Transferrin-Bound Iron in Genetic Hemochromatosis using a New HPLC-Based Method." *J. Hepatol.* **2000**, *32*, 727-733.

14. Parmley, R.; Spicer, S.; Alvarez, C. "Ultrastructural Localization of Nonheme Cellular Iron with Ferrocyanide." *J. Histochem. Cytochem.* **1978**, *26*, 729-741.

15. a) Carter, P. "Spectrophotometric Determination of Serum Iron at the Submicrogram Level with a New Reagent (Ferrozine)." *Anal. Biochem.* **1971**, *40*, 450-458. b) White, J.; Flashka, H. "An Automated Procedure, with Use of Ferrozine, for Assay of Serum Iron and Total Iron-Binding Capacity." *Clin. Chem.* **1973**, *19*, 526-528. c) Kim, J.; Ko, S.; Kwon, S.; Kim, H.; Han, M.; Kim, D.; Cho, S.; Jeon, B. "Ferrous and Ferric Ion Accumulates

in the Brain of Aged Long-Evans Cinnamon Rats, an Animal Model of Wilson's Disease." *Neurosci. Lett.* **2005**, *382*, 143-147.

16. Liang, Z.; Wang, C.; Yang, J.; Gao, H.; Tian, Y.; Tao, X.; Jiang, M. "A Highly Selective Colorimetric Chemosensor for Detecting the Respective Amounts of Iron(II) and Iron(III) Ions in Water." *New J. Chem.* **2007**, *31*, 906-910.

17. Fischer, D.; Price, D. "A Simple Serum Iron Method Using the New Sensitive Chromogen Tripyridyl-s-Triazine." *Clin. Chem.* **1964**, *10, 21-31.*

18. Fakih, S.; Podinovskaia, M; Schaible, U.; Collins, H.; Hider, R. "Monitoring Intracellular Labile Iron Pools: A Novel Fluorescent Iron(III) Sensor as a Potential Non-Invasive Diagnosis Tool." *J, Pharm, Sci,* 2008 (preprint).

19. Sumner, J.; Kopelman, R. "Alexa Fluor 488 as an Iron Sensing Molecule and Its Application in PEBBLE Nanosensors." *Analyst*, **2005**, *130*, 528–533.

20. Breuer, W.; Cabantchik, Z. "A Fluorescence-Based One-Step Assay for Serum Non-Transferrin-Bound Iron." *Anal. Biochem.* **2001**, *299*, 194 –202.

21. Epsztejn, S.; Kakhlon, O.; Glickstein, H.; Breuer, W.; Cabantchik, Z. "Fluorescence Analysis of the Labile Iron Pool of Mammalian Cells." *Anal. Biochem.* **1997**, *248*, 31-40. b) Kartikaasari, A.; Georgiou, N.; Visseren, F.; van Kat-Renaud, H.; van Asbeck, B.; Marx, J. "Intracellular Labile Iron Modulates Adhesion of Human Monocytes to Human Endothelial Cells." *Arterioscler. Thromb. Vasc. Biol.* **2004,** *24,* 2257-226. c) Tenopoulou, M.; Doulias, P.; Barbouti, A.; Brunk, U.; Galaris, D. "Role of Compartmenalized Redox-Active Iron in Hydrogen Peroxide-Induced DNA Damage and Apoptosis. *Biochem J.* **2005**, 703-710. d) Glickstein, H.; Ben El, R.; Shvartsman, M.; Cabantchik, Z. "Intracellular Labile Iron Pools as Direct Targets of Iron Chelators: A Fluorescence Study of Chelator Action in Living Cells." *Blood* **2005**, *106*, 3242-3250.

22. Petrat, F.; Rauen, U.; de Groot, H. "Determination of the Chelatable Iron Pool of Isolated Rat Hepatocytes by Digital Fluorescence Microscopy." *Hepatol.* **1999**, *29*, 1171-1179.

23. a) Hinkle, P.; Shanshala, E.; Nelson, E. "Measurement of Intracellular Cadmium with Fluorescent Dyes. Further Evidence for the Role of Calcium Channels in Cadmium Uptake." *J. Biol. Chem.* **1992**, *267*, 25553-25559. b) Espósito, B.; Breuer, W.; Cabantchik, Z. "Design and Applications of Methods for Fluorescence Detection of Iron in Biological Systems." *Biochem. Soc. Trans.* **2002,** *30*, 729-732.

24. Carter, P. "Spectrophotometric Determination of Serum Iron at the Submicrogram Level with a New Reagent (Ferrozine)." *Anal. Biochem.* **1971**, *40*, 450-458.

25. Zhou, Y.; Wang, S.; Zhang, K.; Jiang, X. "Visual Detection of Copper(II) by Azide- and Alkyne-Functionalized Gold Nanoparticles Using Click Chemistry." *Angew. Chem.* **2008**, *120*, 7564-7566. *Angew. Chem. Int. Ed.* **2008**, *47*, 7454-7456.

26. Lee, J.; Wang, Z.; Liu, J.; Lu, Y. "Highly Sensitive and Selective Colorimetric Sensors for Uranyl (UO_2^{2+}): Development and Comparison of Labeled and Label-Free DNAzyme-Gold Nanoparticle Systems." *JACS* **2008**, *130*, 14217-14226.

27. Cruz, R.; Withers, J.; Li, Y. "Dinucleotide Junction Cleavage Versatility of 8-17 Deoxyribozyme." *Chem. Biol.* **2004**, *11*, 57-67.

28. Schlosser, K.; Gu, J.; Sule, L.; Li, Y. "Sequence-function Relationships Provide New Insight into the Cleavage Site

Selectivity of the 8-17 RNA-Cleaving Deoxyribozyme." *Nucleic Acid. Res.* **2008**, *36*, 1472-1481.

29. Zuker, M. "Mfold Web Server for Nucleic Acid Folding and Hybridization Prediction." *Nucleic Acids Res.* **2003**, *31*, 3406–3415.

[30] Mazumdar, D. "Investigation of Metal-Dependence in DNAzymes and Applications of DNAzymes and Aptamers for Diagnostics." Ph.D. Dissertation, University of Illinois at Urbana-Champaign, 2009.

31. Dickinson, B.; Chang, C.; "A Targetable Fluorescent Probe for Imaging Hydrogen Peroxide in the Mitochondria of Living Cells." *JACS*, **2008**, *130*, 9638-9639.

Chapter 4: Evaluating the Potential of an Acid/Base Catalysis Mechanism in the Pb^{2+}-Dependent 17E DNAzyme by Examining $G^{1.1}$-Mutants

4.1 Note and Acknowledgments

This is a continuation of work conceptualized and first undertaken by Dr. Debapriya Mazumdar. Many thanks to Dr. Debapriya Mazumdar, Dr. Nandini Nagraj, Dr. Eric Null, and Tian Lan for helpful insights into this project.

4.2 Introduction

One class of DNAzymes that have been successfully developed into many metal-ion-based sensors is that of RNA-cleaving DNAzymes. A motif that has been obtained through multiple selection strategies is the 8-17 motif, and one variant of this motif is the 17E DNAzyme, shown in Figure 4.1A. The 17E DNAzyme has been studied by NMR spectroscopy, gel-based methods,[1] and circular dichroism,[2] and fluorescence-detected resonance energy transfer,[3] but no crystal structure of the DNAzyme in its active conformation has yet been obtained. Thus, there is some question as to the mechanism by which 17E carries out its catalytic activity.

The more mature field of ribozyme analysis may provide some insight into this question. Due to their earlier discovery, more is known about ribozyme motifs such as the hammerhead, than DNAzyme motifs such as 8-17. Given the similarity between the structures of RNA and DNA, it is logical to look for parallels between their structure-function relationships. Guanine residues have been found to be key to the reactivity of the self-cleaving hairpin[4,5,6] and hammerhead ribozymes.[7] In these situations, even weak acids with pK_as far from the biological pH of 7.4 participate in catalysis because their Brønsted α and β values enable them to influence the transition state.[8] For example, Han *et al.* performed mutational analysis on the hammerhead ribozyme at three different guanines. They found that while the individual substitution for bases G5, G8, or G12 produced some inhibition, G5 variants were inhibited independent of pH, while G8 and G12 variants saw pH-dependent inhibition. The most dramatic alteration occurred when G8 and G12 were concurrently mutated: this variant saw a markedly different pH-dependence than any other combination of mutations.

This work uses lessons learned in the field of ribozymes to explore a strategic guanine residue's ability to participate in general acid-base catalysis in the 17E DNAzyme, substituting guanine analogs at the $G^{1.1}$ position in its substrate.

4.3 Materials and Methods

4.3.1 Materials

All DNA were obtained from Integrated DNA Technologies (Coralville, IA). Chelex 100 sodium-form beads were obtained from Sigma-Aldrich (St. Louis, MO). All buffer and electrophoresis materials were obtained from Sigma-Aldrich, BIORAD (Hercules, CA), or the USB Corporation (Cleveland, OH). [γ-^{32}P]-ATP was obtained from Perkin-Elmer (Boston, MA). Platinum *Taq* DNA-polymerase and T4 kinase were obtained from Invitrogen (Carlsbad, CA). Millipore water was used to prepare all solutions. Any polypropylene tubes for the long-term storage of solutions, and all glassware were rinsed with concentrated nitric acid before use. Residual divalent cations in non-EDTA-containing solutions were removed by stirring 1 g of Chelex 100 beads in 100 mL of solution for five hours.

4.3.2 Methods

Three different guanine analogs were substituted for $G^{1.1}$, which is the guanine adjacent to the scissile ribonucleotide in the catalytic core of the enzyme. The structures of these analogs are shown in Figure 2.1B. Kinetic assays were carried out under single turnover conditions, with a ratio of five thousand between the enzyme and substrate concentrations. A solution 10 µM in 17E, 2 nM in [γ-^{32}P]-labeled substrate, 100 mM in buffer of an appropriate pH between 5.0 and 6.5, 200 nM in decoy DNA was denaturated at 95 °C and annealed over a thirty-minute time period. It was then mixed with an equal volume of 400 µM Pb^{2+} solution to initiate the reaction. Five-microliter aliquots of the reaction solution were mixed with stop solution to quench the reaction at appropriate time points. The reactions were then purified on a 20% denaturing PAGE gel and exposed to a storage phosphorscreen (Molecular Dynamics). Cleavage products were visualized and intensities were background subtracted by an Amersham Biosciences Molecular Dynamics Storm 430 phosphorimager (Molecular Dynamics). The cleavage efficiency was calculated at time t using the following equation: $y = 100 * [I_c / (I_u +$

I_c)], where y is the percent cleaved product, I_c is the intensity of the cleaved substrate and I_u is the intensity of the uncleaved substrate. Pseudo-first-order rate constants were determined by fitting an equation of the form $y = y_o + a\ (1 - e^{-kt})$ to the data using Origin 8, where y is the percent cleaved product as a function of time t, y_o is the background product at time $t = 0$, a is the fraction of the pool cleaved at time $t = 1$, and k is the observed rate constant.

4.4 Results

The percent cleavage versus time of reaction of each construct was plotted, as shown in Figure 4.2. Once Equation 1 was fitted to these plots, the observed rate constants (k_{obs}) for each reaction were obtained. These are shown in Figure 4.3.

4.5 Discussion

All three analogs inhibited 17E's activity. 2,6-diaminopurine and 2-aminopurine inhibited 17E to a roughly equivalent degree, and inosine inhibited 17E to a lesser extent. What is significant is that the inhibition is pH-independent. In effect, the activity of the native 17E has simply been phase-shifted downward whenever an analog is incorporated into its substrate. This situation is analogous to the G5 substitution Han *et al*. describe in the hammerhead ribozyme. It is strikingly different from the situation when either G8 or G12 in this ribozyme were mutated: in those cases, while inosine maintained a similar pH-dependence to the native enzyme, the diAP and 2-AP variants had significantly different pH-dependencies.

The results from this work, then, implies that $G^{1.1}$ is not involved in a general acid-base mechanism in 17E, but, like the G5 in the hammerhead ribozyme, aids in the overall folding of the DNAzyme.

4.6 Conclusions and Future Directions

$G^{1.1}$ was not found to participate in general acid-base catalysis. What is possible, then, is that another nucleotide in the 17E DNAzyme does, or that 17E uses a different mechanism. One way to decide this question is by exploring the properties of other nucleotides. This should take into account the conserved residues elucidated by Peracchi *et al*.,[9] as well as other work with 8-17. For example, recently, Sekhon *et al.* carried out crosslinking studies on 8-17, and found that C3 and C13 are likely to carry out general acid-base catalysis in this motif.[10] One possible future

direction for this project would be to explore cytosine analogs that alter this nucleotide's pK_a and examine the effect on 17E's activity.

IDT does not currently provide any cytosine analogs in their list of modified bases,[11] but TriLink lists offers nine cytosine analogs, and it is likely that some of these analogs could alter N4's pK_a. These modified bases are 5-bromo-2'-deoxycytidine, N4-ethyl-2'-deoxycytidine, 5-iodo-2'-deoxycytidine, 5-methyl-2'-deoxycytidine, 5-propynyl-2'-deoxycytidine, 5-hydroxy-2'-deoxycytidine, pyrrolo-2'-deoxycytidine, 5-methyl-2'-deoxyisocytidine, and 5-hydroxmethyl-2'-deoxycytidine.[12]

4.7 Figures and Tables

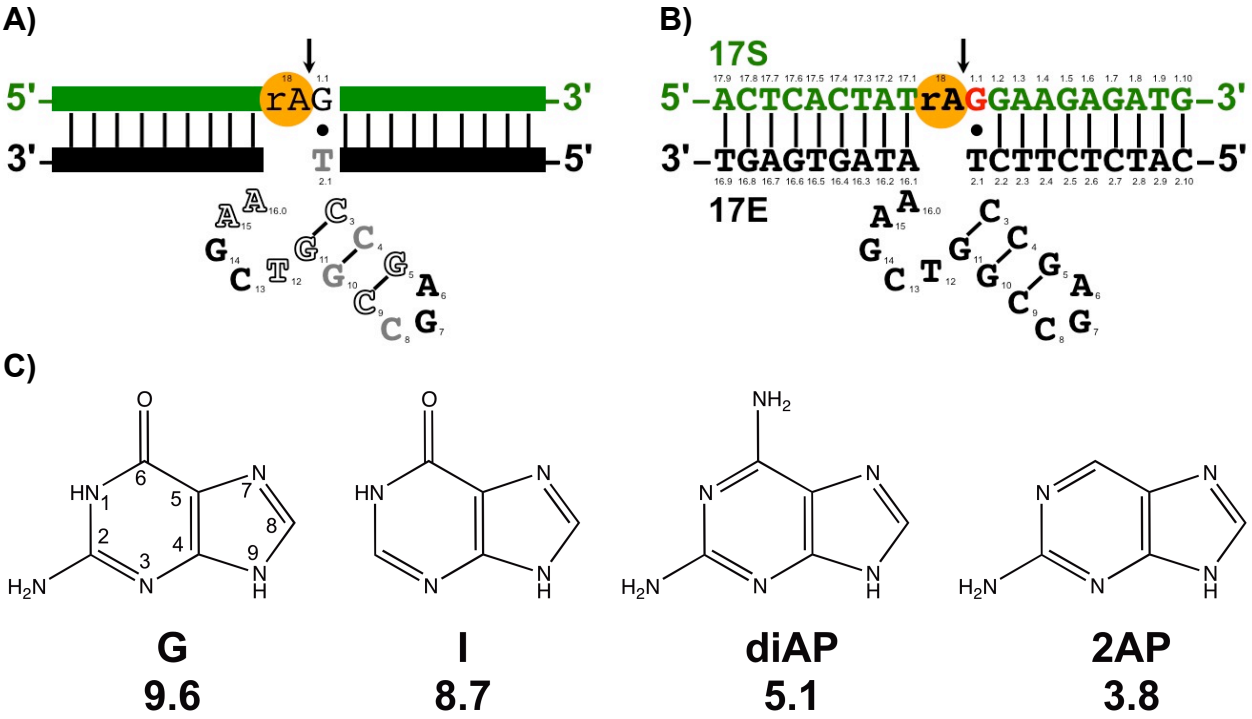

Figure 4.1. The 8-17 motif, 17E DNAzyme, and the $G^{1.1}$ modified bases. A) The 8-17 motif with its conserved nucleotides shown. The cleavage site is indicated by an arrow. Black, grey, and white code the conserved nucleotides' impact on the motif's activity: black denotes nucleotides whose replacement causes a greater than 100-fold decrease in activity, grey denotes nucleotides whose replacement causes a greater than 10-fold decrease in activity, and white denotes nucleotides with lesser impact on the motif's activity. Adapted from ref. 9. B) The 17E DNAzyme and its substrate 17S used in this analysis. The cleavage site is indicated by an arrow. $G^{1.1}$ is the guanine adjacent to the scissile riboadenine. C) Guanine and the guanine analogues substituted for $G^{1.1}$, along with their N1 pK_as (I is inosine, diAP is 2,6-diaminopurine, and 2AP is 2-aminopurine).

Name	Length (nt.)	Sequence (5'→3')
17E	33	CATCTCTTCTCCGAGCCGGTCGAAATAGTGAGT
17S	20	ACTCACTAT**rAG**GAAGAGATG

Table 4.1. The DNA used in this analysis. The $G^{1.1}$ in 17S substituted with inosine, 2,6-diaminopurine, or 2-aminupurine is shown in bold.

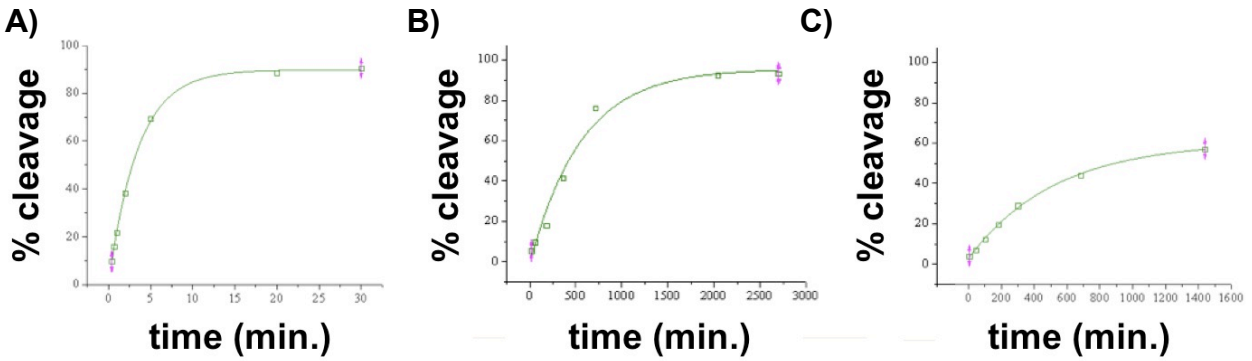

Figure 4.2. Kinetic plots of 17E with three 17S-$G^{1.1}$-substituted variants in the presence of 200 µM Pb^{2+} at pH 5.5. A) Results from the 17S $G^{1.1}$I mutant. B) Results from the 17S $G^{1.1}$diAp mutant. C) Results from the 17S $G^{1.1}$2Ap mutant.

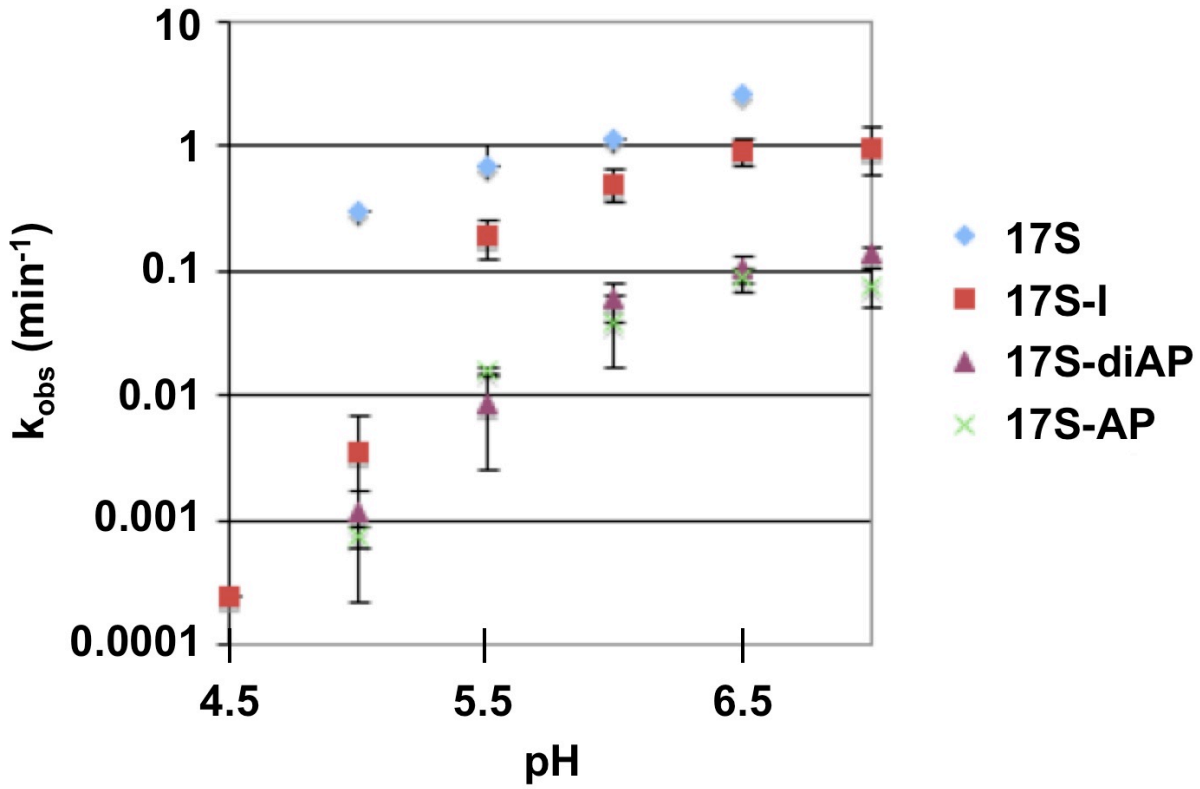

Figure 4.3. Activities of 17E with 17S and three 17S-$G^{1.1}$-substituted variants in the presence of 200 µM Pb^{2+}. (I is inosine, diAP is 2,6-diaminopurine, and 2AP is 2-aminopurine). 17S data is courtesy of Dr. Andrea Brown. For all other data, the averages of at least three data points are shown.

4.8 References

1. Brown, A.; Li, J.; Pavot, C.; Lu, Y. "A Lead-Dependent DNAzyme with a Two-Step Mechanism." *Biochemistry* **2003**, *42*, 7152-7161.

2. Mazumdar, D.; Nagraj, N.; Kim, H.; Meng, X.; Brown, A.; Sun, Q.; Li, W.; Lu, Y. "Activity, Folding, and Z-DNA Formation of the 8-17 DNAzyme in the Presence of Monovalent Ions. *J. Am. Chem. Soc.* **2009**, *131*, 5506-5515.

3. Kim, H.; Liu, J.; Li, J.; Nagraj, N.; Li, M.; Pavot, C.; Lu, Y. "Metal-Dependent Global Folding and Activity of the 8-17 DNAzyme Studied by Fluorescence Resonance Energy Transfer." *J. Am. Chem. Soc.* **2007**, *129*, 6896-6902.

4. Chowrira, B. M.; Berzal-Herranz, A.; Burke, J. M. "Novel Guanosine Requirement for Catalysis by the Hairpin Ribozyme." *Nature* **1991**, *354*, 320-322.

5. Pinard, R.; Hampel, K. J.; Heckman, J. E.; Lambert, D.; Chan, P. A.; Major, F.; Burke, J. M. "Functional Involvement of G8 in the Hairpin Ribozyme Cleavage Mechanism." *EMBO J.* **2001**, *20*, 6434-6442.

6. Cochrane, J. C.; Strobel, S. A. "Catalytic Strategies of Self-Cleaving Ribozymes." *Acc. Chem. Res.* **2008**, *41*, 1027-1035.

7. Han, J.; Burke, J. M. "Model for General Acid-Base Catalysis by the Hammerhead Ribozyme: pH-Activity Relationships of G8 and G12 Variants at the Putative Active Site." *Biochemistry* **2005**, *44*, 7864-7870.

8. Bevilacqua, P. "Mechanistic Considerations for General Acid-Base Catalysis by RNA: Revisiting the Mechanism of the Hairpin Ribozyme." *Biochemistry* **2005**, *42*, 2259-2265.

9. Peracchi, A.; Bonaccio, M.; Clerici, M. "A Mutational Analysis of the 8-17 Deoxyribozyme Core." *J. Mol. Biol.* **2005**, *352*, 783-794.

10. Sekhon, G.; Sen, D. "A Stereochemical Glimpse of the Active Site of the 8-17 Deoxyribozyme from Iodine-Mediated Cross-links Formed with the Substrate's Scissile Site." *Biochemistry* **2010**, *49*, 9072-9077.

11. Integrated DNA Technologies. 10 April 2012. <http://www.idtdna.com/catalog/Modifications/Modifications.aspx?catid=7>.

12. TriLink BioTechnologies. 10 April 2012. <http://www.trilinkbiotech.com/cart/Scripts/prodList.asp?idCategory=65>